

NATIONAL LIBRARY
OTTAWA



BIBLIOTHÈQUE NATIONALE
OTTAWA

8085

NAME OF AUTHOR... WENSON, LON HUTCHISON

TITLE OF THESIS... HUNTER-KILL POTENTIAL OF COGNITIVE
and some sociological
structures

UNIVERSITY... ALBERTA

DEGREE FOR WHICH THESIS WAS PRESENTED... PH.D.

YEAR THIS DEGREE GRANTED... 1960

Permission is hereby granted to THE NATIONAL LIBRARY
OF CANADA to microfilm this thesis and to lend or sell copies
of the film.

The author reserves other publication rights, and
neither the thesis nor extensive extracts from it may be
printed or otherwise reproduced without the author's
written permission.

(Signed) W. Hutchison

PERMANENT ADDRESS:

1817
Woodbine
S.C.

DATED... Nov 1960

THE UNIVERSITY OF ALBERTA

HINDERED ROTOR PROGRAMME AND SOME CRYSTALLOGRAPHIC
STRUCTURES

by



WENDY LOU HUTCHEON

A THESIS

SUBMITTED TO THE FACULTY OF GRADUATE STUDIES
IN PARTIAL FULFILMENT OF THE REQUIREMENTS FOR THE DEGREE
OF DOCTOR OF PHILOSOPHY

DEPARTMENT OF CHEMISTRY

EDMONTON, ALBERTA

SPRING, 1971

UNIVERSITY OF ALBERTA
FACULTY OF GRADUATE STUDIES

The undersigned certify that they have read,
and recommend to the Faculty of Graduate Studies for
acceptance, a thesis entitled "Hindered Rotor Programme
and Some Crystallographic Structures" submitted by
Wendy Lou Hutcheon (née Brooks) in partial fulfilment
of the requirements for the degree of Doctor of
Philosophy.

..... *M.J. Bennett*
M.J. Bennett, Supervisor

..... *W.A. Ayer*
W.A. Ayer

..... *J.E. Bertie*
J.E. Bertie

..... *R.E.D. McClung*
R.E.D. McClung

..... *D. Mash*
D. Mash

..... *C.J.L. Lock*
C.J.L. Lock, External Examiner

Date. November 24, 1970

TABLE OF CONTENTS

	Page
Chapter I: THE HINDERED ROTOR	
Introduction.....	1
Theoretical.....	8
Discussion.....	33
 Chapter II: THE CRYSTAL STRUCTURE OF FERROCINIUM PICRATE	
Introduction.....	54
Experimental.....	55
Solution and Refinement.....	59
Results.....	70
Discussion.....	75
 Chapter III: THE CRYSTAL STRUCTURE OF HYDRIDO- TRIPHENYLSILYL (π -CYCLOPENTADIENYL) DICARBONYL MANGANESE	
Introduction.....	79
Experimental:	
- trichloro derivative.....	80
- triphenyl derivative.....	81
Solution and Refinement.....	84
Results.....	94
Discussion.....	101

Table of Contents
(Continued)

	Page
Chapter IV: THE CRYSTAL STRUCTURE OF DIHYDROOCTACARBONYL DIRHENIUM	
Introduction.....	109
Experimental.....	111
Solution and Refinement.....	113
Results.....	117
Discussion.....	121
References.....	130
Appendix A: Subroutines ROTOR and BESSEL of SFLS5HR.....	136
Appendix B: Programmes Used in Crystal Structure Solution, Refinement and Analysis.....	144
Appendix C: Conventional Crystallographic Symbols.....	146

LIST OF TABLES

		Page
Chapter I:	THE HINDERED ROTOR	
Table I	Refined hindered rotor parameters...	32
Table II	Comparison of corrected C-C bonds...	37
Table III	Comparison of RMS values.....	37a
Table IV	Comparison of temperature factors for ring and metal atom.....	44a
Table V	Refined parameters for Cs[Y(HFA) ₄]..	50
Table VI	Comparison of R factors.....	51a
Chapter II:	THE CRYSTAL STRUCTURE OF FERROCINIUM PICRATE	
Table VII	Possible site symmetries.....	57
Table VIII	Observed and calculated structure factor amplitudes.....	66
Table IX	Positional co-ordinates.....	67
Table X	Atom anisotropic temperature factors.....	68
Table XI	(a) Hindered rotor parameters.....	69
	(b) Derived co-ordinates.....	69
Table XII	(a) Bond lengths.....	73
	(b) Bond angles.....	73
Table XIII	Interionic contacts.....	74
Chapter III:	THE CRYSTAL STRUCTURE OF HYDRIDO- TRIPHENYLSILYL (π -CYCLOPENTADIENYL) DICARBONYL MANGANESE	
Table XIV	Hydrogen peak as a function of $\sin \theta / \lambda$	87

List of Tables
(Continued)

		Page
Table XV	Observed and calculated structure factor amplitudes.....	89
Table XVI	Atom positions.....	90
Table XVII	Anisotropic temperature factors.....	91
Table XVIII	(a) Rigid body, hindered rotor parameters.....	92
	(b) Derived positional parameters for hindered rotors and rigid bodies.....	93
Table XIX	(a) Bond lengths.....	98
	(b) Bond angles.....	99
Table XX	Intermolecular contacts.....	100
Table XXI	Comparison of M-C bonds.....	103
Table XXII	Comparison of M-C bonds trans to -CO.....	105
Chapter IV: THE CRYSTAL STRUCTURE OF DIHYDROOCTACARBONYL DIRHENIUM		
Table XXIII:	Observed and calculated structure factor amplitudes.....	115
Table XXIV:	Atom positions and isotropic temperature factors.....	116
Table XXV:	(a) Bond lengths.....	119
	(b) Bond angles.....	119
	(c) Intermolecular non-bond contacts.....	119
Table XXVI:	Intermolecular contacts.....	120

LIST OF FIGURES

	Page
Chapter I: THE HINDERED ROTOR	
Figure 1 $\frac{1}{2} g(x)f^2(x)$ versus x	19
Figure 2 Molecular structure of ruthenocene.....	28
Figure 3 Molecular structure of benzene.....	28
Figure 4 Molecular structure of $(\pi-C_5H_5)Mn(CO)_3$	29
Figure 5 Molecular structure of $(\pi-C_6H_6)Cr(CO)_2$	29
Figure 6 Molecular structure of $(\pi-C_7H_7)(C_6H_5)Mo(CO)_2$	30
Figure 7 Apparent shortening of radius.....	34
Figure 8 Ratio of radius versus barrier, Bd	35
Figure 9 RMS angular displacement as a function of barrier, Bd	39
Figure 10 Possible potential function for ruthenocene.....	42
Figure 11 $P(\theta')$ versus θ' for a cosine distribution function.....	42
Figure 12 $\Delta B/R^2$ as a function of barrier, Bd	46
Figure 13 ΔB as a function of barrier, Bd	47
CHAPTER II: THE CRYSTAL STRUCTURE OF FERROCINIUM PICRATE	
Figure 14 Structure of ferrocinium picrate.....	71

List of Figures
(Continued)

	Page
Figure 15	Packing of ferrocinium picrate as projected onto the ab plane..... 72
Chapter III: THE CRYSTAL STRUCTURE OF HYDRIDO- TRIPHENYLSILYL (π -CYCLOPENTADIENYL) DICARBONYL MANGANESE	
Figure 16	Molecular structure of $(\pi\text{-C}_5\text{H}_5)(\text{OC})_2\text{Mn}(\text{H})\text{Si}(\text{C}_6\text{H}_5)_3$ 95
Figure 17	Geometry around manganese atom..... 96
Figure 18	Molecular packing projected onto ab plane..... 97
Chapter IV: THE CRYSTAL STRUCTURE OF DIHYDROOCTACARBONYL DIRHENIUM	
Figure 19	Molecular structure of $\text{H}_2\text{Re}_2(\text{CO})_8$...118

ABSTRACTS

Chapter I:

Lipscomb and King's hindered rotor expression was applied to the rigid body routine of M.J. Bennett and B.M. Foxman. The programme SFLS5 was modified to calculate the contribution of the hindered rotor to the structure factors and to do a full matrix least squares refinement of the input parameters. The programme was tested on several sets of published X-ray data. The results showed that the model gives correct bond lengths without recourse to "riding corrections". The barrier parameter B_d is related to the RMS angular displacement of the ring but is not necessarily a measure of activation energy.

Chapter II:

The compound ferrocinium picrate $[\text{Fe}(\text{C}_5\text{H}_5)_2]^+$ $[\text{H}_2\text{C}_6\text{N}_3\text{O}_7]^-$ crystallizes in space group Cmcm ($Z = 4$) with cell dimensions $a = 12.513(7)\text{\AA}$, $b = 20.267(9)\text{\AA}$, $c = 6.903(7)\text{\AA}$. The structure was refined, using SFLS5 as modified for the hindered rotor model, to a conventional R factor of 6.0%. The compound consists of two ionic species, the ferrocinium cation, and the picrate ion. Both ions sit on sites of mm symmetry and show some disorder.

Chapter III:

Hydridotriphenylsilyl (π -cyclopentadienyl) dicarbonyl manganese, $(\pi\text{-C}_5\text{H}_5)(\text{OC})_2\text{Mn}(\text{H})\text{Si}(\text{C}_6\text{H}_5)_3$, crystallizes in the space group $P2_1/n$ with unit cell dimensions $a = 13.200(3)\text{\AA}$, $b = 17.328(4)\text{\AA}$, $c = 9.438(2)\text{\AA}$, $\beta = 92.47(4)^\circ$, $Z = 4$. The structure was refined to a conventional R factor of 4.2%. The geometry around the manganese atom is that of a distorted square pyramid, with that of the silicon atom a distorted tetrahedron. The hydridic hydrogen was located on full data and low angle difference maps and was subject to refinement. It is located in a bridging position, lying $1.54(4)\text{\AA}$ from the manganese and $1.76(4)\text{\AA}$ from the silicon.

Chapter IV:

Dihydrooctacarbonyl dirhenium, $\text{H}_2\text{Re}_2(\text{CO})_8$, crystallizes in space group $P2_1/c$, $a = 8.96(2)\text{\AA}$, $b = 11.62(2)\text{\AA}$, $c = 12.85(2)\text{\AA}$, $\beta = 109.2(1)^\circ$, with four molecules per unit cell. The structure was refined to a conventional R factor of 10.5%, all atoms isotropic. There is octahedral geometry about each rhenium, the hydrogens being assumed to occupy the vacant co-ordinated positions. The doubly hydrogen bridged Re-Re bond of $2.896(3)\text{\AA}$ is shorter than normal Re-Re single bonds.

The topics covered in this thesis involve X-ray diffraction. Undefined symbols have their standard crystallographic meaning and are defined in Appendix C. The standard theoretical and experimental procedures can be found in detail elsewhere^{1,2,3}.

Chapter I

THE HINDERED ROTOR

INTRODUCTION

In X-ray diffraction the structure factor F_{hkl} can be generally expressed as²

$$F_{hkl} = \int \int \int \rho_{xyz} \exp[2\pi i \underline{h} \cdot \underline{r}] dx dy dz . \quad [1]$$

If the assumptions are made that atoms are at rest and the electron density is zero elsewhere in the cell, the expression simplifies to

$$F_{hkl} = \sum_i f_i \exp[2\pi i (hx_i + ky_i + lz_i)] \quad [2]$$

where f_i is the scattering amplitude of atom i at an angle θ and allows for the finite size of the atom.

In general, atoms are not at rest, but are in continual motion. To allow for this, Debye³ derived a temperature parameter B which was related to the mean square displacement of an isotropic harmonic oscillator. Then

F_{hkl} became

$$F_{hkl} = \sum_i f_i \exp[-B(\sin\theta/\lambda)^2] \exp[2\pi i (hx_i + ky_i + lz_i)] . \quad [3]$$

In many cases a better description of the motion of the atoms can be obtained by assuming a general rectilinear harmonic oscillator⁴. This model is conveniently handled in tensor form and the six unique thermal parameters of the general case are related to the root mean square

amplitudes and the direction cosines of the three principal axes of the ellipsoid of vibration. The isotropic and anisotropic models are usually considered practical to describe most crystal structures.

The major disadvantage of these models lies in the large number of parameters required to describe the crystal structure, especially in large molecules such as $\text{RhH}(\text{CO})(\text{P}(\text{C}_6\text{H}_5)_3)_3$ ⁵. Since the isotropic model requires four parameters per atom (x, y, z, B) in the general position and the anisotropic model requires nine parameters per atom (x, y, z and for example $\beta_{11}, \beta_{22}, \beta_{33}, \beta_{12}, \beta_{13}, \beta_{23}$) a full matrix refinement of a large molecule would require excessive computer time and storage. There are two obvious solutions to this problem. The first is to use block diagonal refinement⁶ rather than full matrix refinement. This cuts down greatly on both time and storage requirements, but has the disadvantage that some large parameter correlations can be ignored, even with an apparently sensible choice of blocks.

The second method retains the use of full matrix refinement and utilizes known geometries for certain rigid groups^{7,8}, the disadvantage of the method being that significant deviations from ideal geometry will be missed. In this method, certain groups of atoms are

treated as a unit. It is assumed that the groups are internally rigid and the temperature factors of the atoms are dependent only on the motion of the rigid body as a whole. Such a group may be defined by setting up an internal Cartesian co-ordinate system within the rigid body. The positions of individual atoms within the group can then be specified with reference to the internal co-ordinate system. This co-ordinate system can be related to the crystallographic co-ordinate system by means of a transformation matrix. Since the atoms within the group are assumed to have fixed positions relative to the internal co-ordinate system, it is only necessary to refine the origin and orientation of the co-ordinate system with respect to the crystallographic axes, as well as refining temperature factors for the individual atoms and/or the rigid body as a whole. Use of such a model greatly reduces the number of parameters to be refined.

Use of isotropic temperature parameters for the atoms is based on the assumption that the rigid body is undergoing only relatively small oscillations from its mean position⁹. The opposite extreme occurs if the rigid body is rotating freely. Expressions for the scattering of X-rays from such groups have been calculated by Bijvoet and Ketellar¹⁰ and Zachariasen¹¹.

Intermediate between the two extremes of free rotation and no rotation is the case where the rotation of the group is hindered. Cruickshank¹² found this to be the case in benzene at -3°C . After anisotropic refinement of the carbon atoms, he found that the tangential motion of the atoms was much greater than the radial motion indicating an oscillation of the benzene ring about the hexad axis. In order to describe this motion better, he assumed that the benzene ring was a rigid body. Then its motion could be described in terms of two tensors, T describing the translational motion, and ω associated with oscillations¹³. Using this method of analysis, he showed that the major ring oscillation was about the hexad axis with a RMS (root mean square) angular oscillation of 7.9° . From this it was also possible to calculate the apparent shortening of the C-C bond due to the motion of the ring¹⁴. The method was later extended by Schomaker and Trueblood¹⁵ to the case where there was no pre-ordained centre of rotation and allows for a coupling of rotation and translation via the introduction of a third tensor S. The Cruickshank T and ω tensor elements have been used as model parameters within a structure factor and least squares programme¹⁶ although strictly speaking the site symmetry of the group is limited. The general case of Schomaker and Trueblood

has not been incorporated into a structure factor and least squares programme and its application is currently limited to the analysis of the results of an anisotropic independent atom refinement.

A different approach to the problem of hindered rotation was taken by Lipscomb and King¹⁷ in 1949, at which time the anisotropic tensor description was not known. They derived an expression for the calculation of the intensity of X-ray scattering from rigid groups undergoing hindered rotation. The assumption was made that the rigid group rotates about a fixed axis with a sinusoidal hindering potential. The method was used by Prewitt¹⁸ in 1965 when he treated the cyclopentadienyl rings in $[\text{C}_5\text{H}_5\text{FeS}]_4$ as hindered rotors. He assumed that each cyclopentadienyl ring formed a regular, planar pentagon with D_{5h} symmetry and that the motion of the atoms is predominantly in the plane of the ring. The other motions of the group were described by a single isotropic temperature factor B , this being a modification of the original King and Lipscomb model. This model was refined by means of two matrices in a block diagonal refinement; one 4×4 matrix for x, y, z and B , and a 2×2 matrix for the radius of the ring, and the relative barrier. Use of this model gave cyclopentadienyl C-C bond lengths in good agreement with the average C-C bond

length obtained when corrections for thermal motion had been made for the individual atom models. It also required far fewer parameters to describe the system although this resulted in a higher R factor; 6.9% for the hindered rotor as compared to 5.8% for the individual atom. Also, the hindered rotor model had the advantage that it placed the electron density on the arc of a circle giving a curved distribution rather than attempting to describe the distribution in a rectilinear manner as in the conventional isotropic and anisotropic models. However, there were disadvantages. The particular blocking of the least squares matrix was unfortunate in that the correlation between the two parameters associated with a description of the thermal motion was ignored. This caused severe overshifting and necessitated the introduction of damping factors. Because the ring orientations were well defined from the previous individual atom refinement, these were not refined and the programme was developed with a limited scope. However, the utility of the model had been demonstrated for a routine organometallic structure.

In order to refine n parameters by means of full matrix least squares refinement, a symmetrical matrix containing $(n/2)(n+1)$ unique elements is required. Both the computing time required and the storage demands for

a least squares cycle are proportional² to $(n/2)(n+1)$. Thus, any decrease in the number of parameters to be refined will result in a proportionately greater decrease in time and storage requirements and in the computing cost. It was therefore deemed more economical to develop a programme that allowed the ring orientations to be refined rather than to obtain these parameters from a complete individual atom refinement.

In the following work, the rigid body expressions available in the rigid body modification of the basic full matrix least squares programme SFLS5 by C.T. Prewitt (1966) were used in conjunction with Lipscomb and King's¹⁷ hindered rotor expressions. SFLS5 was then further modified to calculate the contribution to the structure factors by a group undergoing hindered rotation and to do a full matrix least squares refinement on the input parameters.

THEORETICAL

Notation

g_i	complex scattering power of the i^{th} atom
\bar{g}	average complex scattering power of atoms in a ring
$P(\theta')$	probability function of the ring at an angle θ'
\underline{h}	reciprocal lattice vector corresponding to the Miller indices h, k, l
\underline{r}	instantaneous position vector of the atom which may be resolved into two components:
\underline{k}	vector from the real lattice origin to the centre of rotation, and
\underline{v}	vector from the centre of rotation to the instantaneous position of the atom
V_0	potential barrier to rotation
V	potential at rotation angle θ'
n	number of minima in the potential
θ'	instantaneous rotation angle measured from the x axis of the internal Cartesian co-ordinate system in the rigid body

$x_{c_i}, y_{c_i}, z_{c_i}$

fractional co-ordinates of the
centre of gravity of the i^{th} rigid
body

ξ

rotation angle at which the potential
is a minimum

D, E

angles (in radians) defining the
orientation of the plane of the
ring. The direction cosines (with
respect to the chosen internal
Cartesian co-ordinate system) of
the plane are:

$$m_1 = \cos D \sin E$$

$$m_2 = -\sin D$$

and $m_3 = \cos D \cos E$

R

radius of the rigid body in \AA

$\left. \begin{array}{l} X(i) \\ Y(i) \\ Z(i) \end{array} \right\}$

Cartesian co-ordinates in \AA of i^{th} atom

[L]

transformation matrix from the internal
co-ordinate system of the rigid body
to conventional crystallographic
co-ordinates

q_1 to q_6

non-zero elements of the matrix [L]

$$q_1 = 1./(\alpha \sin \beta \sin \gamma^*)$$

$$q_2 = \cot \gamma^* / \beta \sin \alpha$$

$$q_3 = -\frac{1}{c} \left[\cos\alpha \cos\gamma^* - \frac{\cot\beta}{\sin\gamma^*} \right]$$

$$q_4 = 1./(b \sin\alpha)$$

$$q_5 = -c \cot\alpha$$

$$q_6 = 1./c$$

gP_i	population factor of the i^{th} ring
B_i	Debye temperature factor for the i^{th} ring
θ	conventional Bragg angle
λ	wavelength of X-radiation used
f_i	form factor for atoms of the i^{th} ring
T	absolute temperature
k	Boltzman's constant
i	imaginary number = $\sqrt{-1}$
Bd	relative barrier $Bd = V_o/2kT$

The rigid body expression of M.J. Bennett and B.M. Foxman assumes a rigid ring system based on a regular planar polygon of order n possessing D_{nh} symmetry. A right handed Cartesian co-ordinate system is defined such that the origin lies at the centre of the polygon, with the x and z axes being parallel to the a^* and c axes. If the ring lies in the XY plane, then the co-ordinates

of the first atom can be defined as $(R, 0, 0)$. The position of the i^{th} atom is then

$$\begin{aligned} X(i) &= R \cos 2\pi(i-1)/n \\ Y(i) &= R \sin 2\pi(i-1)/n \end{aligned} \quad [4]$$

$$\text{and } Z(i) = 0$$

with respect to the Cartesian co-ordinate system. The direction cosine of the ring normal in its standard orientation is $(0, 0, 1)$. Rotating this polygon about the z axis, the i^{th} vertex becomes

$$\begin{aligned} X(i) &= R \cos(\xi + 2\pi(i-1)/n) \\ Y(i) &= R \sin(\xi + 2\pi(i-1)/n) \\ Z(i) &= 0 \end{aligned} \quad [5]$$

The direction cosines of the plane are still $(0, 0, 1)$. If this is followed by a rotation of D radians about the x axis and E radians about the y axis, the direction cosines of the plane become $(\cos D \sin E, -\sin D, \cos D \cos E)$. The co-ordinates of the i^{th} atom are then

$$\begin{aligned} X(i) &= R[\cos(\xi + 2\pi(i-1)/n) \cos E \\ &\quad + \sin(\xi + 2\pi(i-1)/n) \sin D \sin E] \\ Y(i) &= R[\sin(\xi + 2\pi(i-1)/n) \cos D] \\ Z(i) &= R[-\cos(\xi + 2\pi(i-1)/n) \sin E \\ &\quad + \sin(\xi + 2\pi(i-1)/n) \cos E \sin D] \end{aligned} \quad [6]$$

Transformation to crystallographic co-ordinates using

matrix [L] plus translational correction gives the fractional co-ordinates of the i^{th} atom as

$$\begin{aligned}
 x(i) &= q_1 R[\cos(\xi + 2\pi(i-1)/n) \cos E \\
 &\quad + \sin(\xi + 2\pi(i-1)/n) \sin D \sin E] + x_c \\
 y(i) &= q_2 R[\cos(\xi + 2\pi(i-1)/n) \cos E \\
 &\quad + \sin(\xi + 2\pi(i-1)/n) \sin D \sin E] \\
 &\quad + q_4 R[\sin(\xi + 2\pi(i-1)/n) \cos D] + y_c \\
 \text{and } z(i) &= q_3 R[\cos(\xi + 2\pi(i-1)/n) \cos E \\
 &\quad + \sin(\xi + 2\pi(i-1)/n) \sin D \sin E] \\
 &\quad + q_5 R[\sin(\xi + 2\pi(i-1)/n) \cos D] \\
 &\quad + q_6 R[-\cos(\xi + 2\pi(i-1)/n) \sin E \\
 &\quad + \sin(\xi + 2\pi(i-1)/n) \cos E \sin D] + z_c
 \end{aligned} \tag{7}$$

where q_i are the elements of the transformation matrix [L]. Replacing the fixed angle ξ by the continuous variable θ' , the dot product, $2\pi \underline{h} \cdot \underline{v}$, used in later expressions, becomes

$$2\pi \underline{h} \cdot \underline{v} = e \cos \theta' + d \sin \theta' \tag{8}$$

where

$$e = 2\pi R[(h q_1 + k q_2 + l q_3) \cos E - l q_6 \sin E] \tag{9}$$

$$\begin{aligned}
 \text{and } d &= 2\pi R[(h q_1 + k q_2 + l q_3) \sin D \sin E \\
 &\quad + (k q_4 + l q_5) \cos D + l q_6 \cos E \sin D].
 \end{aligned}$$

If a' is defined as $a' = \sqrt{c^2 + d^2}$ [10]

and $\eta = \text{arc cose}/a'$
 $= \text{arc sin } d/a'$ [11]

then the dot product $2\pi \underline{h} \cdot \underline{v}$ becomes

$$2\pi \underline{h} \cdot \underline{v} = a' \cos(\theta' - \eta). \quad [12]$$

These rigid body expressions can now be used in calculating the contribution of groups in hindered rotation to the structure factor. The derivation parallels that of Lipscomb and King¹⁷.

The contribution of the hindered rotor groups to the structure factor can be expressed as

$$F_{hkl} = \sum_i g_i \quad [13]$$

the summation being over all atoms in the unit cell which are members of a group undergoing hindered rotation. The instantaneous complex scattering power of an atom in a ring is given by

$$g_i = f_i \exp[2\pi i \underline{h} \cdot \underline{r}] \quad [14]$$

$$= f_i \exp[2\pi i \underline{h} \cdot \underline{k}] \exp[2\pi i \underline{h} \cdot \underline{v}].$$

If the probability distribution is given by $P(\theta')$, then

$$\bar{g} = f_i \exp[2\pi i \underline{h} \cdot \underline{k}] \cdot$$

$$\int_0^{2\pi} P(\theta') \exp[2\pi i \underline{h} \cdot \underline{v}] d\theta'. \quad [15]$$

Using a potential function

$$V = -\frac{1}{2} V_0 \cos n(\theta' - \xi) \quad [16]$$

and assuming a Maxwell-Boltzman distribution for the probability function, $P(\theta')$, then

$$P(\theta') = \frac{\exp[V_0 \cos n(\theta' - \xi)/2kT]}{\int_0^{2\pi} \exp[V_0 \cos n(\theta' - \xi)/2kT] d\theta'} \quad [17]$$

Substituting this expression for $P(\theta')$ into equation [15] and using the dot product expression of [12], one obtains

$$\bar{g} = f_i \exp[2\pi i \underline{h} \cdot \underline{k}] \quad [18]$$

$$\frac{\int_0^{2\pi} \exp[Bd \cos n(\theta' - \xi) + ia' \cos(\theta' - \eta)] d\theta'}{\int_0^{2\pi} \exp[Bd \cos n(\theta' - \xi)] d\theta'}$$

where $Bd = V_0/2kT$.

Defining $M_n^\xi(a', Bd) =$

$$\frac{\int_0^{2\pi} \exp[Bd \cos n(\theta' - \xi) + ia' \cos(\theta' - \xi)] d\theta'}{\int_0^{2\pi} \exp[Bd \cos n(\theta' - \xi)] d\theta'} \quad [19]$$

then \bar{g} becomes

$$\bar{g} = f_i \exp[2\pi i \underline{h} \cdot \underline{k}] M_n^\xi(a', Bd). \quad [20]$$

$M_n^\xi(a', Bd)$ can be expanded into an infinite series.

Watson²⁰ gives the following expression:

$$\begin{aligned} \exp[s \cos \tau] &= I_0(s) + 2 \sum_{m=1}^{\infty} I_m(s) \cos m\tau \\ &= \sum_{m=0}^{\infty} \epsilon_m I_m(s) \cos m\tau \end{aligned} \quad [21]$$

where $\epsilon_m = 1$ when $m = 0$, and $\epsilon_m = 2$ when $m \neq 0$. $J_m(s)$ is a Bessel function of order m and $I_m(s)$ is a hyperbolic Bessel function of order m . Using these expressions, the numerator of $M_n^E(a', Bd)$ becomes

$$\begin{aligned} &\int_0^{2\pi} \left[\sum_p \epsilon_p I_p(Bd) \cos p(n\theta' - \xi) \right] \left[\sum_m \epsilon_m I_m(ia') \cos m(\theta' - \xi)\theta' \right] \\ &= \sum_p \sum_m \epsilon_p \epsilon_m I_p(Bd) I_m(ia') \int_0^{2\pi} \cos p(n\theta' - \xi) \cos (\theta' - \eta) d\theta'. \end{aligned} \quad [22]$$

By expanding the cosine term the numerator can be written as

$$\begin{aligned} &\sum_p \sum_m \epsilon_p \epsilon_m I_p(Bd) I_m(ia') \cdot \\ &\int_0^{2\pi} (\cos pn\theta' \cos p\xi \cos m\theta' \cos m\eta \\ &+ \sin pn\theta' \sin p\xi \cos m\theta' \cos m\eta \\ &+ \cos pn\theta' \cos p\xi \sin m\theta' \sin m\eta \\ &+ \sin pn\theta' \sin p\xi \sin m\theta' \sin m\eta) d\theta'. \end{aligned} \quad [23]$$

Making use of (1) summation of integral equalling the integral of summation, and (2) the orthogonality of sines and cosines, this expression simplifies to:

$$2\pi \sum_p \epsilon_p I_p(Bd) I_{pn}(ia') (\cos p\xi \cos pn\eta + \sin p\xi \sin pn\eta). \quad [24]$$

Using the relationship

$$J_m(-is) = (-i)^m I_m(s) \quad [25]$$

given by Watson²⁰ the numerator becomes

$$2\pi \sum_p \epsilon_p i^{pn} I_p(Bd) J_{pn}(a') \cos(pn(\xi - \eta)) \quad [26]$$

and by the same method the denominator is $2\pi I_0(Bd)$.

$M_n^\xi(a', Bd)$ then becomes

$$\frac{\sum_p \epsilon_p i^{pn} I_p(Bd) J_{pn}(a') \cos(pn(\xi - \eta))}{I_0(Bd)}. \quad [27]$$

Using this expression, the contribution to the structure factor from the hindered rotors can be written as

$$F_{hk\ell} = \sum_i f_i g_i \exp[-B_i \frac{\sin^2 \theta}{\lambda^2}] \exp[2\pi i \underline{h} \cdot \underline{k}] M_{n_i}^{\xi_i}(a_i', Bd_i) \quad [28]$$

the summation being over all the rings undergoing hindered rotation.

Programming

The programme SFLS5 was modified to calculate the contribution of a hindered rotor to the structure factor. These modifications were mainly in the addition of two new subroutines ROTOR and BESSEL, as well as modifications to the input and output. It can be seen that there are two

possible routes by which to calculate the M function:

- (1) by means of the integral expression, equation [19], or
- (2) by use of the infinite series summation form (Bessel functions), equation [27].

The first of these, the integral form, can be calculated by means of Weddel's Rule¹⁹. If one divides the range of integration into 7 intervals, then

$$\int_{x_0}^{x_0+6h} \phi(x) dx = \frac{3h}{10} [y_0 + 5y_1 + y_2 + 6y_3 + y_4 + 5y_5 + y_6] \quad [29]$$

This can be expanded for use with $(6n+1)$ intervals, where n is an integer. An integral of the form $\int_a^b e^{f(x)} g(x) dx$ can be expanded into a series of integrals where $f(x)$ and $g(x)$ are two functions of x .

$$\begin{aligned} \int_a^b e^{f(x)} g(x) dx &= \int_a^b [1 + f(x) + \frac{f^2}{2!}(x) + \dots] g(x) dx \\ &= \int_a^b g(x) dx + \int_a^b f(x) g(x) dx \quad [30] \\ &\quad + \frac{1}{2!} \int_a^b f^2(x) g(x) dx + \dots \end{aligned}$$

which hopefully are easier to integrate. Thus the $M_n^\xi(a', Bd)$ function can be broken up into a series of integrals which can be calculated by means of Weddel's Rule, or integrated analytically. However, it was found that even integrals

of the form $\frac{1}{2} \int g(x) f^2(x) dx$ became extremely complicated (Figure 1) and required a minimum of 67 intervals. Since this is an extremely slow method of calculation, it was used only as a check on the results of the infinite Bessel function series calculations.

The infinite series form of $M_n^\xi(a', Bd)$ is

$$M_n^\xi(a', Bd) = \sum_p \epsilon_p i^{pn} J_{pn}(a') \frac{I_p(Bd)}{I_0(Bd)} \cos(pn(\xi - \eta)) \quad [27]$$

$$\text{where } I_p(Bd) = \sum_m \frac{(Bd/2)^{2m+p}}{m!(m+p)!} \quad [31]$$

$$\text{and } J_{pn}(a') = \sum_m \frac{(-1)^m (a'/2)^{2m+pn}}{m!(m+pn)!} \quad [32]$$

$J_{pn}(a')$ being a Bessel summation²⁰ and $I_p(Bd)$ a hyperbolic Bessel summation. It can be seen that whether any term in the summation is real or imaginary depends completely on the value of i^{pn} ; all other functions are real. Thus, if n , the order of the ring, is even, pn is always even and i^{pn} is ± 1 ; $M_n^\xi(a', Bd)$ is then a real summation. If n is odd, then pn alternates even and odd as p increases causing i^{pn} to alternate among ± 1 and $\pm i$. $M_n^\xi(a', Bd)$ is a complex function which can be broken up into real and imaginary contributions:

Figure 1

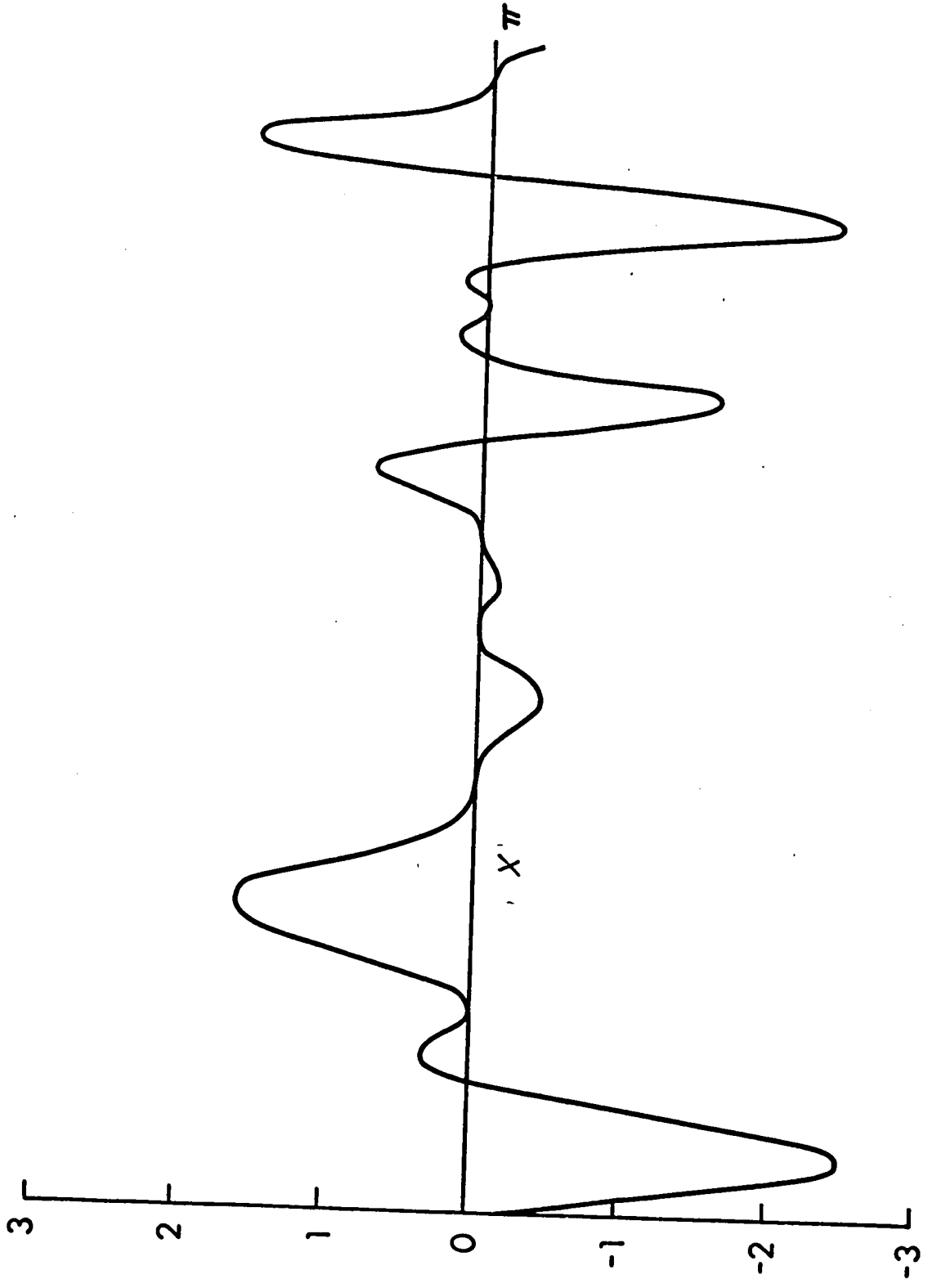
$$\frac{1}{2} g(x) f^2(x) \text{ versus } x$$

$$\text{where } g(x) = \cos[a' \cos(x-\eta)]$$

$$f(x) = B \cos n(x-\xi)$$

The following values were used:

$h = 1$	$k = 2$	$l = 1$
$\xi = 0.23$	$D = 0.60$ radians	
$n = 5$	$E = 0.028$ radians	
$Bd = 2.5$	$R = 1.20 \text{\AA}$	
$q_1 = 0.10$	$q_2 = 0.20$	$q_3 = 0.10$
$q_4 = 0.10$	$q_5 = 0.27$	$q_6 = 0.10$



$$f_2(x)g(x)$$

$$\begin{aligned}
 M_n^\xi(a', Bd) &= M_R + iM_I \\
 &= \sum_{p \text{ even}} (-1)^{pn/2} \epsilon_p J_{pn}(a') \frac{I_p(Bd)}{I_0(Bd)} \cos pn(\xi-\eta) \quad [33] \\
 &\quad + i \sum_{p \text{ odd}} (-1)^{\frac{pn-1}{2}} \epsilon_p J_{pn}(a') I_p(Bd) \cos pn(\xi-\eta).
 \end{aligned}$$

$F_{hk\ell}$ is complex and can also be broken down into real and imaginary terms, generally called $A_{hk\ell}$ and $B_{hk\ell}$.

$$\begin{aligned}
 &= \sum_i f_i \exp(2\pi i \underline{h} \cdot \underline{k}) M_n^\xi(a', Bd) \\
 &= \sum_i f_i (\cos 2\pi \underline{h} \cdot \underline{k} + i \sin 2\pi \underline{h} \cdot \underline{k}) (M_R + iM_I) \quad [34]
 \end{aligned}$$

$$\therefore A_{hk\ell} = \sum_i f_i (M_R \cos 2\pi \underline{h} \cdot \underline{k} - M_I \sin 2\pi \underline{h} \cdot \underline{k}) \quad [35]$$

$$\text{and } B_{hk\ell} = \sum_i f_i (M_I \cos 2\pi \underline{h} \cdot \underline{k} + M_R \sin 2\pi \underline{h} \cdot \underline{k}) \quad [36]$$

Thus for n odd it is necessary to calculate both M_R and M_I as well as the sin and cos terms even for the centrosymmetric case. For the special case of even membered rings in a centrosymmetric space group then

$$A_{hk\ell} = \sum_i f_i M_R \cos 2\pi \underline{h} \cdot \underline{k} \quad [37]$$

In a centric space group with no anomalous dispersion $B_{hk\ell} = 0$. This property was used as a further check on the calculation of M_R and M_I since

$$M_I \cos 2\pi \underline{h} \cdot \underline{k} = -M_R \sin 2\pi \underline{h} \cdot \underline{k} . \quad [38]$$

In order to do a least squares refinement, it is necessary to calculate the derivatives of the $M_n^\xi(a', Bd)$ function. The ring is described by means of ten parameters, and analytical expressions for the derivatives of $F_{hk\ell}$ with respect to each parameter were obtained. Those of the population factor gp , the co-ordinates of the centre of gravity x_c, y_c, z_c and the overall temperature parameter, B , were straightforward, since they are not involved in the calculation of the M function.

Since

$$F_{hk\ell} = \sum gp_i f_i \exp\left[\frac{-B_i \sin^2 \theta}{\lambda^2}\right] \exp[2\pi i \underline{h} \cdot \underline{k}] M_n^\xi(a', Bd) \quad [28]$$

then the derivative with respect to the population factor becomes

$$\frac{\partial F}{\partial (gp)_i} = f_i \exp\left[\frac{-B_i \sin^2 \theta}{\lambda^2}\right] \exp[2\pi i \underline{h} \cdot \underline{k}] M_n^\xi(a', Bd). \quad [39]$$

Using the expansion of $\underline{h} \cdot \underline{k}$ to $(hx_{c_i} + ky_{c_i} + z_{c_i})$ and taking the derivative of F with respect to x_{c_i}

$$\begin{aligned} \frac{\partial F}{\partial x_{c_i}} &= gp_i f_i \exp\left[\frac{-B_i \sin^2 \theta}{\lambda^2}\right] (2\pi i h) \\ &\quad \exp[2\pi i \underline{h} \cdot \underline{k}] M_n^\xi(a', Bd). \end{aligned} \quad [40]$$

Analogous expressions can be written for $\frac{\partial F}{\partial y_{c_i}}$ and $\frac{\partial F}{\partial z_{c_i}}$

where $2\pi i h$ is replaced by $2\pi i k$ and $2\pi i \ell$ respectively. Differentiation with respect to the overall temperature factor gives

$$\frac{\partial F}{\partial B} = - \frac{\sin^2 \theta}{\lambda^2} \exp \left[\frac{B_i \sin^2}{\lambda^2} \right] f_i \exp[2\pi i \underline{h} \cdot \underline{k}] M_n^\xi(a', Bd). \quad [41]$$

The remaining five parameters are used in the calculation of $M_n^\xi(a', Bd)$ and the analytical expressions for their derivatives are somewhat more complicated.

The relative barrier, Bd , is found only in the terms $I_o(Bd)$ and $I_p(Bd)$. The derivative of $M_n^\xi(a', Bd)$ with respect to Bd is given by

$$\begin{aligned} \frac{\partial M_n^\xi(a', Bd)}{\partial Bd} &= \frac{1}{I_o^2(Bd)} [I_o^2(Bd) \sum_p i^{pn} J_{pn}(a') \cdot \\ &\quad \cos pn(\xi - \eta) \frac{\partial I_p(Bd)}{\partial Bd} \\ &\quad - \frac{\partial I_o(Bd)}{\partial Bd} \sum_p \epsilon_p i^{pn} J_{pn}(a') \cdot \\ &\quad I_p(Bd) \cos pn(\xi - \eta)]. \end{aligned} \quad [42]$$

Since

$$I_p(Bd) = \sum_m \frac{(Bd/2)^{2m+p}}{m!(m+p)!} \quad [31]$$

then

$$\frac{\partial I_p(Bd)}{\partial Bd} = \sum_m \frac{2m+p}{Bd} \frac{(Bd/2)^{2m+p}}{m!(m+p)!} \quad [43]$$

That is, each term in this summation is $\frac{2m+p}{Bd}$ times the original Bessel term. An exactly similar expression occurs for

$$\frac{\partial I_0(Bd)}{\partial Bd} = \sum_m \frac{2m}{Bd} \frac{(Bd/2)^{2m}}{(m!)^2} \quad [44]$$

It was for the calculation of such modified Bessel terms that the subroutine BESSEL was written rather than using the computer library function.

In the expression for $M_n^\xi(a', Bd)$, only the term $J_{pn}(a')$ is a function of the radius, R.

$$\frac{\partial M_n(a', Bd)}{\partial R} = \sum_p i^{pn} \epsilon_p \frac{I_p(Bd)}{I_0(Bd)} \cos n(\xi - \eta) \frac{\partial J_{pn}(a')}{\partial R} \quad [45]$$

Since

$$J_{pn}(a') = \sum_m \frac{(-1)^m (a'/2)^{2m+pn}}{m! (m+pn)!} \quad [32]$$

then

$$\begin{aligned} \frac{\partial J_{pn}(a')}{\partial R} &= \sum_m \frac{(-1)^m (a'/2)^{2m+pn-1}}{m! (m+pn)!} \frac{\partial (a')}{\partial R} (2m+pn) \\ &= \sum_m \frac{(-1)^m (a''/2)^{2m+p} (2m+pn)}{m! (m+pn)!} \end{aligned} \quad [46]$$

where $a'' = a'/R$.

As in the case of $\frac{\partial M_n^\xi(a', Bd)}{\partial Bd}$, this is a modified Bessel summation.

The derivative $\frac{\partial M_n^\xi(a', Bd)}{\partial \xi}$ is simply

$$\sum_p -pn i^{pn} \epsilon_p J_{pn}(a') \frac{I_p(Bd)}{I_0(Bd)} \sin(pn(\xi-\eta)). \quad [47]$$

The most complex expressions for the derivatives of F_{hkl} arises from those with respect to the orientation angles D and E. In each term of the $M_n^\xi(a', Bd)$ summation $J_{pn}(a')$ and $\cos(pn(\xi-\eta))$ are functions of both D and E. Dealing first with the derivative with respect to D

$$\begin{aligned} \frac{\partial M_n^\xi(a', Bd)}{\partial D} = & \sum_p i^{pn} \frac{I_p(Bd)}{I_0(Bd)} \left[J_{pn}(a') \sin pn(\xi-\eta) \frac{\partial \eta}{\partial D} \right. \\ & + \cos pn(\xi-\eta) \sum_m \frac{(-1)^m (a'/2)^{2m+pn}}{m! (m+pn)!} \cdot \\ & \left. \frac{2m+pn}{a'} \cdot \frac{\partial a'}{\partial D} \right]. \end{aligned} \quad [48]$$

where $\frac{\partial a'}{\partial D} = \frac{d}{a'} \cdot \frac{\partial d}{\partial D}$

$$\frac{\partial \eta}{\partial D} = - \frac{c}{a' \sqrt{a'^2 - c^2}} \frac{\partial a'}{\partial D} \quad [49]$$

$$\text{and } \frac{\partial d}{\partial D} = 2\pi R \{ (h q_1 + k q_2 + l q_3) \cos D \sin E \\ - (k q_4 + l q_5) \sin D + l q_6 \cos D \cos E \} .$$

The expressions for d, a' and η are given in equations [9], [10] and [11] respectively.

The derivatives of the $M_n^{\xi}(a', Bd)$ function with respect to E are calculated in a similar manner with the result:

$$\frac{\partial M_n(a', Bd)}{\partial E} = \sum_p i^{pn} \frac{I_p(Bd)}{I_0(Bd)} \left[pn J_{pn}(a') \sin pn(\xi - \eta) \frac{\partial \eta}{\partial E} \right. \\ \left. + \cos pn(\xi - \eta) \sum_m \frac{(-1)^m (a'/2)^{2m+pn}}{m!(m+pn)!} \cdot \frac{2m+pn}{a'} \cdot \frac{\partial a'}{\partial E} \right] \quad [50]$$

$$\text{where } \frac{\partial a'}{\partial E} = -2 R \{ (h q_1 + k q_2 + l q_3) \sin E + l q_6 \cos E \}$$

$$\frac{\partial d}{\partial E} = 2\pi R \{ (h q_1 + k q_2 + l q_3) \sin E \cos E \\ - l q_6 \sin D \sin E \} \quad [51]$$

$$\text{and } \frac{\partial \eta}{\partial E} = \frac{d}{(a')^2} \cdot \frac{1}{\sqrt{1 - (d/a')^2}} \frac{\partial a'}{\partial E}$$

The derivatives of the F_{hkl} with respect to the last five parameters can be calculated from the derivatives of M by application of the chain rule to equation [28].

Once written, this programme was tested by several different methods. The M function itself was calculated by two different methods:

- (1) the infinite series, the test for convergence being that the final term was less than 0.01% of the summation, and
- (2) the integral method using Weddel's Rule¹⁹.

The results were also compared with those given by Lipscomb and King¹⁷ and agreed to within the four figures given.

The calculations of derivatives were also checked by several methods:

- (1) by calculating $\frac{\partial M}{\partial \phi}$ analytically from the infinite series form of M, ϕ being one of the variables D, E, ξ , R, or Bd,
- (2) by calculating M at various values of ϕ , plotting the results and obtaining the slope, and
- (3) by means of the numerical analysis technique of forward differences²¹.

Once these tests indicated that the programming was correct, the hindered rotor calculations were tested on several rings found in published crystal structures. These were (1)

benzene¹², ruthenocene²², (3) dicarbonyl- π -cyclohepta-
trienyl- σ -pentafluorophenyl molybdenum²³, (4) cyclo-
pentadienyl manganese tricarbonyl²⁴, and (5) benzene-
chromium tricarbonyl²⁵.

Diagrams of these molecules produced using the
published parameters of the individual atom refinements
are shown in Figures 2 to 6. With the exception of
ruthenocene, the drawings show each molecule projected
onto the plane of the ring. The diagrams were all
produced by C.K. Johnson's ORTEP programme and give
qualitative indications of librations about the ring axes.

Figure 2

The structure of ruthenocene
G.L. Hardgrove and D.H. Templeton
Acta Cryst., 12, 28 (1959)

Figure 3

The structure of benzene
E.G. Cox, D.W.J. Cruickshank and J.A.S. Smith
Proc. Roy. Soc., A247, 1 (1958)

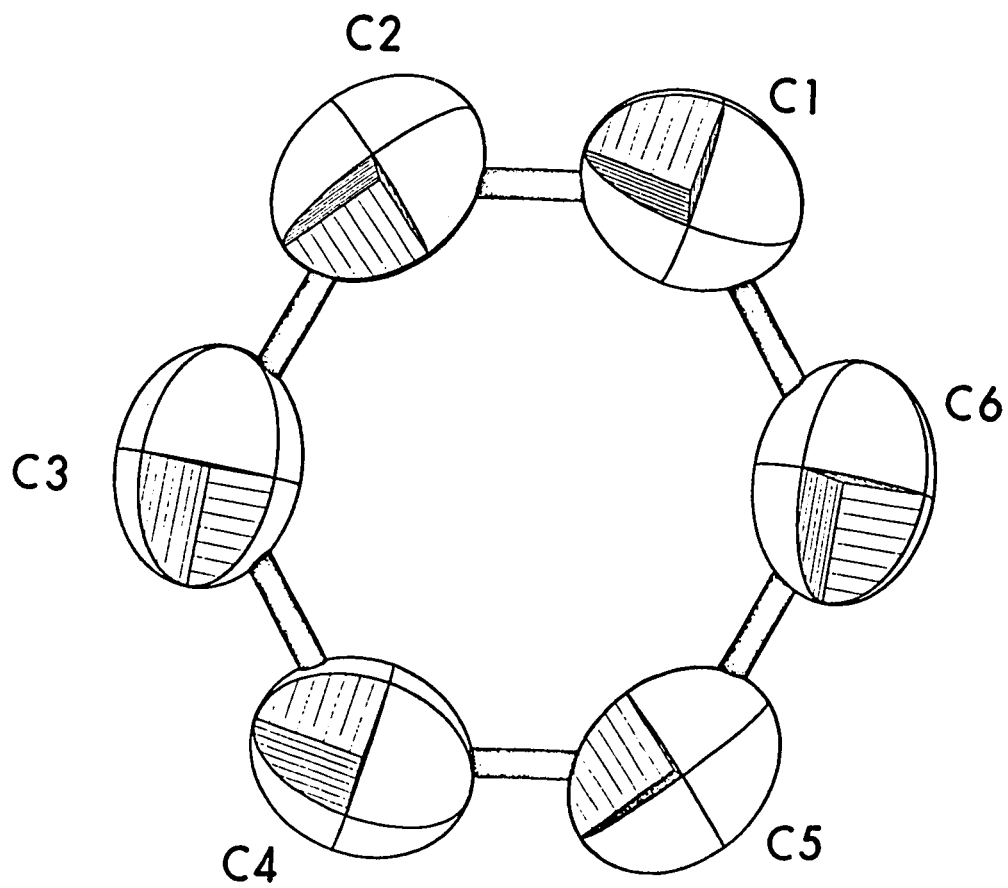
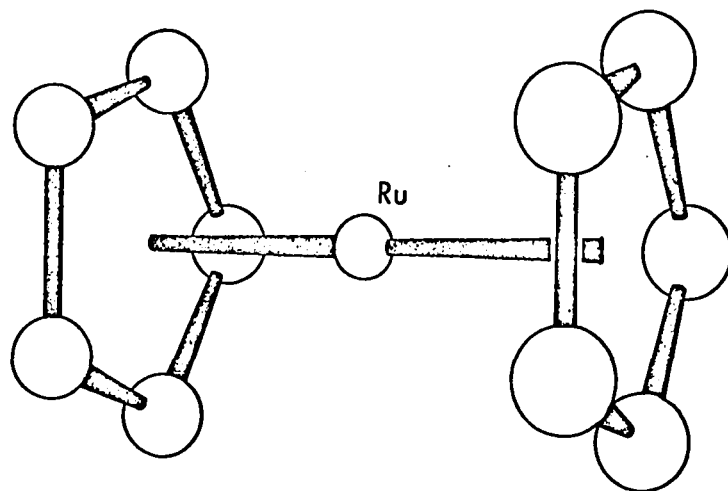


Figure 4

The structure of cyclopentadienyl manganese tricarbonyl

A.F. Berndt and R.E. Marsh

Acta Cryst., 16, 118 (1963)

Figure 5

The structure of benzenechromium tricarbonyl

M.F. Bailey and L.F. Dahl

Inorg. Chem., 4, 1314 (1965)

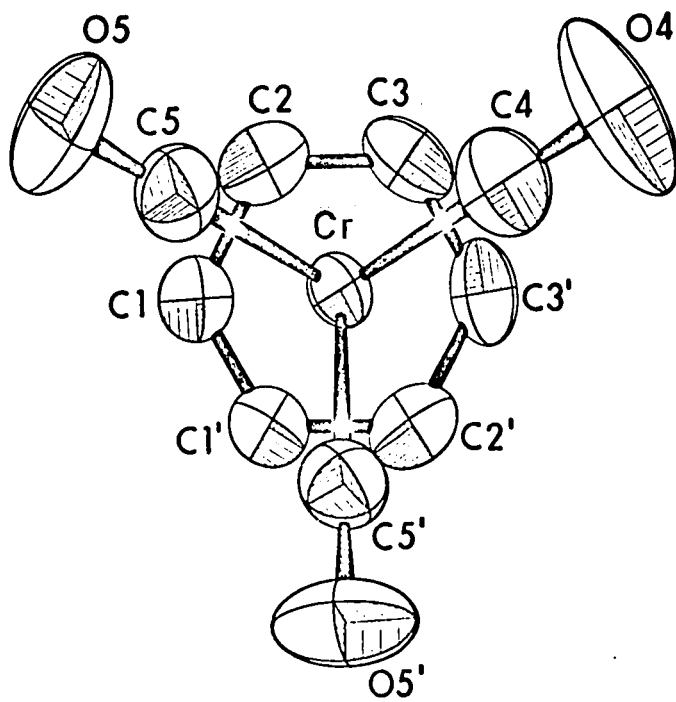
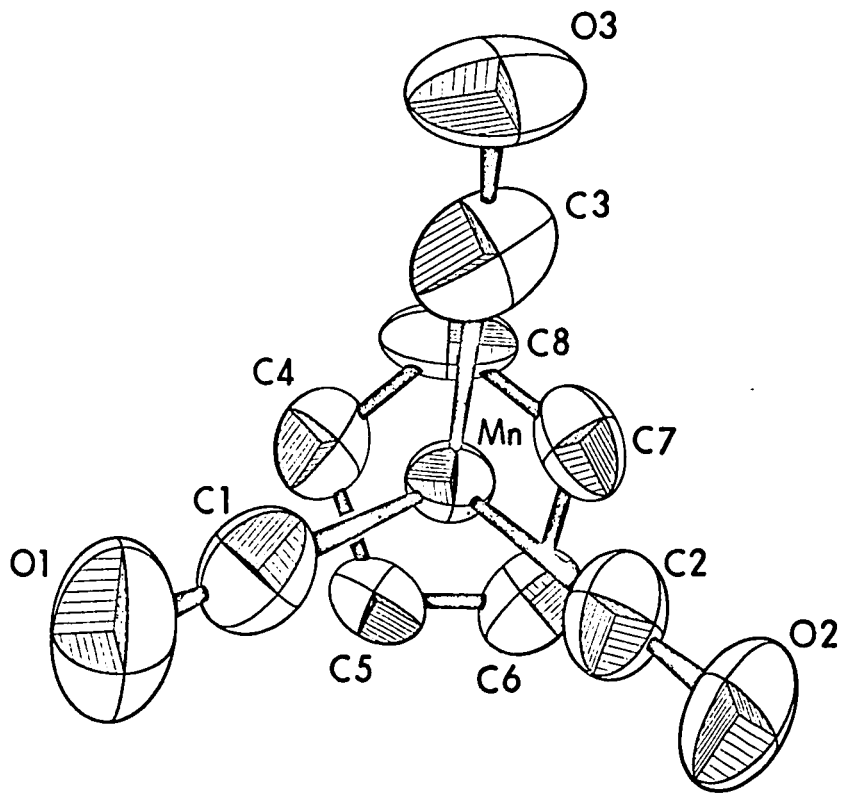
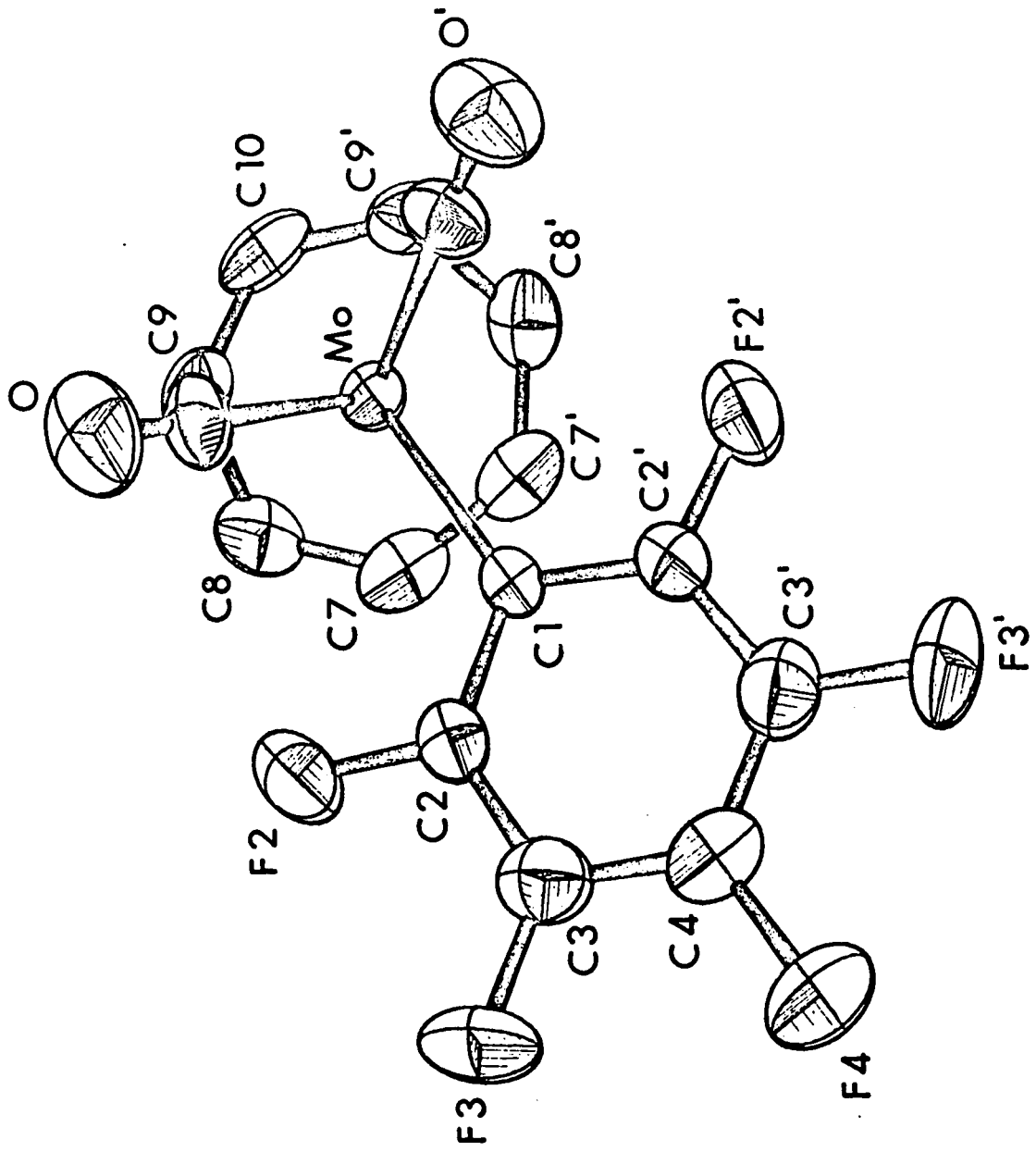


Figure 6

The structure of
dicarbonyl- π -cycloheptatrienyl- σ -pentafluoro-
phenyl molybdenum

M.R. Churchill and T.A. O'Brien

J. Chem. Soc. (A), 1110, (1969)



Results

The refined parameters for the hindered rotor calculations are given in Table I. Parameters for other atoms of the structure did not change significantly from the individual atom refinement values and are not listed. In each case the results of the individual atom refinement given in the published paper were used to obtain the input to the hindered rotor calculation. The centre of gravity and the orientation angles D , E and ξ were obtained from the programme MMR (M.J. Bennett and B.M. Foxman, 1967) which uses the positions of the atoms in the ring as input. The radius was calculated from the average distance between the centre of gravity and the atom positions. The barrier, B_d , was calculated from NMR results where available (benzene²⁷ and ruthenocene²⁸); otherwise set at $B_d = 2$. The isotropic temperature parameter for the ring, B , was set to be slightly greater than that of the metal to which it was attached. In all cases, the hydrogen atoms were placed 1.0\AA from the carbon atoms. The results are discussed under the headings of (1) refined radius, (2) relative barrier, (3) temperature factor of the ring, (4) the R factor, and (5) time and storage requirements.

Table I
Refined parameters of hindered rotor groups

	$\pi C_5H_5Mn(CO)_3$	benzene	$\pi C_6H_6Cr(CO)_3$	Ruthenocene		$\pi C_7H_7Mo(CO)_3$ $\sigma-C_6F_5$
				1	2	
x	0.3010(7)	0.0*	0.3785(6)	0.3632(18)	0.1060(9)	0.2024(7)
y	-0.1882(10)	0.0*	0.2500	0.2500*	0.2500*	0.2500*
z	0.1669(7)	0.0*	-0.2277(5)	0.6292(9)	0.3797(9)	0.1327(4)
B(\AA^2)	3.67(17)	4.64(11)	3.42(9)	2.14(30)	2.49(33)	3.13(13)
Bd	1.50(12)	1.94(11)	1.97(10)	4.9(20)	5.2(33)	1.94(14)
R(\AA)	1.211(6)	1.391(3)	1.415(3)	1.239(13)	1.235(14)	1.626(5)
D rad.	4.024(7)	6.053(3)	6.279*	0.0*	0.0*	3.142*
E radians	2.998(9)	0.821(3)	2.975(3)	0.510(13)	0.531(14)	0.949(4)
ξ	3.018(9)	1.741(3)	0.524*	0.0*	0.0*	0.449(1)
R(%)	8.9	10.1	4.5	8.7	8.7	5.7

* not refined - constrained symmetry element.

Standard deviations in parentheses refer to the last digit listed.

DISCUSSION

Radius

In the refinement of crystal structures by means of the thermal ellipsoid description, the origin of an ellipse tends to refine to the centre of gravity of the local electron density. For the case of an atom moving along a radial track, this centre will not be on the track. If the radial track is the arc AQB of Figure 7, then the centre of gravity would lie at point P. The radius of the ring would show an apparent shortening of the ring by an amount PQ. The ratio of the apparent radius to the true radius would be

$$\frac{\int_0^{\pi} P(\theta') \cos\theta' d\theta'}{\int_0^{\pi} P(\theta') d\theta'} \quad [52]$$

In this case a sinusoidal distribution has been used and $P(\theta')$ can be calculated at various θ' angles as a function of the relative barrier to rotation Bd and the order of the ring. The results are plotted in Figure 8.

For benzene, with a relative barrier from the hindered rotor refinement of 1.95, the ratio of the apparent radius to that of the correct radius would be 0.988. The radius

Figure 7

Radial track of rotation group

where r = radius of ring

OP = apparent radius

$P(\theta)$ probability distribution
along radial track

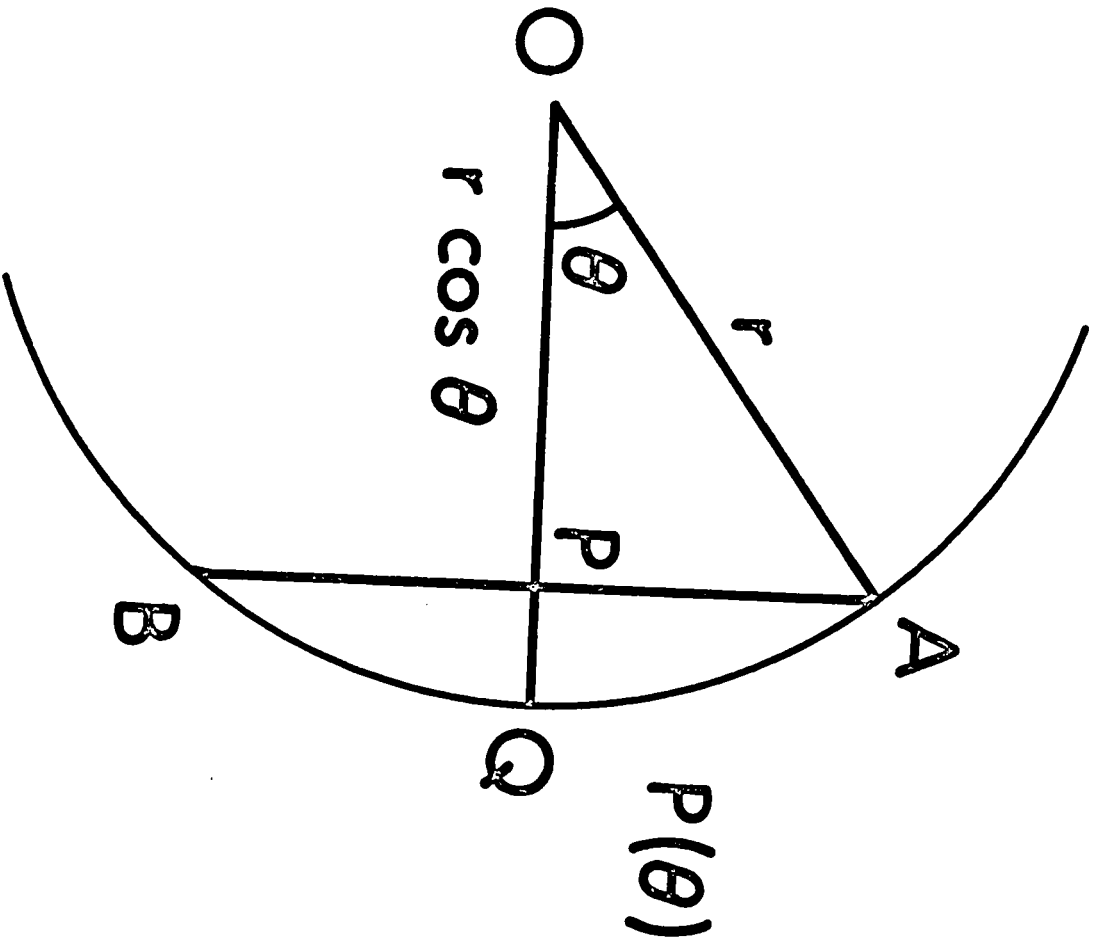
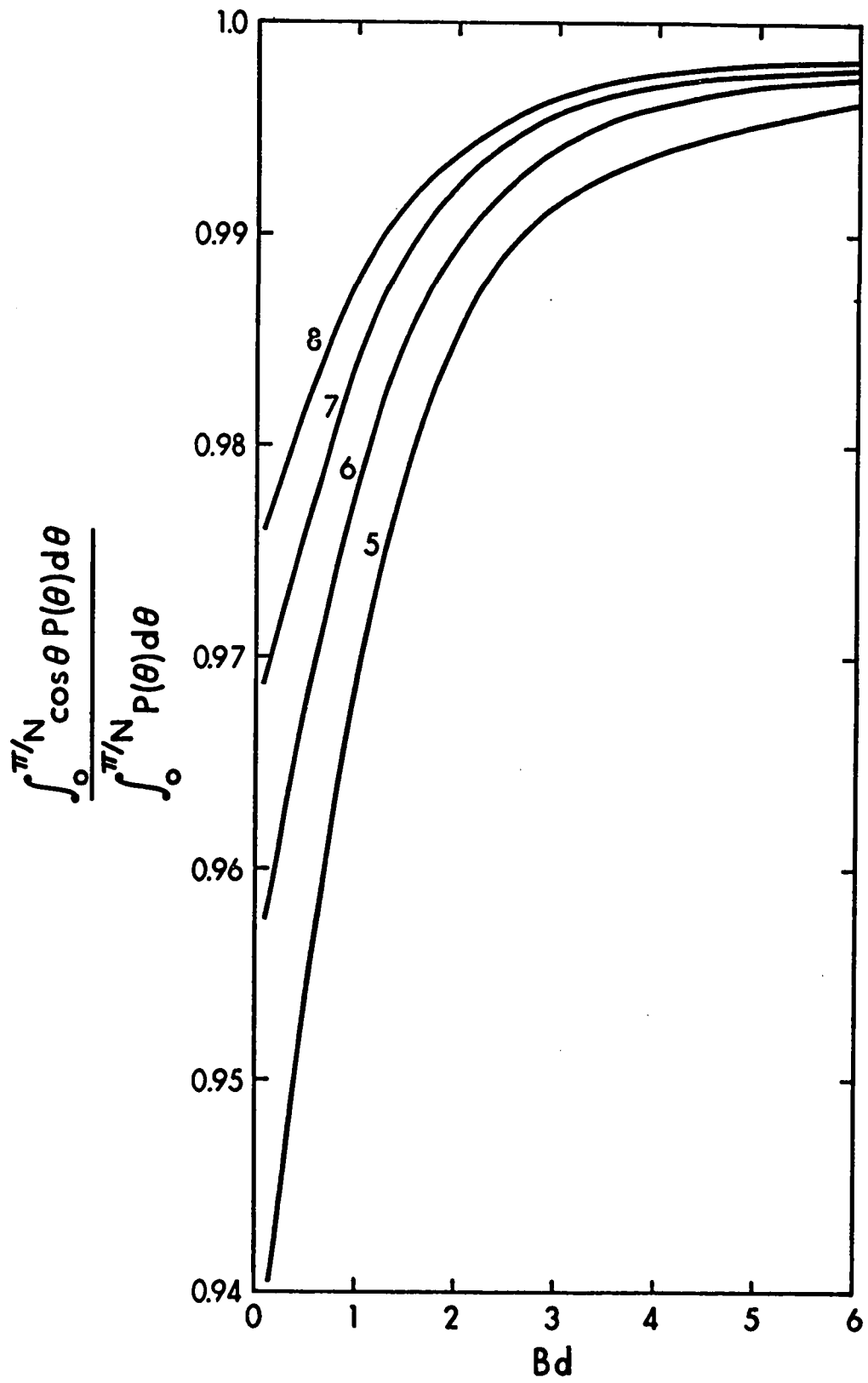


Figure 8

Apparent fractional radius due to the rotation of the ring as a function of the barrier Bd , for various values of n .

$$\text{Apparent fractional radius} = \frac{\int_0^{\pi/N} P(\theta) \cos\theta \, d\theta}{\int_0^{\pi/N} P(\theta) \, d\theta}$$



calculated by means of the hindered rotor method was 1.391\AA . Using this result and the ratio of 0.988, one would expect an uncorrected radius of 1.374\AA in the individual atom treatment. This is close to the result of 1.377\AA obtained by Cruickshank¹². The hindered rotor value of 1.391\AA is in good agreement with Cruickshank's corrected value of 1.392\AA and the Raman²⁹ value of 1.397\AA . Comparable agreement is found for the case of cyclopentadienyl manganese tricarbonyl. A relative barrier from the hindered rotor refinement of 1.50 gives a ratio of 0.978. Using the hindered rotor C-C distance of 1.424\AA and a ratio of 0.978 one would predict an uncorrected individual atom refinement C-C distance of 1.394\AA . Berndt and Marsh²⁴ in fact obtained an average C-C distance of 1.394\AA .

A similar pattern of C-C bond lengthening for the other structures can be seen in Table II. In each case, the C-C distance obtained from the hindered rotor refinement was multiplied by the appropriate ratio to obtain a predicted uncorrected individual C-C distance. As can be seen from Table II, these predicted values agree satisfactorily with the results actually obtained from the individual atom refinement. It would appear that the hindered rotor model correctly allows for the apparent bond shortening due to the motion of the ring, and makes the riding

Table II
Comparison of C-C bonds

	Individual atom model (Å)	Bd	Ratio from graph	Predicted uncorrected C-C bond Å	Hindered Rotor Result Å	Riding corrected result Å
benzene	1.37	1.95	0.988	1.374	1.391	1.392
$\pi C_5H_5Mn(CO)_3$	1.39	1.50	0.978	1.394	1.424	1.42
$Ru(C_5H_5)_2(1)$	1.446	4.5	0.994	1.442	1.451	-
$Ru(C_5H_5)_2(2)$	1.449	5.2	0.995	1.448	1.455	-
$\pi C_6H_5Cr(CO)_3$	1.401	1.97	0.989	1.393	1.408	-
$\pi C_7H_7Mo(CO)_2C_6F_5$	1.407	1.94	0.992	1.400	1.411	-

Table III
Comparison of RMS angular displacement values

Molecule	Barrier Bd	RMS (graph)	RMS (paper)	NMR barrier = $V_0/2kT$
benzene	1.95	8.5°	7.9°	1.8
$(\pi C_6H_6)Cr(CO)_3$	1.97	8.4°	-	-
$(\pi C_7H_7)Mo(CO)_2C_6H_5$	1.94	7.3°	-	-
$\pi C_5H_5Mn(CO)_3$	1.50	12.0°	12°	-
Ruthenocene (1)	4.5	5.8°	-	-
Ruthenocene (2)	5.2	5.4°	-	2.01

correction unnecessary, assuming only one dominant libration.

Barrier to Rotation

The potential function for the hindered rotor was

$$V = - \frac{1}{2} V_0 \cos n(\theta' - \xi) \quad [16]$$

The barrier to rotation in kilocalories per mole is V_0 . The refined relative barrier, B_d , is related to the barrier of rotation V_0 by

$$B_d = \frac{V_0 \times 1000}{2 \times 1.987 \times T} \quad [19]$$

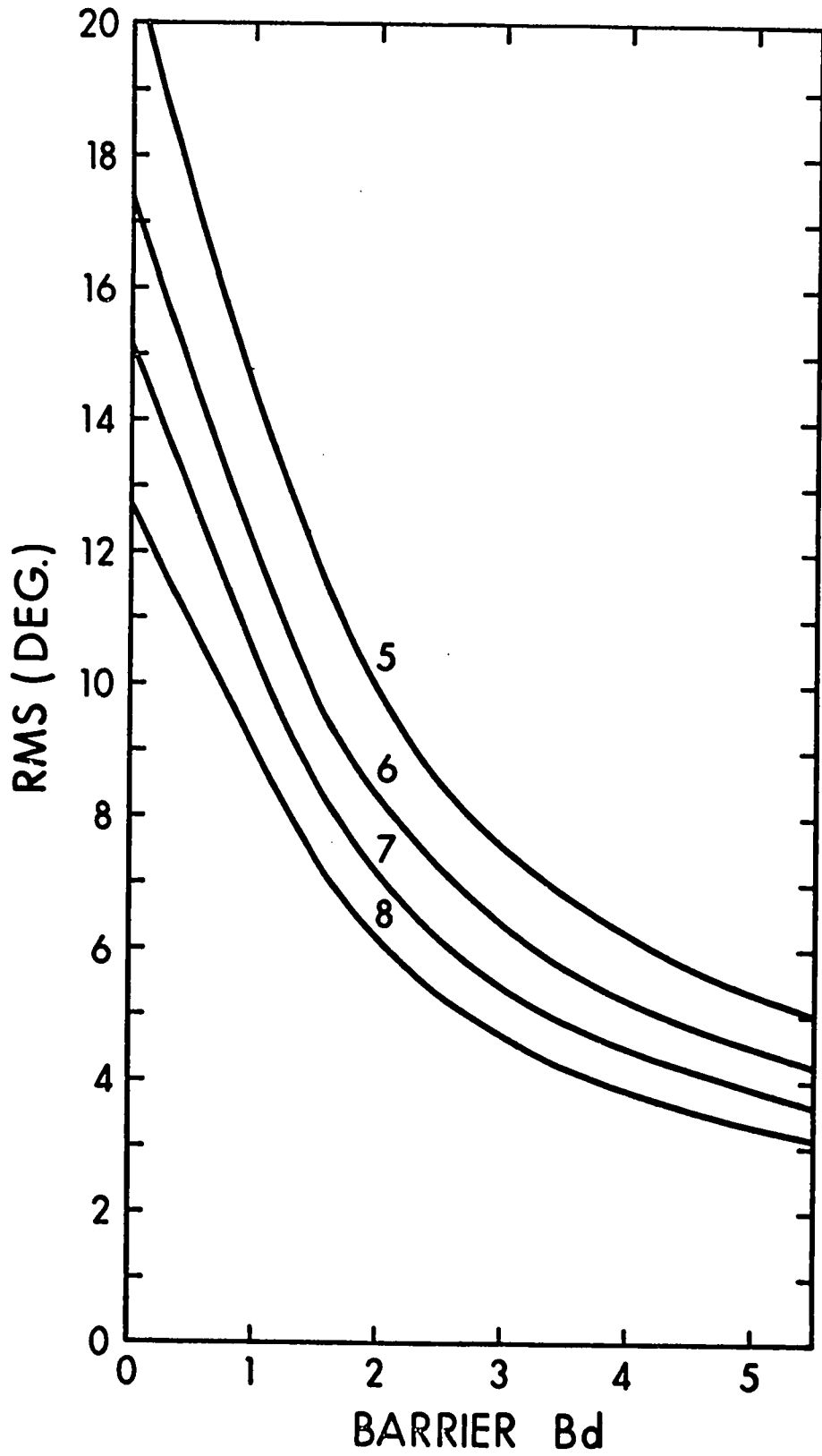
The value of B_d is an indication of the amount of rotation the group undergoes. A barrier of infinity would give no rotation while a barrier of zero would result in free rotation of the rigid group. Intermediate values are directly related to the root mean square angular displacement of the group.

$$\text{RMS} = \sqrt{\frac{\int_0^{\pi/N} \theta'^2 P(\theta') d\theta'}{\int_0^{\pi/N} P(\theta') d\theta'}} \quad [53]$$

Since $P(\theta')$ is a known function of B_d (see equation [17]), angular displacement versus relative barrier can be made for various values of n - the order of the ring. Figure 9

Figure 9

Root mean square angular displacement versus relative
barrier for various values of n



is such a plot for five up to eight membered rings. Thus for $\text{Mn}(\text{CO})_3\text{Cp}$, which has a barrier (Bd) of 1.49, one would expect an RMS angular displacement of 12° . This is also the value obtained by Berndt and Marsh²⁴ by means of Cruickshank's¹³ ω -T analysis. In the case of benzene, the RMS angular displacement obtained from the graph is 8.5° . This agrees satisfactorily with Cruickshank's value of 7.9° ¹². RMS angular displacements for the other molecules are given in Table III. The values of the relative barrier obtained can also be compared to the NMR results for benzene²⁷ and ruthenocene²⁸. Andrews and Eades obtained an activation energy for reorientation of the benzene ring about the hexad axis of 3.7 ± 0.2 kcal/mole below $\sim 240^\circ\text{K}$. Unfortunately, above this temperature the barrier height drops rapidly and one can at best make a rough approximation to the barrier from the slope assuming rotation is still the dominant motion. At -3°C , the temperature at which the crystal structure was done, this was estimated to be 1.8 kcal/mole giving a Bd of 1.7. This is in the same range of values as that of the hindered rotor value of 1.9(1). The agreement of the NMR value with that of the hindered rotor appears to be fortuitous. For $\pi\text{C}_6\text{H}_6\text{Cr}(\text{CO})_3$, $\pi\text{C}_5\text{H}_5\text{Mn}(\text{CO})_3$ and $\pi\text{C}_7\text{H}_7\text{Mo}(\text{CO})_2\text{C}_6\text{H}_5$, NMR results were not available with which to compare the hindered rotor results.

The barriers (B_d) obtained for these compounds were of the same order of magnitude as that of benzene which would be expected for oscillations of the same order as benzene. The results obtained are shown in Table III. The value obtained for ruthenocene was greater than those for the other compounds and had a much larger error associated with it: 5.0 ± 2.6 . This did not agree very well with the NMR result obtained by Holm and Ibers²⁸ of $V_0 = 2.3 \pm 0.2$ kcal/moles which is equivalent to $B_d = 2.01$. The reason for this discrepancy may be in the nature of the potential function used. In a cosine function the activation energy required for rotation of the ring should equal V_0 . If, for example, the potential function were of the form shown in Figure 10 which has a cosine function in the immediate area of the potential minimum and a fixed potential elsewhere, the activation energy would be V_0' while the "Bd" described by a purely cosine function would be $B_d = V_0/2kT$ and not $V_0'/2kT$. A plot of $P(\theta')$ versus θ' (Figure 11) for various values of B_d shows that for $B_d = 4.0$ or greater the atoms are for the most part confined to within a few degrees of the minimum.

In this case, B_d would be insensitive to the shape and height of the potential function outside this region. B_d is then a parameter describing the shape of the function close to the minimum rather than a genuine measure of an

Figure 10

A possible form of the potential function

Figure 11

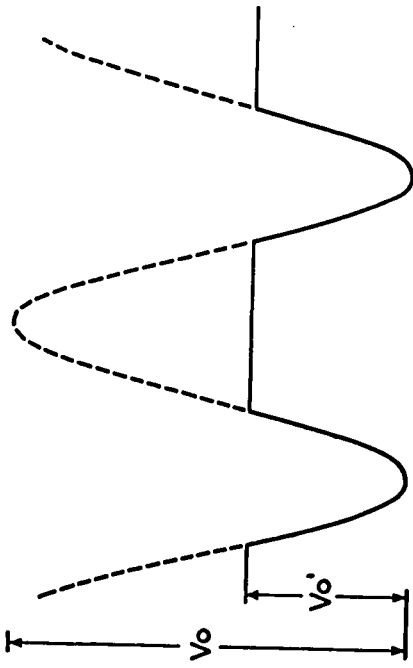
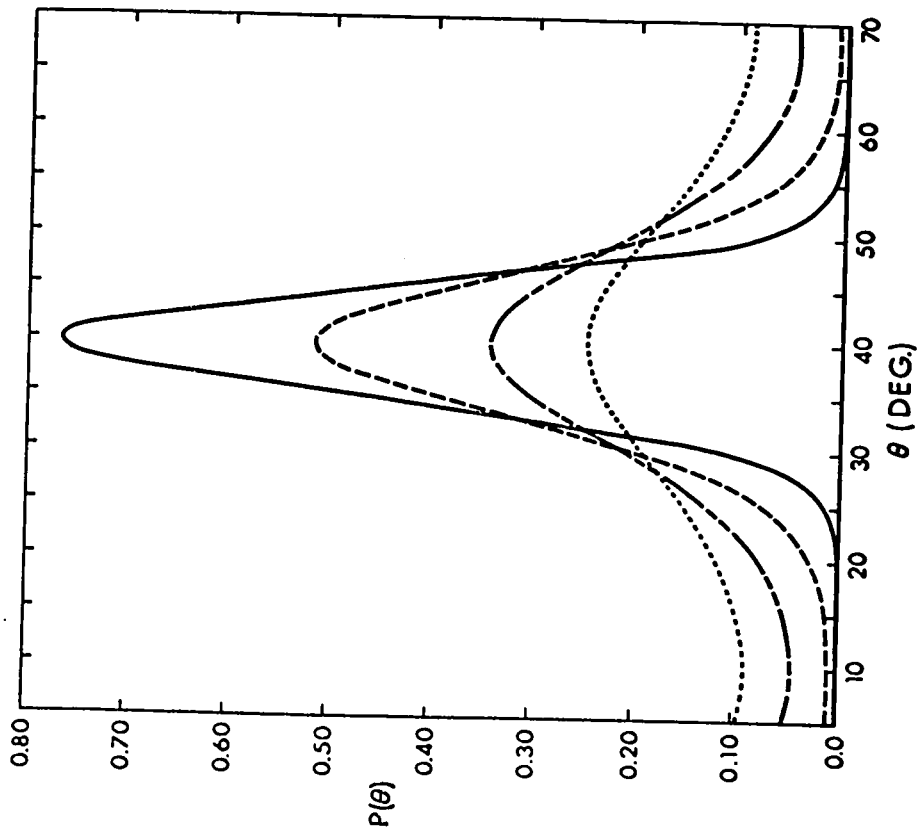
$P(\theta')$ versus θ' for a cosine distribution function

———— $Bd = 4.0$

----- $Bd = 2.0$

----- $Bd = 1.0$

..... $Bd = 0.5$



activation energy.

Temperature Factor B

In the case of hindered rotors, the assumption is being made that most of the motion of the ring is in the plane of the ring and tangential to it. In the case where the ring is strongly bonded to a metal atom, one might expect the ring to ride on the metal. If this were the case, the temperature factors for the rings as a whole, B , should be very similar to the isotropic B of the metal atom, B_M . This indeed seems to be the case as can be seen in Table IV. In each case, the temperature factor seems to be slightly greater than that of the metal to which it is attached. This difference could result from out of plane oscillations by the ring which are not allowed for in the hindered rotor motion, and also by librations of the molecule as a unit.

The observation that the isotropic temperature factor of the ring is slightly greater than that of the metal can be utilized to obtain a starting value of the barrier. This is desirable as it is not always possible to calculate a relative barrier, B_d , from the NMR result, nor would the results be necessarily meaningful.

Application of the hindered rotor model would generally be preceded by individual atom isotropic refinement

or by rigid body refinement. Both of these methods would give B_M and an average temperature factor for atoms in the ring, B_{iso} . These results can be utilized to obtain starting values for the hindered rotor refinement as follows:

If one takes the case where the major motion of an atom is tangential to the ring and this direction is parallel to the z axis, the x and z axes in an orthogonal co-ordinate system being in the plane of the ring, then the elements of the less common tensor description for thermal motion become

$$\begin{aligned}
 B_{11} &= (B_M + 0.6) & B_{12} &= 0 \\
 B_{22} &= (B_M + 0.6) & B_{13} &= 0 \\
 B_{33} &= (B_M + 0.6) + 8\pi^2 \bar{u}_\omega^2 & B_{23} &= 0
 \end{aligned}
 \tag{54}$$

The equivalent isotropic B_{iso} of the atom is

$$B_{iso} = B_M + 0.6 + \frac{8\pi^2}{3} \bar{u}_\omega^2 .
 \tag{55}$$

The root mean square displacement (in Å) is

$$\bar{u}_\omega = R \sqrt{\frac{\int_0^{\pi/N} \theta'^2 P(\theta') d\theta'}{\int_0^{\pi/N} P(\theta') d\theta'}}
 \tag{56}$$

Substituting for \bar{u}_ω in equation [55], one obtains:

Table IV
 Comparison of temperature factors for ring
 and metal atom

	$B \text{ (\AA)}^2$	$B_M \text{ (\AA)}^2$	$\Delta B \text{ (\AA)}^2$
$\pi\text{-C}_5\text{H}_5\text{Mn}(\text{CO})_3$	3.64(17)	3.18	0.46
$\pi\text{-C}_6\text{H}_6\text{Cr}(\text{CO})_3$	3.09(9)	2.63	0.46
ruthenocene (1)	2.11(30)	1.50	0.61
ruthenocene (2)	2.48(30)		0.98
$\pi\text{-C}_7\text{H}_7\text{Mo}(\text{CO})_2\text{-C}_6\text{F}_5$	3.13(13)	2.60	0.53
			Average 0.60

$$B_{\text{iso}} = B_M + 0.6 + \frac{8\pi^2}{3} R^2 \frac{\int_0^{\pi/N} \theta'^2 P(\theta') d\theta'}{\int_0^{\pi/N} P(\theta') d\theta'} \quad [57]$$

Since $P(\theta')$ is known as a function of B_d ,

$$\frac{8\pi^2}{3} \frac{\int_0^{\pi/N} \theta'^2 P(\theta') d\theta'}{\int_0^{\pi/N} P(\theta') d\theta'} \quad \text{can be plotted as a function}$$

of the barrier B_d (Figure 12) for various values of n . In Figure 13 a C-C bond distance of 1.392\AA is assumed and

$$\begin{aligned} \Delta B &= B_{\text{iso}} - (B_M + 0.6) \\ &= \frac{8\pi^2}{3} R^2 \frac{\int_0^{\pi/N} P(\theta') \theta'^2 d\theta'}{\int_0^{\pi/N} P(\theta') d\theta'} \quad [58] \end{aligned}$$

is plotted against the barrier B_d . Thus, knowing the average B_{iso} of the atoms in the ring and the isotropic temperature factor of the metal, ΔB , can be calculated and a starting value of the barrier obtained from Figure 12 or 13. For example, in $\pi\text{-C}_6\text{H}_6\text{Cr}(\text{CO})_3^{25}$ the individual atom refinement gives B_{iso} of 4.5 for carbon atoms in the

Figure 12

$\Delta B/R^2$ as a function of barrier, B_d

$$\text{where } \Delta B = \frac{8\pi^2}{3} R^2 \frac{\int_0^{\pi/N} \theta'^2 P(\theta') d\theta'}{\int_0^{\pi/N} P(\theta') d\theta'}$$

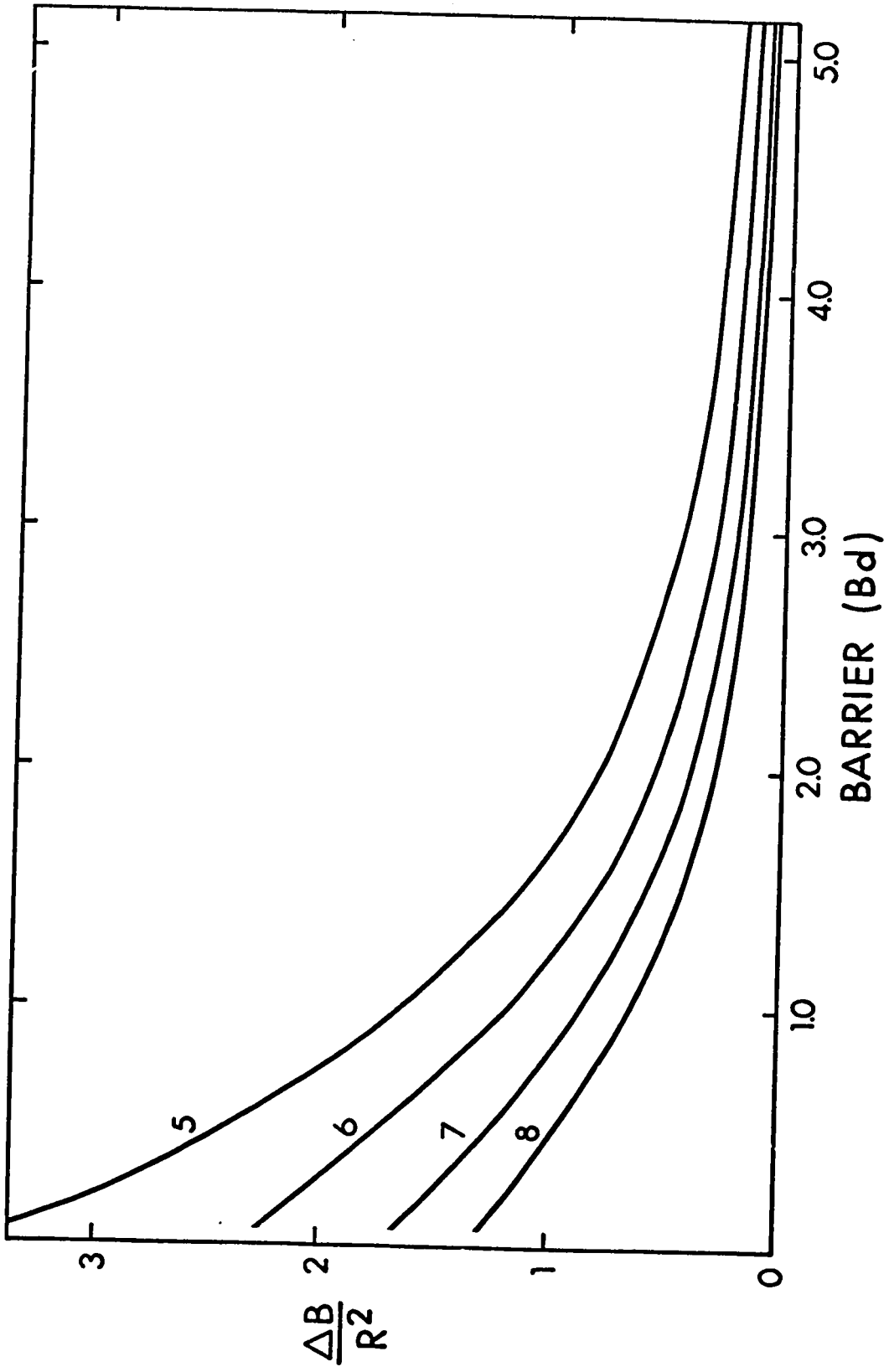
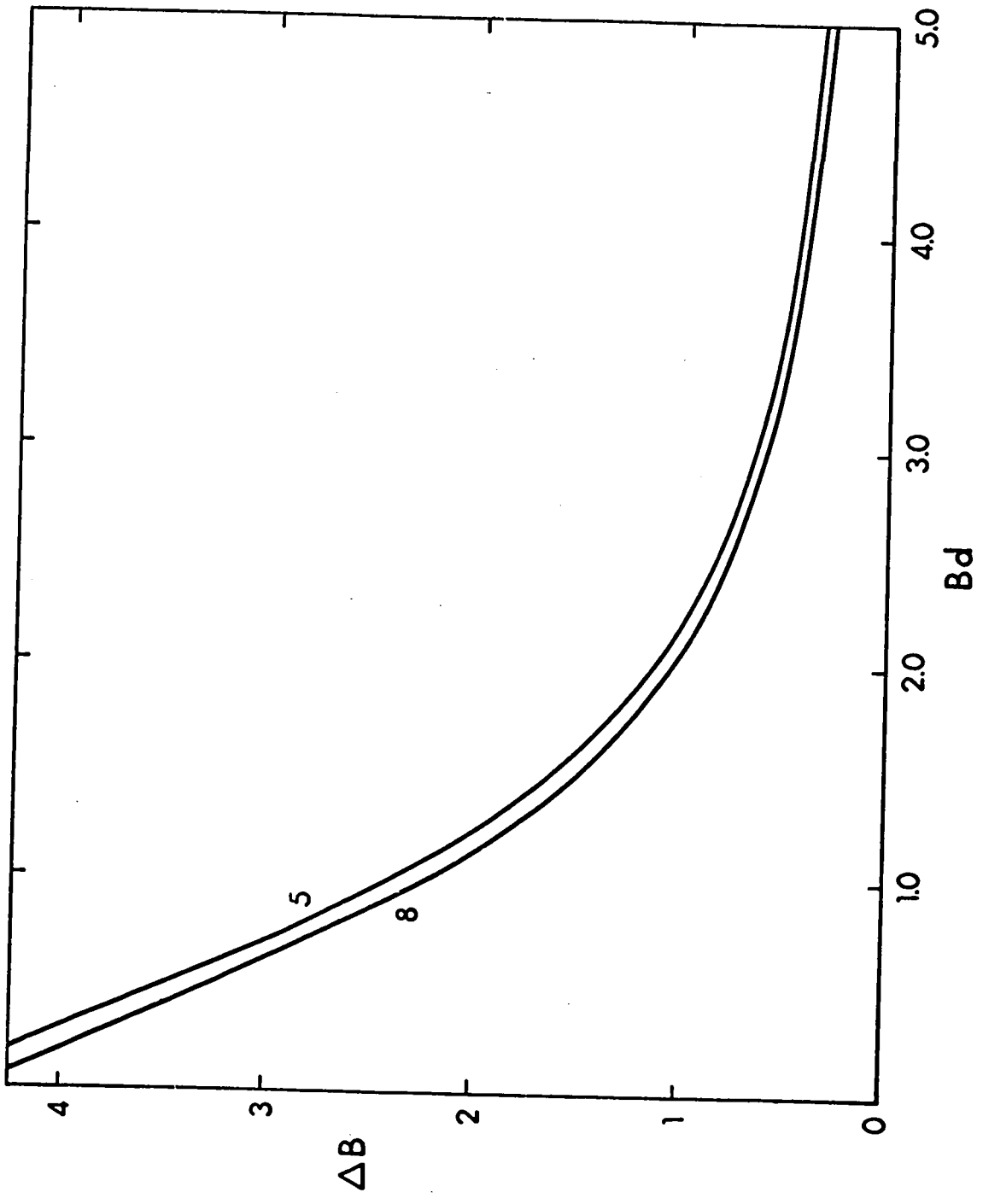


Figure 13

ΔB as a function of barrier, B_d
(C-C distance of 1.392\AA is assumed)



benzene ring and $B_{iso} = 2.6$

$$\begin{aligned}\therefore \Delta B &\approx B_{iso} - (B_M + 0.6) \\ &= 4.5 - (2.6 + 0.6) \\ &= 1.3\end{aligned}$$

From Figure 13 one would obtain a starting value of $B_d = 1.7$. The final refined value of the barrier was 1.97. For $\pi\text{-C}_5\text{H}_5\text{Mn}(\text{CO})_3$ a starting value of 1.5 would be calculated while that for $\pi\text{-C}_7\text{H}_7\text{Mo}(\text{CO})_2\text{C}_6\text{F}_5$ would be 1.8. The final refined values were 1.50 and 1.94 respectively. Although not too accurate a method, this has the practical application that one is able to obtain a starting value for the relative barrier that is acceptably close to the final result. This reduces the number of cycles required for refinement, since the method of non-linear least squares requires a good starting value. A starting value of the temperature factor of the ring would be $B = B_M + 0.6$. The use of reasonably correct starting values of the temperature factor is important since there is a high correlation between the two parameters, B_d and B , typically being of the order of 0.60. Thus a poor starting value of one could greatly affect the other and slow down refinement. Such a high correlation between the two parameters could explain the oscillation problems experienced by Prewitt¹⁸ et al. as they refined using block diagonal least squares, the

barrier and ring temperature factor being in separate matrices.

Test on $-\text{CF}_3$ Groups

The hindered rotor model was also tested out on the fluorines of the four $-\text{CF}_3$ groups in $\text{Cs}[\text{Y}(\text{HFA})_4]^{26}$, where HFA represents the hexafluoroacetylacetonate ion, $\text{CF}_3\text{COCHOCF}_3$. $-\text{CF}_3$ groups as well as such groups as perchlorates are noted for undergoing large thermal motions. The assumption was made that the fluorine groups had D_{3h} symmetry and that the dominant motion was in the plane of the fluorine atoms. The results of the hindered rotor calculations are given in Table V. Although the R factor is not as good as that of the individual atom model, the hindered rotor model does lengthen the C-F and C- CF_3 bonds and brings them close to the corrected values obtained by Cruickshank, Jones and Walker in ammonium trifluoroacetate³⁰. Since $-\text{CF}_3$ groups are less rigid, the assumption of D_{3h} symmetry of the fluorine groups is probably not very good and is the probable cause of the poor structure factor amplitude agreement of the hindered rotor model. This view gains some support from the deformations observed in the individual atom refinement.

Table V
Results of hindered rotor refinement of Cs[Y(HFA)₄]

(a) Hindered rotor parameters for CF₃ groups

Group	x	y	z	B	Bd	R	D	E	F
1	-.4526(7)	.4162(6)	.3871(5)	5.6(2)	0.65(4)	1.249(7)	0.175(8)	1.832(6)	2.511(9)
2	.1730(8)	.5064(5)	.3983(4)	7.5(3)	1.67(5)	1.234(7)	5.534(9)	1.121(9)	4.279(8)
3	-.2499(11)	.1165(6)	.3442(6)	8.3(3)	0.44(4)	1.228(8)	5.453(13)	1.509(16)	3.545(17)
4	.3133(9)	.2188(6)	.4640(5)	7.7(3)	0.84(5)	1.233(8)	3.232(8)	0.870(8)	3.755(17)

(b) Bond lengths (Å)

	Cs[Y(HFA) ₄]		Other molecules	
	Hindered rotor	Individual atom (uncorrected)	Uncorrected	Corrected
Average C-F	1.319	1.26(1)	1.334	1.346(5) ³⁰
Average C-CF ₃	1.576	1.501(16)	-	{ 1.54(2) ³¹ 1.55-1.60 ³²

Reliability Factor

Another test of the validity of the hindered rotor model is on purely statistical grounds. An increased number of parameters being refined will normally result in a lower R factor. Going from the hindered rotor model to the individual atom model requires more parameters and should result in a drop in the R factor. Whether such a drop is significant can be decided by comparing the ratio of R factors with those given by Hamilton³³. If the ratio is greater than that given by Hamilton then the increase in the number of parameters is statistically justified at the significance level chosen (in this case 90%). Thus the hindered rotor model, which has fewer parameters, would be statistically justified only if $\frac{R_{HR}}{R_{IA}} < \text{Hamilton ratio}$. This appears to be true for only $\pi\text{-C}_5\text{H}_5\text{Mn}(\text{CO})_3$ and $\text{Ru}(\text{C}_5\text{H}_5)_2$.

Time and Storage Requirements

One practical advantage of the hindered rotor model over that of the isotropic or anisotropic atom model is that it requires fewer parameters. Since the matrix size = $n(n+1)/2$ where n is the number of parameters refined, the storage requirements increase approximately in proportion to n^2 . Furthermore, the time required to build the matrix and later to invert it is also related

Table VI
R factors (%)

	Published R Factor	Individual Atom R ₁ # Parameters	Hindered Rotor R ₁ # Parameters	Hamilton Ratio	Ratio of R's
π -C ₅ H ₅ Mn(CO) ₃	9.0	8.9	8.9	1.033	1.00
benzene	9.9	8.6	10.1	1.078	1.17
π -C ₆ H ₆ Cr(CO) ₃	4.1	4.1	4.6	1.039	1.12
π -C ₇ H ₇ Mo(CO)-C ₆ F ₅	5.9	5.5	5.7	1.015	1.03
Ru(C ₅ H ₅) ₂	9.8	8.6	8.7	1.010	1.01

to the matrix size and also increases as n^2 . This effect is especially noticeable in large structures such as $(C_5H_5CoCO)_2(GeCl_2)_2Fe(CO)_4^{34}$. In this structure refinement of both molecules in the asymmetric unit, with the heavy atoms anisotropic and all others isotropic, requires 339 parameters, 350K bytes of storage and two hours of computing time per cycle. Use of the hindered rotor for the four cyclopentadienyl rings drops the number of parameters to 295 and the storage to 300K bytes. The time per cycle is cut in half to 63 minutes. Thus, although the addition of subroutines to handle the hindered rotor calculations lengthens the programme (~12K bytes), it is far outweighed by the core saved due to the large drop in the number of parameters to be refined, and concomitant reduction in storage assigned to the matrix.

For crystal structures such as benzene in which only a few parameters are refined, a large percentage of the computing time is spent in calculating structure factors. Because calculation of the M function is slower than the corresponding individual atom expressions, the cycle time will be slower for the hindered rotor model than for the individual atom model. However, for larger structures such as $\pi-C_7H_7Mo(CO)_2C_6F_5$, in the order of 75% of computing time² is spent in building and inverting the matrix. In

this case, the slow calculation of the M function is outweighed by the reduction in matrix building time and the hindered rotor model is faster. The break even point appears to be for structures of the size of $\pi\text{-C}_5\text{H}_5\text{Mn}(\text{CO})_3$ for which approximately the same time was required in both methods.

Conclusions

The development of the hindered rotor model within the framework of a conventional structure factor and least squares programme was undertaken for specific application to $\pi\text{-C}_n\text{H}_n$ groups bonded to metal atoms. The model is attractive in that it emphasizes the physically real phenomenon of hindered rotation of these groups in the solid state. The fixed form of the potential function does not appear to be a serious problem as long as no physical significance is attached to the height of the barrier to rotation that is obtained. Bond lengths derived from the hindered rotor model agree well with those obtained from independent atom models after corrections for thermal motion have been made. The model has been found to be competitive with independent atom models as judged by a statistical comparison of conventional crystallographic R factors.

Chapter II

THE CRYSTAL STRUCTURE OF FERROCINIUM PICRATE

INTRODUCTION

Once the hindered rotor programme was written and tested it was decided to test the programme for use in a routine crystal structure. The compounds ferrocene and ferrocinium picrate both contain cyclopentadienyl rings. The crystal structure of ferrocene by Dunitz, Orgel and Rich³⁵ shows a libration of the cyclopentadienyl rings about the five fold axis, making it ideal for the hindered rotor treatment. Such libration could also occur in the ferrocinium ion of such salts as ferrocinium picrate. Since use of the hindered rotor model gives good average bond lengths, the structural results could be used as evidence in determining the bonding in such structures. For these reasons, the data for ferrocene were re-collected by Kathleen Simpson³⁶ and the structure of ferrocinium picrate undertaken.

EXPERIMENTAL

The compound ferrocinium picrate $[\text{Fe}(\text{C}_5\text{H}_5)_2^+]$
 $[\text{H}_2\text{C}_6\text{N}_3\text{O}_7^-]$ was prepared by Ester Lorah³⁷ from
ferrocene dissolved in a benzene/ethanol solution.
This was oxidized with quinone in the presence of a
stoichiometric amount of picric acid. Her analysis
showed

	C	H	N
calculated	46.36%	2.92%	10.15%
found	46.00%	3.06%	10.40%

A thermogram run to 150° - 160° gave no weight loss,
indicating no solvent and no excess ferrocene present
in the crystals. The crystals were long black needles
extinguishing along the needle axis. The symmetry of
rotation, Weissenberg (hk0 - hk3) and precession photo-
graphs (0kl) showed the compound to be orthorhombic.
Systematic absences of $hk\ell$: $h+k = 2n+1$ and $h0\ell$: $\ell = 2n+1$
allowed three possible space groups - $\text{Cmc}2_1$, Cmcm or
 $\text{C}2\text{cm}$, a non-standard setting of $\text{Ama}2$. Of these, only
 Cmcm is centrosymmetric. The unit cell $a = 12.513(7)\text{\AA}$,
 $b = 20.267(9)\text{\AA}$ and $c = 6.903(7)\text{\AA}$ ($V = 1750.6\text{\AA}^3$) was
obtained from least squares refinement of 2 θ values
of carefully centred, high angle reflections measured
on the Picker four circle manual diffractometer. The

density was determined by flotation, using a mixture of benzene and dibromomethane, to be 1.60 gm/cc. This is consistent with a calculated density of 1.57 gm/cc for 4 molecules per unit cell. Since both space groups $Cmc2_1$ and $Ama2$ have eight general positions and $Cmcm$ has sixteen, this would require the ionic species to sit on special positions such as a mirror or two fold axis. Each space group has one or more special positions. $Cmcm$ has site symmetries of mm and $2/m$. Site symmetry of mm is possible for both the ferrocinium and picrate ions. It would require the ferrocinium ion to be in the eclipsed formation while the picrate would be required to be planar. Site symmetry $2/m$ is possible for the ferrocinium ion requiring a staggered arrangement of the cyclopentadienyl rings, but is impossible for the picrate ion unless highly disordered. The space groups $Cmc2_1$ and $C2cm$ both have site symmetry m . Both the ferrocinium and picrate ions can possess this symmetry as well as the two-fold symmetry found in $C2cm$. The possibilities of site symmetries in the three space groups, assuming no major disorder, are summarized in Table VII.

Data were collected using a crystal (0.23 mm x 0.057 mm x 0.062 mm) mounted along the needle axis (c)

Table VII
Possible site symmetry

	Space Group	Site Symmetry of FeCp_2^+	Site Symmetry of Picrate Ion
1	Cmcm	mm	mm
2	Cmcm	2/m	mm
3	Cmc2 ₁	m	m
4	C2cm	m	m
5	C2cm	m	2
6	C2cm	2	m
7	C2cm	2	2

and with the c^* axis co-incident with the diffractometer ϕ axis. A moving crystal, moving counter technique ($\theta/2\theta$) was used with a scan width of 2° at two degrees per minute. CuK_α X-radiation was used, monochromated by an oriented graphite crystal (002 reflection). The diffracted beam aperture used was 1.0 mm and the pulse height analyser was centred on the CuK_α peak to accept 90% of the radiation. Stationary background counts of 30 seconds were taken on each side of the scan. Six hundred and forty-two unique reflections (hkl ; h , k and l positive only) were collected, of which 276 were rejected using the criteria (1) $I \leq 0$ and (2) $I \leq 3\sigma$ where $I = [P - t(B_1 + B_2)]$ and $\sigma = [P + t^2(B_1 + B_2)]^{1/2}$

where P peak count

$\left. \begin{array}{l} B_1 \\ B_2 \end{array} \right\}$ background counts

and t ratio of total peak count to total background count

Seven well distributed standard reflections measured periodically throughout the data collection showed no decomposition of the crystal. No absorption correction was made ($\mu(\text{Cu}) = 75.1 \text{ cm}^{-1}$).

SOLUTION AND REFINEMENT

A three dimensional Patterson map gave the iron position as $x = 0.0$ and $y = 0.185$, the z co-ordinate being undefined. Although simple interpretation of the Patterson does not determine the space group, site symmetry considerations given in Table VII reduced the possible arrangements from seven to two. The Patterson solution eliminates possibilities 2, 4, 5, 6 and 7, leaving only 1 and 3 for serious consideration and reduces the space group choice to either $Cmcm$ or $Cmc2_1$. The space group $Cmc2_1$ was chosen for initial refinement because the crystal showed $mm2$ symmetry. Since this space group is polar, the z co-ordinate was fixed at $z = 0.0$. A difference map ($F_o - F_c$, F_c phased on iron only) revealed the location of all other non-hydrogen atoms. With the space group chosen as $Cmc2_1$, the iron only phased Fourier map is centrosymmetric and has the symmetry of $Cmcm$. If the non-centrosymmetric space group is correct, the effect of the extra symmetry is to show the true electron density distribution, together with its superimposed mirror image. The picrate atoms, with the exception of the ortho nitro group, were found on the mirror plane ($z = 0.0$). The appearance of diffuse ortho nitro group peaks on either side of the plane could result from

either non-centric space group with its superimposed mirror image, or centrosymmetric space group with disorder of the nitro group. The cyclopentadienyl rings of the ferrocinium cation were revealed as smears of electron density and possessing mm symmetry. This could also be due to superposition of the mirror image in the non-centrosymmetry space group, or if centrosymmetric, due to a large oscillation of the rings. Calculation of the structure factors using all non-hydrogen atoms gave an R factor of $R_1 = 26.7\%$, $R_2 = 28.3\%$, where

$$R_1 = \frac{\sum ||F_o| - |F_c||}{\sum |F_o|}$$

and

$$R_2 = \left[\frac{\sum w (|F_o| - |F_c|)^2}{\sum w |F_o|^2} \right]^{1/2}$$

The weights used were obtained from peak and background counts (weight $w = 1/\sigma^2(F)$, $\sigma(F) = (P + t^2(B_1 + B_2) + p^2I)^{1/2}$, $p = 0.03$).

Four cycles of refinement, minimizing the function $\sum w (|F_o| - |F_c|)^2$, with all atoms isotropic and the cyclopentadienyl ring as a hindered rotor brought the R factor down to $R_1 = 11.6\%$.

The final orientation of the cyclopentadienyl ring

was 18° from the orientation required by the additional mirror of Cmc_m. There remained the distinct possibility of refinement into a false minimum corresponding to the pseudo-mirror at $z = 0.0$. Also, in a non-polar space group such as Cmc2₁, anomalous dispersion³⁸ (in this case for the iron atom) can produce significant co-ordinate changes. Four models were then refined with the inclusion of anomalous scattering for iron:

- (1) Previous model; refinement terminated with Bd negative.
- (2) Mirror image of previous model; R = 11.9%.
- (3) Ferrocinium ion as in (1), picrate as in (2); R = 11.8%.
- (4) Mirror image of (3); refinement terminated with Bd negative.

Refinement of models (1) and (4) resulted in negative values for Bd indicating that the mirror image of the cyclopentadienyl ring was preferred. This suggests that the omission of anomalous scattering favoured the choice of a false minimum for the cyclopentadienyl ring in the initial model.

For the ferrocinium ion, it is reasonable to expect the centres of gravity of the rings and the iron atom to be approximately collinear. In this crystal structure, this would require the z co-ordinate of the ring centre to be zero. However, models (2) and (3) showed a diff-

erence in z corresponding to -0.03\AA .

Cruickshank and MacDonald's³⁸ formula

$$\Delta z \text{ (in } \text{\AA}) = \frac{2}{\pi S_{\max}} \left(\frac{\Delta f''}{|f|} \right)_{\frac{1}{2} S_{\max}}$$

where $S = \frac{2 \sin \theta}{\lambda}$

predicts a difference in the z co-ordinate of 0.03\AA in the incorrect model which agrees with the observed shifts. This suggests that models (2) and (3) are also wrong and that none of the cases considered so far are correct.

The structure was then refined using the centrosymmetric space group $Cmcm$. This group requires a mirror plane through the plane of the picrate ion and the iron atom. Isotropic refinement of all atoms brought the R factor to $R_1 = 10.7\%$, $R_2 = 13.7\%$, with disorder allowed for the ortho nitro group. These atoms (N1, O2 and O3) were given half weight above and below the mirror plane for the following reasons:

(1) The initial difference map showed considerable smearing of the peaks for these atoms off the mirror plane.

(2) When confined to the mirror plane, the B_{33} values obtained were very large, suggesting that the atoms were in fact off the $z = \frac{1}{2}$ plane, and that the ortho nitro group was not planar with the rest of the

picrate group.

(3) If O1, O2 and O3 were all in the plane, there would be a very short O1-O2 contact of 2.64\AA , and an even shorter O2-O3 contact of 1.90\AA , which is much shorter than the Van der Waal's radius sum. These short contacts would be lengthened if O2 and O3 were off the mirror plane.

(4) Work by Maartmann-Moe³⁹ on the structure of potassium and ammonium picrates showed that the ortho nitro groups are twisted $25^\circ - 27^\circ$ out of the plane of the benzene ring, making a non-planar picrate ion a plausible structure.

(5) Study of the packing diagram (Figure 15) suggests that the nitro group could be accommodated in either the "up" ($z(O3) > 0.25$) or "down" position. In the "up" position, O3 is within Van der Waal's contact of H14 of the neighbouring ferrocinium ion, while in the "down" it is the same distance from H13. Similarly, O2 is equidistant from H11 and also O1 in either position. This would suggest that the picrate ion crystallizes with a random arrangement of "up" or "down" meta nitro groups. The disordered centric model was chosen rather than a non-centric model as:

(1) no clear distinction could be made among the four possible arrangements of the ferrocinium and

picrate ion;

(2) use of Cruickshank and MacDonald's³⁸ formula for the error in co-ordinates due to the wrong hand when using anomalous dispersion indicated that both hands were incorrect and that the mean - a disordered model - would be a better description; and

(3) the R factor was consistently higher for the non-centric model than for the centric model, despite the fact that the latter has fewer variable parameters.

Allowing the iron atom anisotropic motion and adding the hydrogens of the cyclopentadienyl rings as hindered rotors with C-H distance of $1.0\overset{\circ}{\text{A}}$, dropped the R factor to $R_1 = 8.4\%$, $R_2 = 12.3\%$. Further refinement with all atoms anisotropic and the picrate hydrogen added gave a final reliability factor of $R_1 = 6.0\%$, $R_2 = 8.5\%$. It was noticed during anisotropic refinement that some atoms, noticeably O1 as well as the disordered nitro group, had much larger thermal parameters in the z direction. For this reason, O1 was also moved off the mirror plane and given a half population above and below the mirror plane. Refinement of this disordered model gave a final z co-ordinate of $z = 0.1794 \pm .1842$. Because of this large error in the z co-ordinate, O1 was returned to the mirror plane and no other atoms were allowed to become disordered.

In the final cycle of refinement no shift was greater than 1/10 of an esd. A final difference map gave no peak greater than $0.42 \text{ e}^-/\text{A}^3$. The observed and calculated structure factor amplitudes (x10) are given in Table VIII. Table IX gives the final positional co-ordinates of the individual atoms and the anisotropic B values are listed in Table X. Hindered rotor parameters for the cyclopentadienyl rings are in Table XI.

Table VIII

Observed and calculated structure factor amplitudes
(x10) in electrons for $[\text{Fe}(\text{C}_5\text{H}_5)_2^+][\text{H}_2\text{C}_6\text{N}_3\text{O}_7^-]$

H	K	FO	FC	H	K	FO	FC	H	K	FO	FC	H	K	FO	FC	H	K	FO	FC
	L = 0			10	0	597	641	8	6	206	229	9	1	196	187		L = 4		
0	2	252	334	10	2	700	155	8	10	188	192	9	3	257	281	0	0	960	930
0	4	83	78	10	4	132	80	9	1	409	424	9	5	341	363	0	4	123	116
0	6	948	959	10	6	175	180	9	9	264	273	9	11	215	197	0	6	180	135
0	8	721	693	10	8	394	363	9	11	146	140	9	13	146	152	0	8	521	455
0	10	249	248	10	14	249	221	9	15	263	247	10	0	664	702	0	10	142	88
0	12	142	129	11	1	355	349	10	4	383	382	10	6	181	208	0	14	267	299
0	14	654	604	11	3	176	203	10	6	181	197	10	8	319	309	0	16	218	237
0	16	503	451	11	11	235	258	10	10	366	366	11	3	263	270	1	1	428	439
1	1	833	985	12	0	159	210	10	12	177	143	11	5	207	181	1	3	237	196
1	3	1489	1572	12	6	204	192	11	7	269	274	12	0	260	289	1	5	209	178
1	5	1002	1005	12	8	286	251	12	2	205	204	12	2	146	97	1	11	264	250
1	7	80	66		L = 1			12	4	180	147	12	6	209	180	2	0	814	794
1	9	175	179	0	2	1281	1350	13	1	157	142		L = 3						
1	11	318	316	0	4	2734	2660		L = 2			0	2	237	221	2	2	138	168
1	13	155	127	0	6	498	537	0	0	3450	3525	0	4	730	649	2	6	413	417
1	19	291	258	0	8	91	89	0	2	407	298	0	6	375	335	2	8	326	331
1	21	144	113	0	10	1167	1120	0	4	303	310	0	8	229	237	2	10	142	110
2	0	852	695	0	12	122	117	0	6	790	284	0	10	568	553	2	16	152	170
2	2	1106	1195	0	14	223	212	0	8	604	608	0	12	238	228	3	1	207	210
2	4	543	576	0	18	226	215	0	14	510	516	0	18	191	195	3	3	315	326
2	6	707	737	0	20	430	434	0	16	372	406	1	1	100	120	3	5	455	466
2	8	993	994	1	1	1254	1341	1	1	1086	1072	1	1	119	107	3	11	206	212
2	10	130	161	1	3	233	211	1	3	454	450	1	7	119	107	3	13	199	194
2	12	172	164	1	5	161	143	1	5	364	358	1	11	264	266	4	0	509	512
2	14	177	176	1	7	130	120	1	11	273	296	1	13	148	167	4	2	405	401
2	16	435	437	1	9	160	114	1	13	124	146	1	15	234	256	4	4	321	333
2	20	143	158	1	11	455	440	1	19	218	216	2	17	169	204	4	8	253	299
3	1	217	359	1	15	356	339	2	0	1190	1204	2	2	736	748	5	3	264	287
3	3	513	467	1	17	299	264	2	2	554	599	2	4	600	608	5	5	471	514
3	5	346	348	2	2	1374	1433	2	6	761	798	2	6	305	315	5	11	236	209
3	7	484	474	2	4	478	475	2	8	677	664	2	10	531	526	6	0	234	232
3	9	483	491	2	6	792	826	2	10	202	209	2	12	267	269	6	8	157	175
3	11	623	645	2	8	200	217	2	12	141	140	3	1	548	566	7	5	268	254
3	13	553	589	2	10	590	609	2	14	181	155	3	3	330	334	7	11	236	216
3	15	133	122	2	12	622	626	2	16	337	327	3	5	301	337	7	13	203	227
3	17	224	222	2	14	218	238	2	18	126	140	3	7	518	537	8	0	201	199
4	0	188	186	3	1	466	440	2	20	337	327	3	9	409	436	8	8	196	152
4	2	894	804	3	3	355	329	2	22	126	140	3	11	142	121	9	3	222	192
4	4	443	438	3	5	315	291	3	1	319	300	3	13	142	121	9	5	179	169
4	6	198	197	3	7	803	824	3	3	358	396	3	15	309	275	10	0	430	417
4	8	462	454	3	9	593	561	3	5	753	775	4	2	300	334		L = 5		
4	10	486	488	3	11	235	224	3	7	393	377	4	4	716	764	0	2	200	244
4	12	136	119	3	13	212	184	3	9	321	310	4	6	353	377	0	4	339	332
4	14	229	270	3	15	397	392	3	11	512	502	4	8	126	142	0	6	234	244
5	1	106	137	3	17	212	265	3	13	492	461	4	10	218	228	0	10	302	309
5	3	231	203	4	0	825	793	4	0	825	793	4	12	320	316	0	12	188	168
5	5	1582	1559	4	2	396	396	4	2	396	396	4	16	226	221	1	7	178	167
5	7	131	113	4	4	575	555	4	4	575	555	5	1	728	718	1	11	141	139
5	9	408	404	4	6	777	724	4	6	180	208	5	7	489	518	2	2	297	259
5	11	669	685	4	8	227	250	4	8	607	578	5	9	398	388	2	4	281	299
5	13	267	313	4	10	607	615	4	10	400	370	5	11	138	118	2	10	141	207
5	19	298	301	4	12	376	399	4	14	200	159	5	15	504	480	2	12	138	130
6	0	751	775	4	16	190	201	4	16	154	138	6	2	132	130	3	1	236	202
6	2	829	827	4	20	149	152	5	3	343	343	6	4	330	323	3	7	154	173
6	4	632	612	5	1	826	815	5	5	1213	1189	6	10	169	173	4	2	153	151
6	6	109	94	5	3	370	375	5	9	320	318	6	12	203	223	4	4	226	243
6	8	342	333	5	5	157	122	5	11	513	510	7	1	177	182	5	1	216	235
6	10	114	66	5	7	619	589	5	13	300	280	7	3	210	225	5	7	182	191
6	16	209	199	5	9	745	703	5	19	235	223	7	7	210	222	6	4	186	184
7	1	609	555	5	11	123	108	6	0	541	484	7	9	207	207	6	12	168	153
7	3	1008	993	5	15	817	849	6	2	379	344	7	15	316	341	7	7	184	179
7	5	635	595	6	2	343	345	6	4	321	311	8	2	205	188	7	9	193	172
7	7	328	328	6	4	628	566	6	8	223	222	8	4	142	137		L = 6		
7	9	173	185	6	6	174	183	6	16	186	167	8	6	161	128	0	0	392	437
7	11	239	253	6	12	318	340	7	1	324	334	8	12	186	168	0	8	172	227
7	13	404	398	6	14	285	277	7	3	350	307	9	1	223	242	1	3	188	173
7	17	164	179	6	16	234	249	7	5	400	382	9	9	143	136	2	0	262	289
8	0	1203	1117	7	1	934	871	7	7	148	131	9	13	132	101	2	8	161	159
8	2	572	557	7	3	519	477	7	11	235	245	10	2	164	180	4	0	178	97
8	6	335	362	7	5	748	257	7	13	335	337	10	4	335	333				
8	10	148	130	7	7	491	516	7	17	151	154	10	6	152	147				
8	16	242	190	7	9	158	187	8	0	455	460	10	10	232	234				
9	3	279	288	7	15	369	359	8	2	281	282	11	1	176	171				
9	5	535	565	7	17	312	279	8	4	161	143	11	7	206	198				
9	11	235	243	8	2	588	600	8	6	128	171	12	2	192	206				
9	13	198	178	8	4	428	432	8	16	158	174								

Table IX
Positional co-ordinates for ferrocinium picrate

Atom	x	y	z
Fe	0.0	0.1851(1)	0.2500
C1	0.0	0.4408(8)	0.2500
C2	0.0932(9)	0.4829(6)	0.2500
C3	0.9464(9)	0.5500(5)	0.2500
C4	0.0	0.5827(7)	0.2500
N1	0.1996(11)	0.4511(5)	0.2010(29)
N2	0.0	0.6533(7)	0.2500
O1	0.0	0.3801(5)	0.2500
O2	0.2092(8)	0.3960(5)	0.266(10)
O3	0.2733(9)	0.4814(5)	0.1285(21)
O4	0.0862(7)	0.6822(4)	0.2500
H1	0.1680	0.5730	0.2500

Parameters without estimated
errors were not refined.

Table XI

(a) Hindered rotor parameters

	x	y	z	B	Bd	R	D	E	ξ
C ring	0.2500	.1354 (4)	.1856 (3)	5.6 (2)	.40 (7)	1.186 (5)	0.0	$\pi/2$.3141
H ring	0.2500	.1354	.1856	5.6	.40	2.186	0.0	$\pi/2$.3141

(b) Derived co-ordinates for hindered rotor atoms

	x	y	z
C11	0.1354	0.2441	0.2500
C12	0.1354	0.2037	0.4134
C13	0.1354	0.1382	0.3510
H11	0.1354	0.2935	0.2500
H12	0.1354	0.2189	0.5512
H13	0.1354	0.0983	0.4361

RESULTS

A drawing of the ferrocinium picrate molecule is shown in Figure 14. The packing of the ions projected onto the *ab* plane is given in Figure 15. The atoms in the upper picrate ion are dotted in, while those below are not. Bond angles and bond lengths are given in Table XII, while some interionic contacts are listed in Table XIII.

Figure 14

Drawing of ferrocinium picrate
showing numbering system used

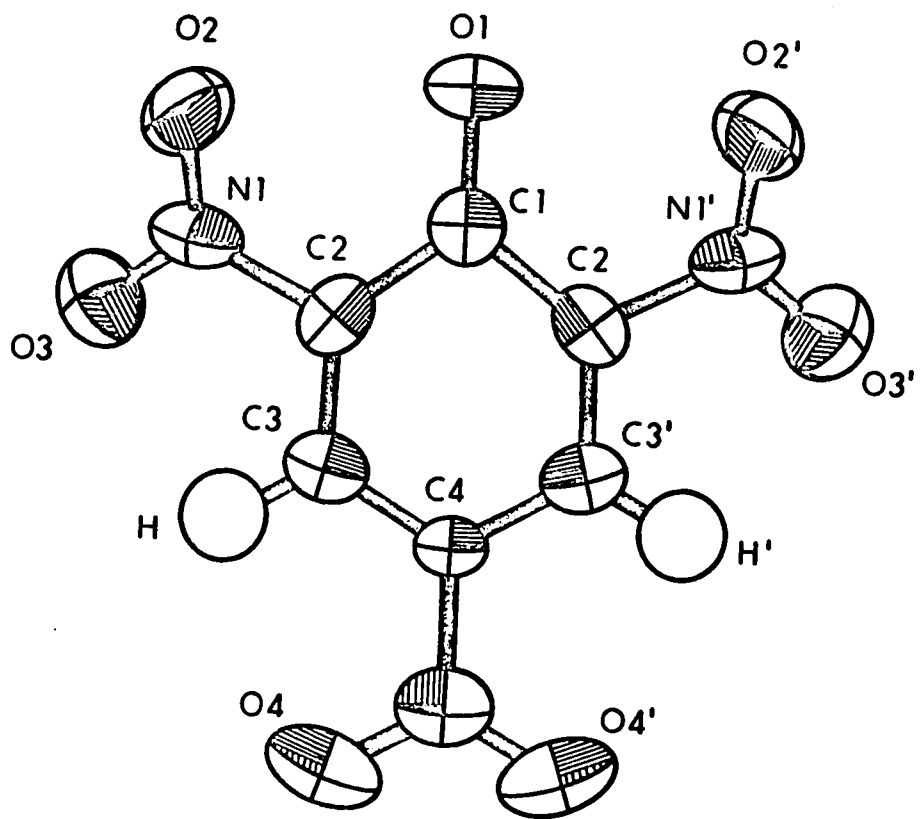
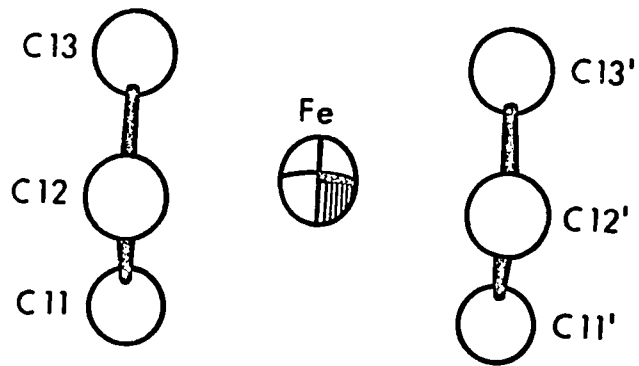


Figure 15

Packing of ferrocinium picrate
as projected onto the ab plane

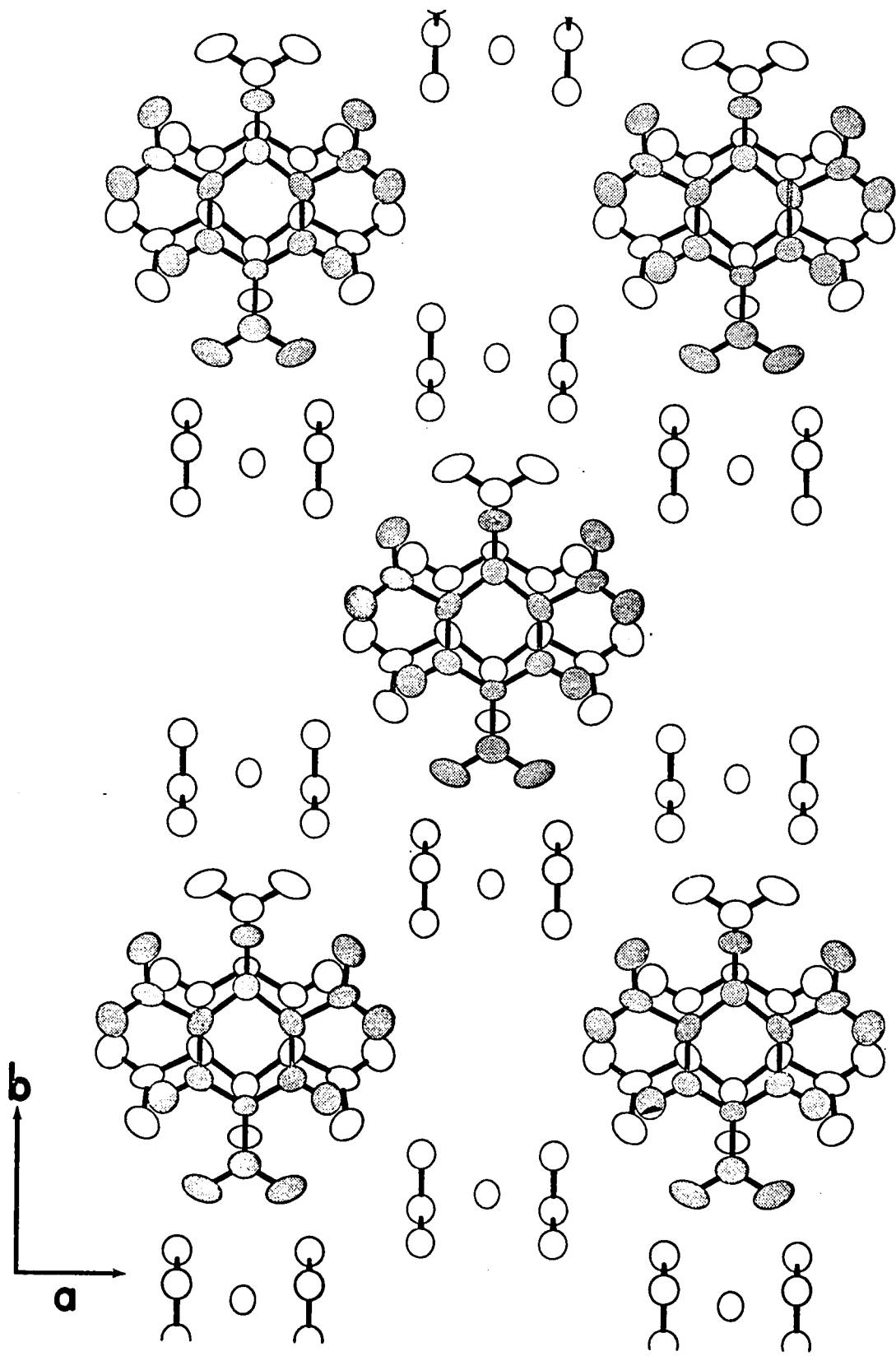


Table XII

(a) Intramolecular bond lengths in
ferrocinium picrate (\AA)

Fe - C11	2.074(7)	C1 - O1	1.231(17)
Fe - C12	2.070(5)	C1 - C2	1.445(14)
Fe - C13	2.064(6)	C2 - C3	1.360(15)
		C3 - C4	1.357(12)
C11 - C12	1.395(6)	C2 - N1	1.517(16)
C11 - H11	1.00	C4 - N2	1.429(18)
		N1 - O2	1.210(32)
H12 - O1	2.439(8)	N1 - O3	1.216(15)
H12 - O2	2.277(10)	N2 - O4	1.228(9)
O1 - O2	2.641(10)	(C3 - H1)	1.029(11)

(b) Bond angles (deg)

C2 - C1 - C2'	107.6(14)
O1 - C1 - C2	126.2(7)
C1 - C2 - C3	126.9(12)
C1 - C2 - N1	117.2(9)
C2 - C3 - C4	118.5(12)
C3 - C4 - C3'	121.5(14)
C3 - C4 - N2	119.2(7)
C4 - N2 - O4	118.6(8)
O4 - N2 - O4	122.9(15)
C2 - N1 - O2	113.(2)
C2 - N1 - O3	123.(1)
O2 - N1 - O3	123.(2)

dihedral angle: ($z = 0.25$ plane) and

(N1, O2, O3 plane) 26.6°

Table XIII
Interionic contacts

Fe - O1	3.951(11)	O3 - H13	2.383(12)
O1 - H11	2.439(18)	O3 - H13	2.668(12)
O1 - O2	2.641(10)	O3 - O3	1.928(29)
O1 - C11	3.234(12)	O4 - H11	2.505(7)
O1 - O4	3.830(6)	O2 - H11	2.277(10)

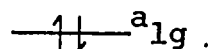
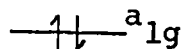
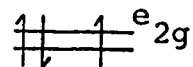
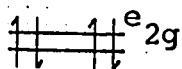
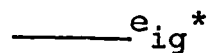
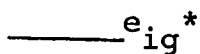
DISCUSSION

The compound ferrocinium picrate is an ionic species consisting of the ferrocinium ion $\text{Fe}(\text{Cp})_2^+$ in which the iron may be considered to be in the formal +3 oxidation state, and the picrate ion $[\text{H}_2\text{C}_6\text{N}_3\text{O}_7]^-$.

The ferrocinium ion has two cyclopentadienyl rings which are related by a mirror plane, and thus unlike ferrocene in the solid state^{35,36}, the rings are eclipsed. Ferrocene in the gaseous state⁴⁰, as well as ruthenocene²² in the solid state, are also eclipsed. The Fe-C distances were found to be longer (average $2.070(5)\text{\AA}$) than those of ferrocene³⁶ ($2.047(5)\text{\AA}$) while the average C-C distance of $1.395(6)\text{\AA}$ for ferrocinium was shorter ($1.416(4)\text{\AA}$) as obtained from the hindered rotor model.

Although distortions from D_{5h} symmetry may be present, because of the disorder in the crystal and large oscillations of the rings (RMS- 18°), the results of any individual atom refinement would likely be unreliable. Evidence of this can be seen in the results of Pettersen⁴¹ in which the C-C distance ranges from 1.33\AA to 1.44\AA with an error of $\pm 0.02\text{\AA}$ or greater. Use of the hindered rotor model allows for the oscillation of the rings and should give a good average value for the C-C distance. The lengthening of the Fe-C distances and shortening of the

C-C distances in the ferrocinium ion is in agreement with the molecular orbital calculations^{42,43} and spectral results⁴⁴⁻⁴⁸ which indicated that the ground state of ferrocene in the eclipsed formation is $E_{2g}[(a_{1g})^2(e_{2g})^4]$ and that of the ferrocinium ion is $E_{2g}[(a_{1g})^2(e_{2g})^3]$. Since a_{1g} and e_{2g} are the highest bonding orbitals, removal of one electron from the e_{2g} level



ferrocene

ferrocinium ion

would weaken the Fe-C(ring) bonds and result in a longer Fe-C distance in ferrocinium ion than in ferrocene. It would also strengthen the C-C bond thus shortening it in

$\text{Fe}(\text{Cp})_2^+$ since an electron is being removed from a C-C antibonding orbital. These calculations were done⁴² assuming D_{5d} symmetry. However, the symmetry of the ferrocinium ion in this structure is D_{5h} rather than D_{5d} . Molecular orbital calculations using D_{5h} symmetry give the same pattern of energy levels. If the assumption is made that the order of the energy levels is the same in the eclipsed form as in the staggered form, then a ground state of the ferrocinium ion would be $E_2'(a_1'^2, e_2'^3)$ and the argument given above would still apply.

The picrate ion lies on a mirror plane at $z = 0.2500$ and across a second mirror at $x = 0.0$. However, three atoms, namely those of the ortho nitro group (N1, O2 and O3), were allowed to move off the mirror, and have "half atoms" above and below the $z = \frac{1}{4}$ mirror. The reasons for this were discussed in some detail earlier.

Although because of the disorder problem the results are somewhat suspect, the geometry calculated from the disordered picrate model agrees fairly well with those of potassium and ammonium picrate³⁹. The N-O distances within the ortho nitro group ($1.210(32)\text{\AA}$ and $1.216(15)\text{\AA}$) are the same within experimental error as those of the potassium and ammonium structures ($1.232(5)\text{\AA}$, $1.229(5)\text{\AA}$, $1.237(5)\text{\AA}$ and $1.206(5)\text{\AA}$) respectively. The ortho nitro group was found to be twisted 26.6 degrees from the

plane of the benzene ring, while in the potassium and ammonium compounds it was $25^\circ - 27^\circ$. The C-N bond is slightly shorter ($1.429(18)\text{\AA}$) than those found by Maartmann-Moe ($1.457(6)\text{\AA}$ and $1.461(5)\text{\AA}$). The rest of the molecule also has a geometry very similar to the potassium and ammonium picrates.

Chapter III

THE CRYSTAL STRUCTURE OF HYDRIDOTRIPHENYLSILYL
(π -CYCLOPENTADIENYL) DICARBONYL MANGANESE

INTRODUCTION

The ultraviolet irradiation of metal carbonyls in the presence of substituted silanes has led to the preparation of a new class of metal-silicon hydrides. These compounds seem to fall into two groups; for example, those prepared from triaryl silanes such as $(\pi\text{-C}_5\text{H}_5)(\text{OC})_2\text{Mn}(\text{H})\text{Si}(\text{C}_6\text{H}_5)_3$ (1), and those containing the more electronegatively substituted silyls such as $(\pi\text{-C}_5\text{H}_5)(\text{OC})_2\text{Mn}(\text{H})\text{SiCl}_3$ (2). The latter group of compounds shows well defined infrared bands in the region of "normal" terminal metal-hydrogen stretching frequencies (1887 cm^{-1} , deuteride 1360 cm^{-1})⁴⁹. The former group, however, showed no bands in either terminal or bridging M-H regions. The solid state Raman spectra⁴⁹ shows a weak broad band at 1900 cm^{-1} which shifts to 1350 cm^{-1} in the deuteride, these bands being in what is considered the terminal metal-hydrogen region. In order to understand the differences in the spectral results, the crystal structures of (1) and (2) were undertaken.

EXPERIMENTAL

The compound hydridotrichlorosilyl (π -cyclopentadienyl) dicarbonyl manganese, $(\pi\text{-C}_5\text{H}_5)(\text{OC})_2\text{Mn}(\text{H})\text{SiCl}_3$ (2), forms light brown needle crystals. Rotation, Weissenberg ($h0\ell\text{-}h4\ell$ and $0k\ell\text{-}9k\ell$) and precession ($h0\ell\text{-}h3\ell$) photographs using several crystals showed the crystals to be monoclinic with unit cell $a = 14.71\text{\AA}$, $b = 11.46\text{\AA}$, $c = 14.85\text{\AA}$ and $\beta = 107.75^\circ$. Systematic absences of $hk\ell$; $h+\ell = 2n+1$, $0k0$; $k = 2n+1$ and $h0\ell$; $\ell = 2n+1$ fixed the space group at $B2_1/c$ (a non-standard setting of $P2_1/c$). Eight molecules per unit cell gave a calculated density of 1.75 gm/cc. Since the molecule does not possess a centre of symmetry, it is most likely that the molecules lie in general positions with one molecule per asymmetric unit. The crystal was mounted on the PAILRED automatic diffractometer in order to collect data. However, measurement of standard reflections showed that decomposition of the crystal in the X-ray beam was so rapid (over 30% in 20 hours), an accurate crystal structure was impossible. The determination was terminated at this point.

The compound hydridotriphenylsilyl (π -cyclopentadienyl) dicarbonyl manganese (π -C₅H₅)(OC)₂Mn(H)Si(C₆H₅)₃ was prepared by J.K. Hoyano⁴⁹ by the ultraviolet radiation of (C₅H₅)Mn(CO)₃ in the presence of an excess of triphenylsilane and recrystallized from a mixed hexane-dichloromethane solvent system to obtain crystals suitable for single crystal X-ray diffraction study. The yellow crystals were mounted parallel to an extinction direction (a face diagonal). Rotation, Weissenberg (0k ℓ -2k ℓ) and precession (kh0-hk2 and h0 ℓ -h2 ℓ) photographs showed the crystal to be monoclinic. Systematic absences of 0k0, k = 2n+1 and h0 ℓ , h + ℓ = 2n+1 fixed the space group as P2₁/n. The general positions in this space group are

$$\begin{array}{ccc} x & y & z \\ \bar{x} & \bar{y} & \bar{z} \\ \frac{1}{2}+x, & \frac{1}{2}-y, & \frac{1}{2}+z \\ \frac{1}{2}-x, & \frac{1}{2}+y, & \frac{1}{2}-z \end{array}$$

The unit cell dimensions were obtained from least squares refinement of 2 θ values of reflections that had been carefully centred in the counter window on the Picker four circle manual diffractometer, using CuK _{α 1} radiation ($\lambda = 1.5405\text{\AA}$). The cell dimensions are a = 13.200(3) \AA , b = 17.328(4) \AA , c = 9.438(2) \AA and $\beta = 92.47(4)^\circ$. The density was determined by

flotation to be 1.347(3) gm/cc which agrees well with the calculated density of 1.342 gm/cc ($Z = 4$, $V = 2156.8\text{\AA}^3$) and is consistent with one molecule per asymmetric unit.

The crystal used in data collection was a prism bound by the faces 010, $0\bar{1}0$, 203, $\bar{2}0\bar{3}$, 212 and $\bar{2}\bar{1}\bar{2}$ with dimensions 0.17 mm x .097 mm x 0.097 mm. It was mounted along a face diagonal, the a^* axis being coincident with the diffractometer ϕ axis. Data was collected manually on the Picker four circle diffractometer using CuK_α X-radiation and a coupled $\omega/2\theta$ scan technique. The angular settings (ϕ , χ , 2θ) were calculated using MIXG2 for unique sections of the reciprocal lattice limited by $\sin \theta/\lambda \leq 0.5$. A scan width of 2 degrees at a scan speed of 2 degrees per minute was employed with a stationary background count of 30 seconds on each side of the scan. The beam was monochromated by means of a graphite crystal (002 reflection). The diffracted beam collimator aperture was 0.5 mm and the pulse height analyser was centred on the CuK_α peak. Intensities were calculated using $I = P - t(B_1 + B_2)$ where P is the peak count, B_1 and B_2 are the background counts and t is the ratio of total time of peak count to total time of background count. Two thousand, two hundred and thirteen unique (hkl

and $h\bar{k}\bar{l}$, h , k and l positive) reflections were measured of which 662 were rejected using the criteria (1) $I \leq 0$, or (2) $I \leq 3\sigma$ where $\sigma = [P + t^2(B_1 + B_2)]^{1/2}$. Lorentz and polarization corrections were applied to the remaining 1551 reflections. Twelve well distributed standard reflections measured at various times throughout the data collection indicated no decomposition of the crystal. The maximum variation was ± 5 sigma. There was no apparent pattern in the peak height variation. Absorption corrections ($\mu_{Cu} = 58.8 \text{ cm}^{-1}$) were applied to the data. Transmission factors ranged from 0.51 to 0.63 with the majority lying close to 0.59.

SOLUTION AND REFINEMENT

The three dimensional Patterson map gave a set of three peaks agreeing with a manganese position of $x = -0.112$, $y = 0.250$ and $z = 0.060$. A further set of peaks gave the position of the silicon atom as $x = -.043$, $y = 0.199$ and $z = -.165$. A structure factor calculation using these co-ordinates returned

$$R_1 = \frac{\sum ||F_o| - |F_c||}{\sum |F_o|} \text{ of } 51.6\% \text{ and } R_2 = \left[\frac{\sum w ||F_o| - |F_c||^2}{\sum w |F_o|^2} \right]^{\frac{1}{2}}$$

of 64.0%. The weights used were calculated from $\sigma(F)$: $w = 1/\sigma(F)^2$ where $\sigma(F) = [P + t^2(B_1 + B_2) + p^2 I]^{\frac{1}{2}}$, $p = .03$. The scattering factors were calculated from Cromer's co-efficients⁵⁰ for all atoms except hydrogen. These were obtained from Mason and Robertson⁵¹. A difference map phased using the manganese and silicon atom positions revealed the location of the two carbonyl groups. A further difference map, phased using the six atoms located gave the positions of all remaining non-hydrogen atoms. After one cycle in which the phenyl groups were treated as rigid bodies and the cyclopentadienyl ring as a hindered rotor, the R factor dropped to $R_1 = 28.6\%$ and $R_2 = 38.9\%$. The starting parameters for the four rings were calculated using MMR with a radius of 1.397\AA for the rigid bodies. At the end of isotropic refinement the R factor was $R_1 = 8.6\%$ and

$R_2 = 10.5\%$. A difference map at this time showed the hydrogen atoms attached to the aromatic rings, the peak heights ranging from $0.76e^{-\circ 3}/\text{\AA}^3$ to $0.38e^{-\circ 3}/\text{\AA}^3$. These were added as rigid bodies with the same orientation and centre of gravity as the carbon rings to which they were bonded and with a C-H distance of 1.0\AA . The hydrogens on the cyclopentadienyl ring were added as a hindered rotor rather than as a rigid body. The difference map also showed a peak in a bridging position between the manganese and silicon atoms. This peak was of the same magnitude as those of the twenty aromatic hydrogens ($\sim 0.5 e^{-\circ 3}/\text{\AA}^3$) and was the twelfth largest peak on the map. Adding the hydrogen atoms, giving the manganese, silicon and carbonyls anisotropic temperature factors of the form: $\exp(-(\beta_{11}h^2 + \beta_{22}k^2 + \beta_{33}l^2 + \beta_{12}hk + \beta_{13}hl + \beta_{23}kl))$ and allowing for anomalous dispersion ($\Delta f'_{\text{Mn}} = -0.050$, $\Delta f''_{\text{Mn}} = 2.90$, $\Delta f'_{\text{Si}} = 0.20$ and $\Delta f''_{\text{Si}} = 0.40$) dropped the R factor to $R_1 = 6.2\%$, $R_2 = 7.3\%$ after four cycles. A difference map showed that the peak previously found at the bridging position ($x = -0.009$, $y = 0.248$ and $z = -0.014$) was still present with a peak height of $0.53e^{-\circ 3}/\text{\AA}^3$ and was the second largest peak present. This hydrogen peak is of very similar density to those of the hydrogen peaks

found by Ibers et al.⁵² in the structure $\text{CoH}(\text{N}_2)(\text{P}(\text{C}_6\text{H}_5)_3)_3$. The largest peak was located near the para carbon of a phenyl ring (C44), and since it disappeared on the low angle ($\sin \theta/\lambda \leq 0.30$) difference map, was most likely due to the thermal motion of the phenyl ring. To further check the validity of the hydride peak, difference maps were calculated using various $\sin \theta/\lambda$ data cutoffs ($\sin \theta/\lambda \leq 0.35$, ≤ 0.30 , ≤ 0.25 , and ≤ 0.20). In all four maps, the hydrogen peak was the largest peak on the map and was approximately a factor of two greater than the next highest. The peak positions remained constant on all four maps while its height varied according to the $\sin \theta/\lambda$ cutoff. Table XIV gives the observed and calculated peak heights. The calculations are the same as those of La Placa and Ibers⁵.

The hydridic hydrogen was added as an isotropic atom and allowed to refine. At the same time the carbons in the phenyl rings were refined using the individual atom, anisotropic temperature factor model. Three cycles of refinement gave a final R factor of $R_1 = 4.2\%$ and $R_2 = 4.7\%$. In the final cycle no shift was greater than 1/10 of an e.s.d. A final difference map showed no peak greater than $0.19\text{e}^{-\text{\AA}^3}$

Table XIV
Hydrogen peak as a function of $\sin \theta/\lambda$

$\sin \theta/\lambda$ cutoff(\AA^{-1})	Number of terms in the unique section	$\rho^E (e/\text{\AA}^3)$	$\rho^C (e/\text{\AA}^3)^b$
0.20	149	0.20	0.16
0.25	278	0.29	0.25
0.30	464	0.37	0.34
0.35	703	0.41	0.42
0.50 ^a	1551	0.53	0.53

a full data set

$$b \quad \rho^C = \frac{1}{2\pi^2} \int_0^{s_0} (1+a^2s^2/4)^{-2} \exp(-Bs^2/16\pi^2) s^2 ds$$

$$s = 4\pi \sin \theta/\lambda$$

a = Bohr's radius

or less than $-0.20\text{e}^{-\text{\AA}^3}$.

Table XV lists the observed and calculated structure factor amplitudes; $10|F_o|$ and $10|F_c|$, both in absolute units of electrons. The final positional parameters for the individual atoms are given in Table XVI and their anisotropic temperature factors in Table XVII. Parameters for the hindered rotors are found in Table XVIII. The estimated standard deviations were obtained from the inverse matrix of the final least squares cycle.

Table XV

Observed and calculated structure factor amplitudes
(x 10) in electrons for $(\pi\text{-C}_5\text{H}_5)(\text{OC})_2\text{Mn}(\text{H})\text{Si}(\text{C}_6\text{H}_5)_3$

Table with multiple columns containing numerical data, organized in a grid-like structure. The data appears to be a list of values for various categories, possibly representing a dataset or a series of measurements. The columns are labeled with letters and numbers, and the rows contain numerical values, some with signs (+/-).

Table XVI

Final atom co-ordinates for $(C_5H_5)(OC)_2Mn(H)Si(C_6H_5)_3$

Atom	x	y	z
Mn	-0.1187 (1)	0.2382 (1)	0.0658 (1)
Si	-0.0492 (1)	0.1991 (1)	-0.1567 (1)
C1	-0.0827 (4)	0.3331 (4)	0.1165 (6)
O1	-0.0578 (3)	0.3956 (3)	0.1474 (5)
C2	-0.2109 (4)	0.2782 (3)	-0.0535 (6)
O2	-0.2751 (3)	0.3056 (2)	-0.1262 (5)
C21	-0.1459 (4)	0.1368 (3)	-0.2546 (6)
C22	-0.2167 (5)	0.1689 (3)	-0.3513 (6)
C23	-0.2910 (5)	0.1250 (5)	-0.4210 (7)
C24	-0.2964 (6)	0.0476 (5)	-0.3957 (8)
C25	-0.2278 (7)	0.0136 (4)	-0.3015 (8)
C26	-0.1538 (5)	0.0574 (4)	-0.2314 (6)
C31	-0.0206 (4)	0.2819 (3)	-0.2787 (6)
C32	-0.0198 (4)	0.3590 (3)	-0.2374 (6)
C33	0.0085 (5)	0.4173 (3)	-0.3274 (7)
C34	0.0374 (4)	0.4005 (3)	-0.4615 (7)
C35	0.0382 (4)	0.3247 (4)	-0.5066 (6)
C36	0.0096 (4)	0.2661 (3)	-0.4157 (6)
C41	0.0721 (4)	0.1415 (3)	-0.1424 (6)
C42	0.0997 (5)	0.9020 (3)	-0.2512 (6)
C43	0.1950 (6)	0.0545 (4)	-0.2480 (8)
C44	0.2608 (5)	0.0676 (4)	-0.1333 (10)
C45	0.2378 (5)	0.1154 (4)	-0.0260 (8)
C46	0.1435 (4)	0.1515 (3)	-0.0306 (7)
H1	-0.0132 (32)	0.2467 (23)	0.0020 (45)

Table XVIII
 (a) Rigid body and hindered rotor parameters

Ring	x	y	z	B	Bd	R	D	E	ξ
1	-.2218	.0917	-.3253			2.392	3.313	2.469	4.785
2	.0088	.3414	-.3717			2.392	3.233	1.263	3.319
3	.1678	.1040	-.1389			2.392	2.257	2.480	6.524
4	-.1448(2)	.1654(1)	.1906(3)	3.91(8)	3.36(28)	1.203(2)	2.351(3)	2.849(3)	4.461(3)
5	-.1448	.1654	.1903	3.91	3.36	2.203	2.351	2.849	4.461

The parameters for which no estimated errors are given were not refined.

Table XVIII
(Contd.)

(b) Derived positional parameters for hindered rotors and rigid bodies

Ring	Atom	x	y	z
1	H22	-.2128	.2274	-.3701
	H23	-.3415	.1510	-.4899
	H24	-.3505	.0152	-.4451
	H25	-.2308	-.0440	-.2805
	H26	-.1021	.0324	-.1607
2	H32	-.0427	.3657	-.1358
	H33	.0051	.4708	-.2833
	H34	.0566	.4465	-.5192
	H35	.0603	.3171	-.6076
	H36	.0126	.2119	-.4600
3	H42	.0490	.0831	-.3347
	H43	.2109	.0199	-.3283
	H44	.3297	.0408	-.1325
	H45	.2867	.1249	.0569
	H46	.1248	.1881	.0505
4	C11	-.1412	.2126	.2839
	C12	-.2287	.1915	.2007
	C13	-.2002	.1343	.1036
	C14	-.0952	.1207	.1267
	C15	-.0587	.1685	.2381
5	H11	-.1383	.2519	.3614
	H12	-.2985	.2132	.2091
	H13	-.2463	.1084	.0312
	H14	-.0538	.0824	.0736
	H15	.0129	.1710	.2777

RESULTS

The molecular geometry and the numbering system used is shown in Figure 16, while the geometry of the manganese atom is shown in Figure 17. The molecular packing as viewed down the c axis is depicted in Figure 18. The drawings were made using the programme ORTEP. Table XIX gives the bond lengths and angles within the molecule. Some intermolecular contacts are listed in Table XX. The results and estimated errors associated with them were calculated using the programme ORFFE2.

Figure 16

Molecular structure of $(\pi\text{-C}_5\text{H}_5)(\text{OC})_2\text{Mn}(\text{H})\text{Si}(\text{C}_6\text{H}_5)_3$

Figure 17

Geometry around manganese atom

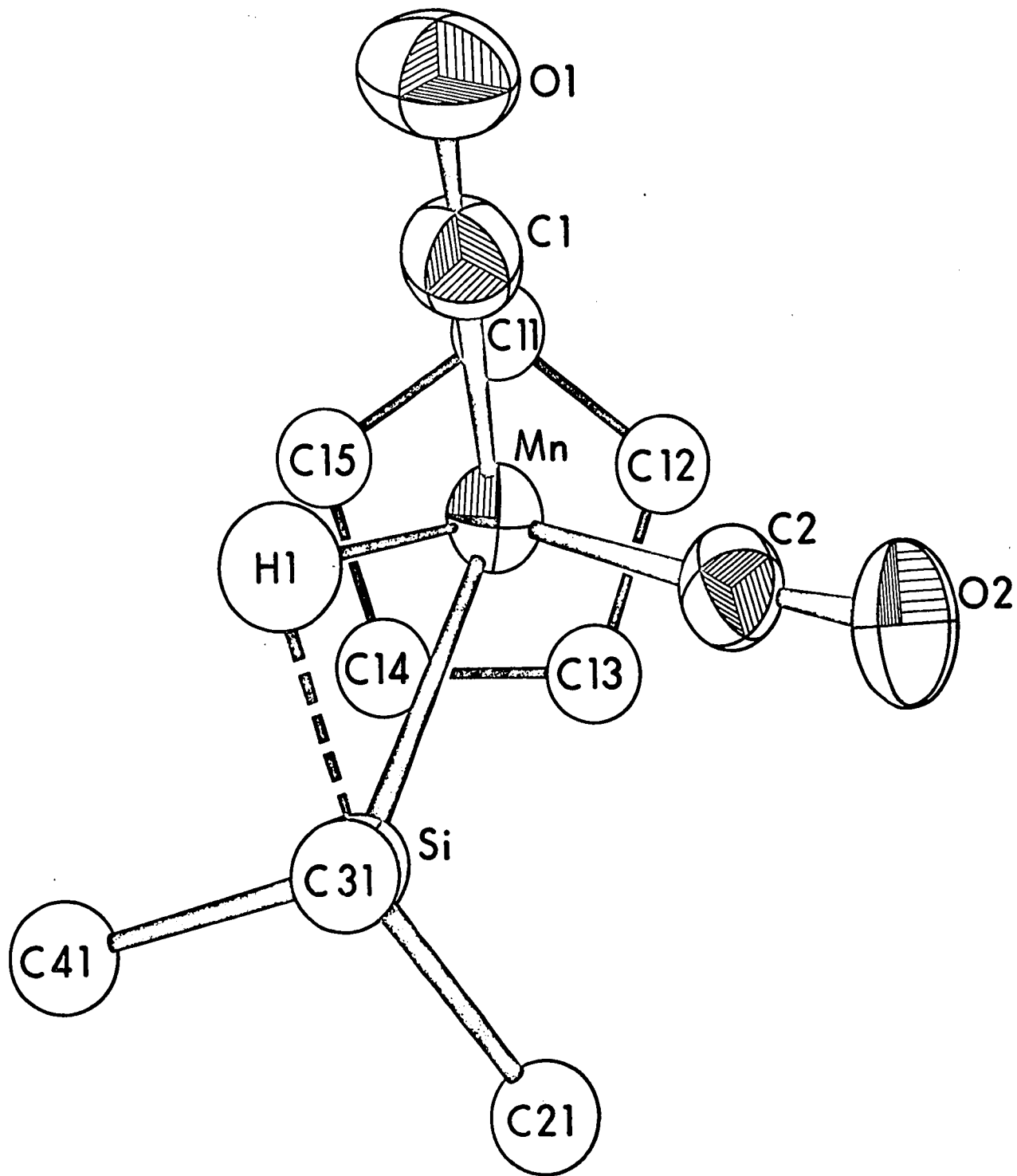


Figure 18

Molecular packing projected onto ab plane

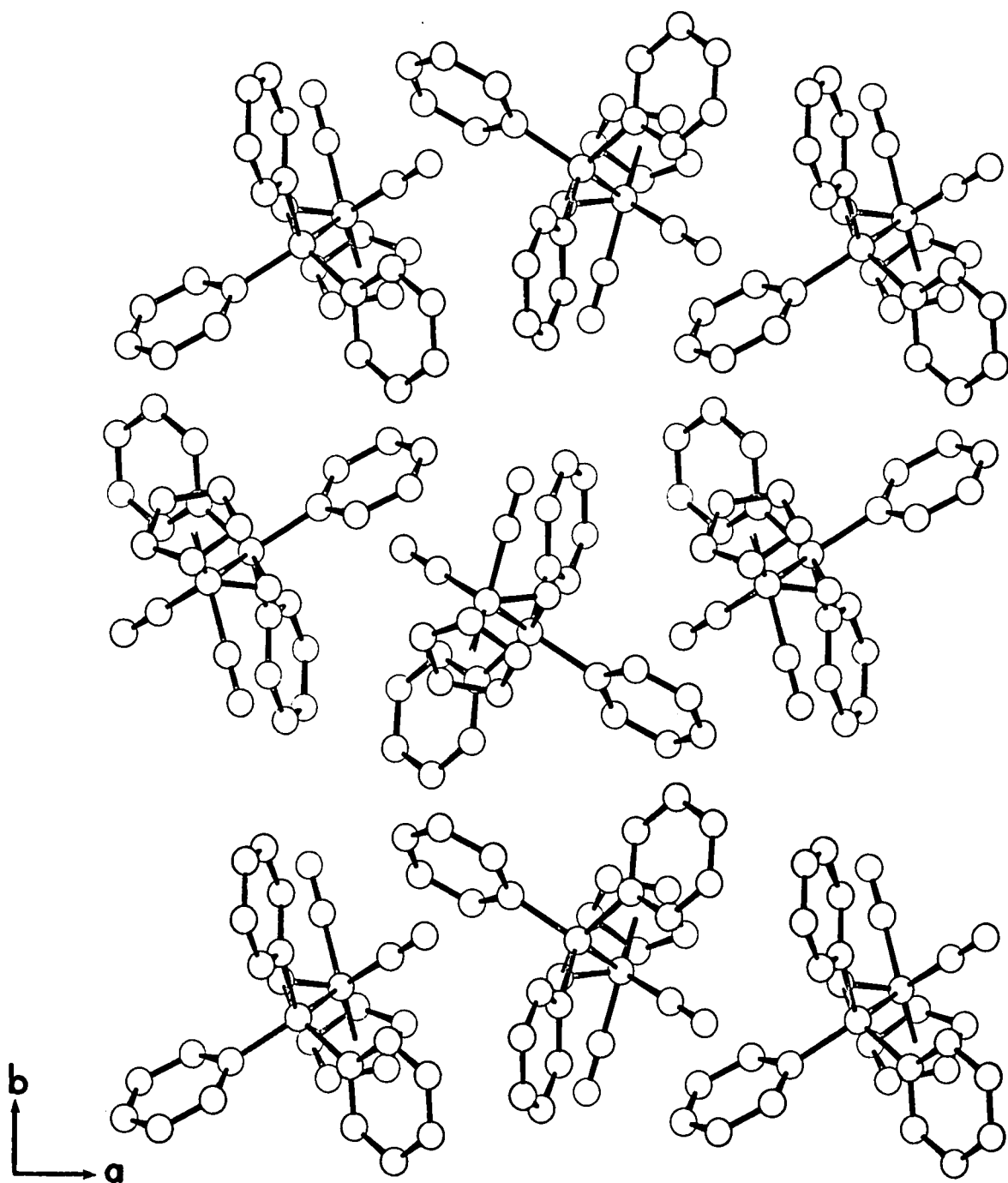
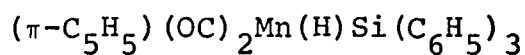


Table XIX

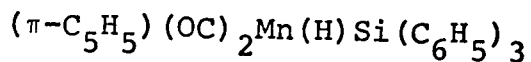
(a) Bond lengths (Å) in



Mn-Si	2.424(2)	C21-C22	1.393(7)
Si-H	1.76(4)	C21-C26	1.398(7)
Mn-H	1.55(4)	C22-C23	1.385(8)
Mn-Cl	1.771(7)	C23-C24	1.365(9)
Mn-C2	1.764(7)	C24-C25	1.374(9)
Cl-O1	1.162(6)	C25-C26	1.384(8)
C2-O2	1.168(6)	C31-C32	1.391(7)
Mn-Cl1	2.140(4)	C31-C36	1.396(7)
Mn-Cl2	2.132(4)	C32-C33	1.382(7)
Mn-Cl3	2.136(4)	C33-C34	1.369(8)
Mn-Cl4	2.146(4)	C34-C35	1.382(8)
Mn-Cl5	2.148(4)	C35-C36	1.392(7)
ave Mn-C	2.140(4)	C41-C42	1.398(7)
Cl1-Cl2	1.414(3)	C41-C46	1.395(7)
Si-C21	1.883(5)	C42-C43	1.415(9)
Si-C31	1.888(5)	C43-C44	1.378(9)
Si-C41	1.886(5)	C44-C45	1.353(9)
Cl-H	2.08(4)	C45-C46	1.391(8)

Table XIX
(Contd.)

(b) Bond angles (degrees) in



Mn-H1-Si	94(2)	C26-C21-C22	116.3(5)
Mn-Si-H1	39(1)	C21-C22-C23	122.3(6)
Si-Mn-H1	46(2)	C22-C23-C24	119.9(6)
C1-Mn-C2	88.7(3)	C23-C24-C25	119.8(6)
Si-Mn-Cp	118.0(1)	C24-C25-C26	120.4(6)
C1-Mn-Cp	122.6(2)	C25-C26-C21	121.4(6)
C2-Mn-Cp	123.7(2)	C36-C31-C32	116.6(5)
H1-Mn-Cp	122.0(1)	C31-C32-C33	122.0(5)
C1-Mn-H	77.0(1)	C32-C33-C34	120.4(5)
C2-Mn-H	109.0(2)	C33-C34-C35	119.5(5)
Mn-Si-C21	108.1(2)	C34-C35-C36	119.9(5)
Mn-Si-C31	114.1(2)	C35-C36-C31	121.6(5)
Mn-Si-C41	115.9(2)	C46-C41-C42	116.2(5)
C21-Si-C31	106.6(2)	C41-C42-C43	121.8(6)
C21-Si-C41	106.7(2)	C42-C43-C44	118.1(6)
C31-Si-C41	104.7(2)	C43-C44-C45	122.3(7)
O1-C1-Mn	178.6(6)	C44-C45-C46	118.8(6)
O2-C2-Mn	176.3(5)	C45-C46-C41	122.9(6)

Table XX

Intermolecular contacts

O1-H33	2.723 (5)	O1-H24	3.038 (5)
O1-H44	2.829 (5)	O1-H35	3.048 (5)
O1-H23	3.288 (5)	O2-H25	2.749 (4)
O2-H15	2.937 (4)	O2-H35	3.049 (4)
O2-H46	3.270 (5)	O2-H36	3.284 (4)
H22-H45	2.646 (1)	H22-H46	2.671 (1)
H22-H11	2.787 (1)	H23-H46	2.849 (1)
H25-H45	2.662 (1)	H33-H34	2.457 (1)
H33-H44	2.647 (1)	H34-H34	2.415 (1)
H34-H44	2.610 (2)	H34-H13	2.796 (1)
H36-H15	2.576 (1)	H36-H11	2.645 (1)

DISCUSSION

A drawing of the compound $(\pi\text{-C}_5\text{H}_5)(\text{OC})_2\text{Mn}(\text{H})\text{Si}(\text{C}_6\text{H}_5)_3$ is found in Figure 16. The geometry about the manganese atom (Figure 17) can be described as a distorted square pyramid and that of the silicon atom as a distorted tetrahedron. The molecule has a hydrogen cis to the silicon and close enough ($1.76(4)\text{\AA}$) to interact with it.

The Si-C(C_6H_5) distances of $1.883(5)\text{\AA}$, $1.888(5)\text{\AA}$ and $1.886(5)\text{\AA}$ are the same within experimental error. There is some distortion from tetrahedral geometry about the silicon atom, the Mn-Si-C(C_6H_5) angles varying from $108.1(2)^\circ$ to $115.9(2)^\circ$ and the C(C_6H_5)-Si-C(C_6H_5) (different rings) from $104.7(2)$ to $106.7(2)$. Angles within the phenyl rings range from $116.3(5)$ at the attached carbons to $122.3(6)$. It will be noticed that in the phenyl rings there is a range in C-C bond lengths from $1.365(9)$ to $1.415(9)\text{\AA}$. This bond length range and distribution is not that expected for a single population of formally identical bond lengths with an estimated standard deviation of 0.008\AA as determined from the least squares refinement. The variation of bond lengths follows a definite pattern, the longest being those close to the silicon-bonded carbon (average 1.395\AA). The shortest, with an average C-C distance of

1.370^oÅ, are those furthest away. A similar pattern was observed by Beauchamp et al.⁵³ and results from the wagging motion of the rings. The apparent shortening of the C-C bond is due to the same effect as discussed in the hindered rotor section; that is, the atoms move along an arc, the centre of which lies near the silicon atom. Attempts to describe the distribution of electron density resulting from such motion by means of anisotropic temperature factors would give an error in the centre of electron density of each atom, and hence in the calculated bond lengths. The greatest apparent shortening would occur between those atoms which have the greatest motion, i.e., CR3-CR4 and CR4-CR5 where R is the number of the ring (R = 2,3,4).

The Mn-C(π -C₅H₅) and Mn-C(CO) distances were not unusual and agree with those of such compounds as (C₆H₇)Mn(CO)₃⁵⁴, (C₁₀H₈)Mn₂(CO)₆⁵⁵, (π -C₅H₅)Mn(CO)₃²⁴ and [(π -C₅H₄CH₃)Mn(CO)₂]₂C₆H₄(As(CH₃)₂)₂⁵⁶, as can be seen in Table XXI. The variations, where significant, are consistent with the trends that would be predicted on the basis of the relative π acceptor properties of the other ligands present. In all these compounds the carbonyl groups lie trans to a delocalized π system. One would expect that the

Table XXI
Comparison of bond lengths

Molecule	Mn-C(π -C ₅ H ₅)	Mn-C(CO)	C-O
this work			
(π -C ₅ H ₅)Mn(CO) ₃	2.140 (4)	1.767 (7)	1.165 (6)
(C ₁₀ H ₈ Mn ₂ (CO) ₆)	2.16 (2)	1.80 (2)	1.15 (3)
(C ₆ H ₇)Mn(CO) ₃	2.169 (4)	1.803 (5)	1.151 (6)
[(π -C ₅ H ₄ CH ₃)Mn(CO) ₂] ₂ diars	2.141(9) to 2.219(7)	1.788(6)	1.157(8)
	2.15(3)	1.77(3)	

Mn-C(O) distances trans to other carbonyls would be longer than those trans to π -ring systems. This more dramatic demonstration of the trans effect can be seen in such compounds as $\text{HMn}(\text{CO})_5$ ⁵⁷, $(\text{CO})_4\text{Mn}(\text{H})(\text{P}(\text{C}_6\text{H}_5)_2)_2\text{Mn}(\text{CO})_4$ ⁵⁸, $\text{Mn}_2(\text{CO})_{10}$ ⁵⁹, and $\text{HRe}_2\text{Mn}(\text{CO})_{14}$ ⁶⁰ in which Mn-C distances trans to carbonyl groups are longer (Table XXII).

The Mn-Si bond length of $2.424(2)\text{\AA}$ ^o lies between that found in $(\text{OC})_4\text{Mn}(\text{Si}(\text{C}_6\text{H}_5)_2)_2\text{Mn}(\text{CO})_4$ ⁶¹ of 2.40\AA ^o and that of $2.497(5)\text{\AA}$ in $\text{Mn}(\text{Si}(\text{CH}_3)_3)(\text{CO})_5$ ⁶². It is significantly shorter than the calculated single bond distance of 2.56\AA ^o (using 1.17\AA ⁶³ for the radius of silicon and 1.39\AA ⁶⁴ for manganese), and would suggest some double bond character between the manganese and silicon.

The most exciting part of the work is the location of the bridging hydrogen. It lies in an otherwise empty space between the manganese and silicon atoms, and as described earlier was found to be the highest peak on all low angle difference maps. It is bonded to the manganese with a distance of $1.55(4)\text{\AA}$ ^o or ca 1.62\AA ^o when corrected for the use of a spherical electron distribution⁶⁵. This is close to the terminal Mn-H distance of 1.60\AA ^o found by neutron diffraction techniques in $\text{HMn}(\text{CO})_5$ ⁵⁷, $1.60(12)\text{\AA}$ ^o in $\text{RhH}(\text{CO})(\text{P}(\text{C}_6\text{H}_5)_3)_3$ ⁴

Table XXII
Comparison of bond lengths

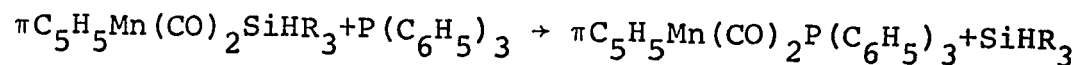
Molecule	Mn-C trans to carbonyl	Mn-C not trans to carbonyl
$\text{HMn}(\text{CO})_5$	1.836(5)	1.821(9)
$\text{Mn}_2(\text{CO})_{10}$	1.830(8)	1.792(14)
$(\text{CO})_4\text{Mn}(\text{H})(\text{P}(\text{C}_6\text{H}_5)_2)_2\text{Mn}(\text{CO})_4$	1.840(9)	1.788(9)
$\text{HRe}_2\text{Mn}(\text{CO})_{14}$	1.840(15)	1.80(3)

and 1.6(1) in $\text{CoH}(\text{N}_2)(\text{P}(\text{C}_6\text{H}_5)_3)_3$ ⁵², the latter two being done using X-ray methods. The Si-H distance of 1.76(4)Å, although considerably longer than the Si-H bond distance of 1.48Å in SiH_4 ⁶⁶, is much shorter than would be expected for a normal Si-H intramolecular contact. Because silicon has a larger radius than carbon, one would expect the C····H contact to be less than that of Si····H. This is not the case, Cl-H being 2.08(4)Å and Si-H being 1.76(4)Å. This would suggest an interaction between the Si-H and formation of a weak bond. A similar type of interaction was found in $\text{bipy}(\text{OC})_3\text{ClMoSnCH}_3\text{Cl}_2$ ⁶⁷ in which the Sn-Cl distance of 2.805(4)Å was longer than would be expected for a bridging chlorine distance, but much shorter than Van der Waals distance (4.0Å). The bond length evidence would suggest a bent 3 centre, 2 electron bond $\left[\text{Mn} \begin{array}{c} \text{H} \\ \diagup \quad \diagdown \\ \text{Si} \end{array} \right]$ with the predominant atomic orbitals lying on the manganese and hydrogen atoms.

The presence of such a bridge would help to explain the different spectral and kinetic properties observed between this compound and the trihalogenated silyl derivatives. In the structure of $(\pi\text{-C}_5\text{H}_5)(\text{OC})\text{Fe}(\text{H})(\text{SiCl}_3)_2$ ⁶⁸, the hydrogen atom was not located. However, if an Fe-H distance of ca 1.6Å is assumed, the hydrogen atom lying midway between the Si's and ca 120° from

Fe-Centre (ring), then one would obtain a Si-H distance of 2.3Å. This is greater than the Cl····H distance of 2.08(4)Å and implies that there is no $\text{Fe}-\overset{\text{H}}{\text{Si}}$ bridge. The more electronegative chlorines pull sufficient electron density from the silicon to destroy any Si-H interaction. Alternatively, taking the electrostatic view of the hydrogen bond $\overset{\delta-}{\text{X}}-\overset{\delta+}{\text{H}}\cdots\overset{\delta-}{\text{Y}}$, the requirement is that the Y group (in this case silicon) have a partial negative charge. In SiCl_3 , the highly electronegative chlorine would be expected to produce a slight positive charge on the silicon, which while improving the electron acceptor properties as far as transition metal interactions were concerned, would reduce the ability to hydrogen bond. It would thus appear that the difference in physical properties of the two types of compound is due, in part at least, to the presence or lack of a bridging hydrogen. The chlorinated silyl compounds have a terminal M-H bond and clearly show this in the infrared. The phenyl substituted silyl class have a Mn-H bond that is close to, but not exactly the same as, a terminal bond. This difference, due to the Si····H interaction, could help to explain the lack of a peak in the infrared M-H terminal region, but the appearance of a weaker peak in the Raman.

The preliminary results of a kinetic study⁶⁹ of the displacement of a silane by a phosphine, which may be represented by the following general chemical equation:



may be rationalized in terms of the structural results reported here. In the case of the triphenyl silyl derivative, the dominant reaction proceeds via an initial dissociation in which triphenyl silane is eliminated and the second step involves very rapid phosphine attack on the electron deficient species $\pi\text{C}_5\text{H}_5\text{Mn}(\text{CO})_2$. The reaction is the first order in transition metal complex and zero order with respect to phosphine. However, for the trichlorosilyl derivative the main reaction is found to be bimolecular. The formation of a weak silicon hydrogen bond corresponds to a partial activation of the leaving group and significant formation of the silicon hydrogen bond in the trichlorosilyl derivative occurs only with the involvement of the entering phosphine ligand.

Chapter IV

THE CRYSTAL STRUCTURE OF DIHYDROOCTACARBONYL DIRHENIUM

INTRODUCTION

There has been great interest lately in the bonding and geometry of M-H-M bridges. The presence of the hydrogen should result in a lengthening of the M-M distance, since a 2 electron/3 centre bond is postulated. This was observed in the structure of $\text{HRe}_2\text{Mn}(\text{CO})_{14}$ ⁶⁰ in which a Re-Re distance of 3.39\AA was found. This is longer than the Re-Re distance of 2.96\AA to 3.02\AA found in such structures as $\text{Re}_4(\text{CO})_{16}$ ⁷⁰. A similar result was found by Dahl in the structure of $(\text{HCr}_2(\text{CO})_{10})$ ⁷¹. In this molecule a Cr-Cr distance of 3.41\AA was obtained. If a linear, symmetrical M-H-M bond is assumed, both compounds have a M-H distance of 1.70\AA which is similar to the neutron diffraction result of $1.68(1)\text{\AA}$ for Re-H in ReH_9 ⁷². It should also be possible to have a bent M-H-M bridge. One would then expect a M-M bond shorter than that found in the linear bridge, but longer than that in the unbridged M-M bond. This has been found in such structures as $(\text{H}_2\text{Re}_3(\text{CO})_{12})^-$ ⁷³ in which bridged Re-Re distances of $3.181(7)\text{\AA}$ and $3.173(7)\text{\AA}$ were found, and in $(\text{H}_6\text{Re}_4(\text{CO})_{12})^-$ ⁷⁴ having an average Re-Re distance of $3.160(7)\text{\AA}$. Having established a pattern for single bridged metal-metal bonds, one wonders what

would occur in doubly hydrogen bridged bonds such as occur in $\text{H}_2\text{Re}_2(\text{CO})_8$ and $\text{H}_2\text{Os}_3(\text{CO})_9$ ⁷⁵. These bridges are now 4 centre rather than 3 centre systems. Bonding schemes such as protonated metal-metal double bonds (M=M) have been suggested as well as a 4 centre delocalization of electrons. In an attempt to understand the bonding in such systems, the crystal structure of $\text{H}_2\text{Re}_2(\text{CO})_8$ was undertaken.

EXPERIMENTAL

The compound $\text{H}_2\text{Re}(\text{CO})_8$, molecular weight 598.4 gm/mole, was prepared by J.K. Hoyano and was recrystallized from a mixture of dichloromethane and hexane to obtain crystals suitable for single crystal X-ray diffraction studies. The yellow crystals were mounted parallel to the elongated edge of the crystal. Rotation, Weissenberg ($0k\ell$, $h0\ell$ - $h7\ell$, $hk0$ - hkl) and precession ($h0\ell$, $0k\ell$) photographs showed the crystal to be monoclinic with systematic absences $h0\ell$: $\ell = 2n+1$ and $0k0$: $k = 2n+1$, fixing the space group at $P2_1/c$. The unit cell was found to be $a = 8.96(2)\text{\AA}$, $b = 11.62(2)\text{\AA}$, and $c = 12.85(2)\text{\AA}$, $\beta = 109.2(1)^\circ$ from precession and Weissenberg photographs⁷⁶. The density was determined experimentally by means of flotation in a solution of Clerici's Reagent and water to be 3.16 gm/cc which agreed with the calculated density of 3.18(2) gm/cc for four molecules per unit cell. This would require that the molecules lie in general positions in the unit cell. Data within the 1.0\AA sphere were collected on the PAILRED automatic diffractometer using Weissenberg geometry and a moving crystal/stationary counter technique (ω scan). The hexagonal crystal was mounted along the b axis, and 13 layers ($h0\ell$ - $h12\ell$) were collected

using MoK_α -radiation. The X-ray beam was monochromated using a graphite single crystal (002 reflection). A scintillation counter, aperture 2.5° , was used, with the pulse height analyser centred on the MoK_α peak and set to accept 90% of the peak. A half scan of 1.5° for the inner reflections ($\sin \theta/\lambda \leq 0.20$) and 1.0° for the outer reflections was used at a scan speed of $2.5^\circ/\text{min}$. The scan widths were increased to 2.0° and 1.5° for inner and outer reflections for the higher levels. The peak was scanned three times or until the peak count passed 4,000 counts. A stationary background was counted for twenty seconds on each side of the scan. Because the crystal was found to decompose in light, and to a lesser extent in radiation, the data were collected in a darkened room. Twelve standard reflections were measured at the end of each layer and a decomposition correction applied as a function of time and $\sin \theta/\lambda$. The intensities were calculated using $I = P - t(B_1 + B_2)$ where P is the peak count, B_1 , B_2 the background count, and t is the ratio of peak count time to that of total background. Four hundred and twenty-two reflections were rejected using the criteria (1) $I = 0$ and (2) $I \leq 3\Delta I$ where $\Delta I = (P + t^2(B_1 + B_2))^{\frac{1}{2}}$. Absorption corrections were applied ($\mu(\text{Mo}) = 217.\text{cm}^{-1}$, max crystal dimensions: $.14 \text{ mm} \times .11 \text{ mm} \times .14 \text{ mm}$, mean $\mu r = 1.4$).

SOLUTION AND REFINEMENT

The positions of the rhenium atoms were obtained from a three dimensional Patterson map as Re1:

x = 0.295, y = 0.130, z = 0.273 and Re2: x = -0.046, y = 0.130, z = 0.180. A structure factor calculation

using the form factors calculated from Cromer's coefficients⁵⁰ gave reliability factors of $R_1 =$

27.9%, $R_2 = 31.3\%$, where $R_1 = \frac{\sum ||F_o| - |F_c||}{\sum |F_o|}$,

$$R_2 = \left[\frac{\sum w (|F_o| - |F_c|)^2}{\sum w |F_o|^2} \right]^{\frac{1}{2}}, \quad w = 1/\sigma(F)^2 \quad \text{and} \quad \sigma(F) =$$

$(P + t^2(B_1 + B_2) + p^2I)^{\frac{1}{2}}, \quad p = 0.06.$ A difference map phased by the two rhenium atoms gave the positions of

all other non-hydrogen atoms. Four cycles of full matrix least squares refinement, minimizing the

function $\sum w (|F_o| - |F_c|)^2$ with all atoms isotropic, reduced the R factors to $R_1 = 16.0\%$ and $R_2 = 20.4\%$.

It was noticed that four layers (h1l, h2l, h3l and h9l) had much higher R factors (of the order of 20%)

than the others (~10%). For this reason, data for these layers were recollected using a second crystal of similar dimensions (.12 mm x .13 mm x .10 mm).

The data were treated as for the first crystal, corrected for absorption and combined with the previous

data using a second scale factor. Inclusion of the anomalous dispersion corrections for rhenium ($\Delta f' = -1.40$, $\Delta f'' = 7.70$) in the calculated structure factors and further refinement dropped the reliability factors to $R_1 = 10.3\%$, $R_2 = 12.0\%$. A difference map at this point showed peaks of 3 - 4 electrons near each of the rheniums, suggesting an error in the absorption correction. Since any anisotropic refinement would be meaningless for this reason, and also because of the large decomposition correction (~30%) applied, refinement was terminated at this point. In the final cycle, all atoms isotropic, no shift was greater than 1/10 the corresponding e.s.d. The observed and calculated structure factor amplitudes (x10) are listed in Table XXIII. The positional parameters and temperature factors are given in Table XXIV.

Table XXIII

Observed and calculated structure factor
amplitudes ($\times 10$) in units of electrons

K	L	FO	FC	K	L	FO	FC	K	L	FO	FC	K	L	FO	FC	K	L	FO	FC	K	L	FO	FC								
0	4	1755	1830	3	8	1177	1082	3	7	793	736	2	11	1113	1337	1	7	1771	1818	0	6	1828	1847	3	-3	2544	1814	0	4	1418	1314
0	8	735	747	3	10	1042	986	3	0	817	720	2	11	1144	1052	1	5	1505	1553	0	-	827	932	3	-3	1342	1154	0	0	641	683
0	12	451	420	3	11	716	802	3	12	455	489	2	-1	454	372	1	9	1237	1318	0	-8	1545	1545	3	-12	814	807	0	-6	767	877
0	14	875	747	3	13	1622	1575	3	-4	1372	1200	2	-5	980	889	0	-10	1664	1672	3	-14	788	845	0	-8	837	784				
1	1	1774	1215	3	-3	2748	2755	3	-6	1584	1133	2	-7	1275	1220	1	-2	1546	1742	0	-2	162	164	2	0	1281	1474				
1	4	955	1212	3	-5	2351	2355	3	-7	1649	1731	2	-11	1043	1423	1	-3	1662	1536	4	6	516	581	0	-4	953	817				
1	6	378	485	3	-1	1718	1435	3	-8	1549	1433	1	5	0	2312	2015	1	-4	2173	2373	1	3	911	645	1	1	1141	1132			
1	7	455	663	3	-4	792	701	4	2	1558	1418	3	2	2328	2104	1	-8	926	903	4	15	0	1237	1	5	971	758				
1	8	1420	1374	4	1	557	539	4	4	2373	2533	3	7	946	889	1	-11	736	623	1	-4	1076	827	4	15	0	1047				
1	10	1436	1870	4	4	2602	2246	4	6	476	805	3	3	1932	1816	1	-11	736	623	1	-5	1824	1843	4	-2	1351	870				
1	11	1240	1733	4	8	2232	2310	4	12	1295	1229	3	7	940	889	1	-9	1403	1614	1	-9	2410	2425	5	0	2076	1977				
1	12	1635	1621	4	11	1106	1127	4	15	0	1023	3	7	946	877	1	-14	971	1084	1	-9	1842	1845	5	1	1811	1750				
1	13	710	958	4	-1	1067	1293	4	0	755	404	3	10	1032	1152	1	-10	826	927	5	2	1353	1285	1	-10	1761	1510				
1	-2	1165	1215	4	-2	1125	1464	4	-1	762	885	3	15	0	1206	2	3	1257	1290	2	3	936	812	2	1	2064	1841				
1	-3	187	832	4	-3	1274	1482	4	-5	674	794	3	15	0	1206	2	3	1257	1290	2	3	936	812	2	1	2064	1841				
1	-4	1291	1212	4	-4	1027	1285	4	-6	427	461	3	-1	1488	1362	2	5	1640	1711	2	3	2330	2341	5	-2	401	463				
1	-5	875	665	4	-5	1004	1218	4	-6	1648	1376	3	-3	1019	777	2	-1	943	1045	2	-1	1173	1166	5	-3	871	1115				
1	-6	1005	1100	4	-6	1255	55	4	-7	2543	2482	3	-5	1120	1079	2	-5	2854	2543	2	-11	1794	1194	6	3	729	637				
1	-7	1816	1803	4	-7	889	782	4	-7	2671	2835	3	-10	1220	1131	2	-5	1249	1213	3	0	944	902	7	7	742	778				
1	-8	1622	1875	4	-8	854	463	4	4	1491	1464	3	-11	1596	1456	2	-13	746	823	3	1	1544	1312	7	0	1495	1674				
1	-9	1454	1403	4	-8	981	738	4	5	1438	1545	3	-12	1407	1370	3	3	981	959	3	3	847	574	7	-1	1162	1031				
1	-10	1268	1421	4	-9	938	866	4	6	1198	1195	3	-13	1607	1584	3	5	1156	1143	3	-4	1415	1294	7	-2	528	465				
1	-11	1454	1403	4	-9	814	801	4	-1	732	824	3	-14	1407	1370	3	5	1156	1143	3	-4	1415	1294	7	-2	528	465				
1	-12	1268	1421	4	-10	872	723	4	1	933	1105	3	-15	1277	1244	3	5	1156	1143	3	-4	1415	1294	7	-2	528	465				
1	-13	1454	1403	4	-10	742	718	4	2	1362	1304	3	-16	1407	1370	3	5	1156	1143	3	-4	1415	1294	7	-2	528	465				
1	-14	1454	1403	4	-11	814	801	4	-1	732	824	3	-17	1407	1370	3	5	1156	1143	3	-4	1415	1294	7	-2	528	465				
1	-15	1454	1403	4	-11	814	801	4	-1	732	824	3	-17	1407	1370	3	5	1156	1143	3	-4	1415	1294	7	-2	528	465				
1	-16	1454	1403	4	-12	814	801	4	-1	732	824	3	-17	1407	1370	3	5	1156	1143	3	-4	1415	1294	7	-2	528	465				
1	-17	1454	1403	4	-12	814	801	4	-1	732	824	3	-17	1407	1370	3	5	1156	1143	3	-4	1415	1294	7	-2	528	465				
1	-18	1454	1403	4	-13	814	801	4	-1	732	824	3	-17	1407	1370	3	5	1156	1143	3	-4	1415	1294	7	-2	528	465				
1	-19	1454	1403	4	-13	814	801	4	-1	732	824	3	-17	1407	1370	3	5	1156	1143	3	-4	1415	1294	7	-2	528	465				
1	-20	1454	1403	4	-14	814	801	4	-1	732	824	3	-17	1407	1370	3	5	1156	1143	3	-4	1415	1294	7	-2	528	465				
1	-21	1454	1403	4	-14	814	801	4	-1	732	824	3	-17	1407	1370	3	5	1156	1143	3	-4	1415	1294	7	-2	528	465				
1	-22	1454	1403	4	-15	814	801	4	-1	732	824	3	-17	1407	1370	3	5	1156	1143	3	-4	1415	1294	7	-2	528	465				
1	-23	1454	1403	4	-15	814	801	4	-1	732	824	3	-17	1407	1370	3	5	1156	1143	3	-4	1415	1294	7	-2	528	465				
1	-24	1454	1403	4	-16	814	801	4	-1	732	824	3	-17	1407	1370	3	5	1156	1143	3	-4	1415	1294	7	-2	528	465				
1	-25	1454	1403	4	-16	814	801	4	-1	732	824	3	-17	1407	1370	3	5	1156	1143	3	-4	1415	1294	7	-2	528	465				
1	-26	1454	1403	4	-17	814	801	4	-1	732	824	3	-17	1407	1370	3	5	1156	1143	3	-4	1415	1294	7	-2	528	465				
1	-27	1454	1403	4	-17	814	801	4	-1	732	824	3	-17	1407	1370	3	5	1156	1143	3	-4	1415	1294	7	-2	528	465				
1	-28	1454	1403	4	-18	814	801	4	-1	732	824	3	-17	1407	1370	3	5	1156	1143	3	-4	1415	1294	7	-2	528	465				
1	-29	1454	1403	4	-18	814	801	4	-1	732	824	3	-17	1407	1370	3	5	1156	1143	3	-4	1415	1294	7	-2	528	465				
1	-30	1454	1403	4	-19	814	801	4	-1	732	824	3	-17	1407	1370	3	5	1156	1143	3	-4	1415	1294	7	-2	528	465				
1	-31	1454	1403	4	-19	814	801	4	-1	732	824	3	-17	1407	1370	3	5	1156	1143	3	-4	1415	1294	7	-2	528	465				
1	-32	1454	1403	4	-20	814	801	4	-1	732	824	3	-17	1407	1370	3	5	1156	1143	3	-4	1415	1294	7	-2	528	465				
1	-33	1454	1403	4	-20	814	801	4	-1	732	824	3	-17	1407	1370	3	5	1156	1143	3	-4	1415	1294	7	-2	528	465				
1	-34	1454	1403	4	-21	814	801	4	-1	732	824	3	-17	1407	1370	3	5	1156	1143	3	-4	1415	1294	7	-2	528	465				
1	-35	1454	1403	4	-21	814	801	4	-1	732	824	3	-17	1407	1370	3	5	1156	1143	3	-4	1415	1294	7	-2	528	465				
1	-36	1454	1403	4	-22	814	801	4	-1	732	824	3	-17	1407	1370	3	5	1156	1143	3	-4	1415	1294	7	-2	528	465				
1	-37	1454	1403	4	-22	814	801	4	-1	732	824	3	-17	1407	1370	3	5	1156	1143	3	-4	1415	1294	7	-2	528	465				
1	-38	1454	1403	4	-23	814	801	4	-1	732	824	3	-17	1407	1370	3	5	1156	1143	3	-4	1415	1294	7	-2	528	465				
1	-39	1454	1403	4	-23	814	801	4	-1	732	824	3	-17	1407	1370	3	5	1156	1143	3	-4	1415	1294	7	-2	528	465				
1	-40	1454	1403	4	-24	814	801	4	-1	732	824	3	-17	1407	1370	3	5	1156	1143	3	-4	1415	1294	7	-2	528	465				
1	-41	1454	1403	4	-24	814	801	4	-1	732	824	3	-17	1407	1370	3	5	1156	1143	3	-4	1415	1294	7	-2	528	465				
1	-42	1454	1403	4	-25	814	801	4	-1	732	824	3	-17	1407	1370	3	5	1156	1143	3	-4	1415	1294	7	-2	528	465				
1	-43	1454	1403	4	-25	814	801	4	-1	732	824	3	-17	1407	1370	3	5	1156	1143	3	-4	1415	1294								

Table XXIV

Positional parameters for $\text{H}_2\text{Re}_2(\text{CO})_8$

Atom	x	y	z	Isotropic B
Re1	.2948(2)	.1289(2)	.2691(1)	1.69(5)
Re2	-.0467(2)	.1190(2)	.1800(2)	1.80(5)
C1	.2948(78)	.2262(53)	.1432(50)	2.6(11)
O1	.3114(65)	.2936(42)	.0798(41)	4.0(10)
C2	.4701(67)	.0340(48)	.2412(43)	1.8(9)
O2	.5621(65)	-.0183(40)	.2354(40)	3.8(9)
C3	.4502(65)	.2249(42)	.3710(43)	1.7(9)
O3	.5460(64)	.2812(43)	.4340(41)	4.0(10)
C4	.2994(71)	.0220(47)	.3921(46)	2.1(10)
O4	.3135(69)	-.0325(48)	.4675(46)	2.0(10)
C5	-.0512(85)	.0178(56)	.3111(55)	3.0(13)
O5	-.0721(61)	-.0365(40)	.3680(41)	3.7(9)
C6	-.2190(88)	.2035(56)	.2005(54)	3.0(12)
O6	-.3072(59)	.2611(40)	.2199(38)	3.4(9)
C7	-.1934(95)	.0163(61)	.0827(58)	3.6(13)
O7	-.2868(76)	-.0499(51)	.0298(48)	5.3(12)
C8	-.0451(73)	.2144(51)	.0457(48)	2.3(10)
O8	-.0743(73)	.2576(50)	-.0362(49)	5.1(12)

RESULTS

A drawing of the molecule is shown in Figure 19, giving the numbering scheme used. The diagram was drawn using the Calcomp plotter and Carroll K. Johnson's programme ORTEP. The bond lengths and angles within the molecule are found in Table XXV, while Table XXVI gives some intermolecular contacts. These distances and their associated errors were calculated using ORFFE2.

Figure 19

View of $\text{H}_2\text{Re}_2(\text{CO})_8$ down b axis

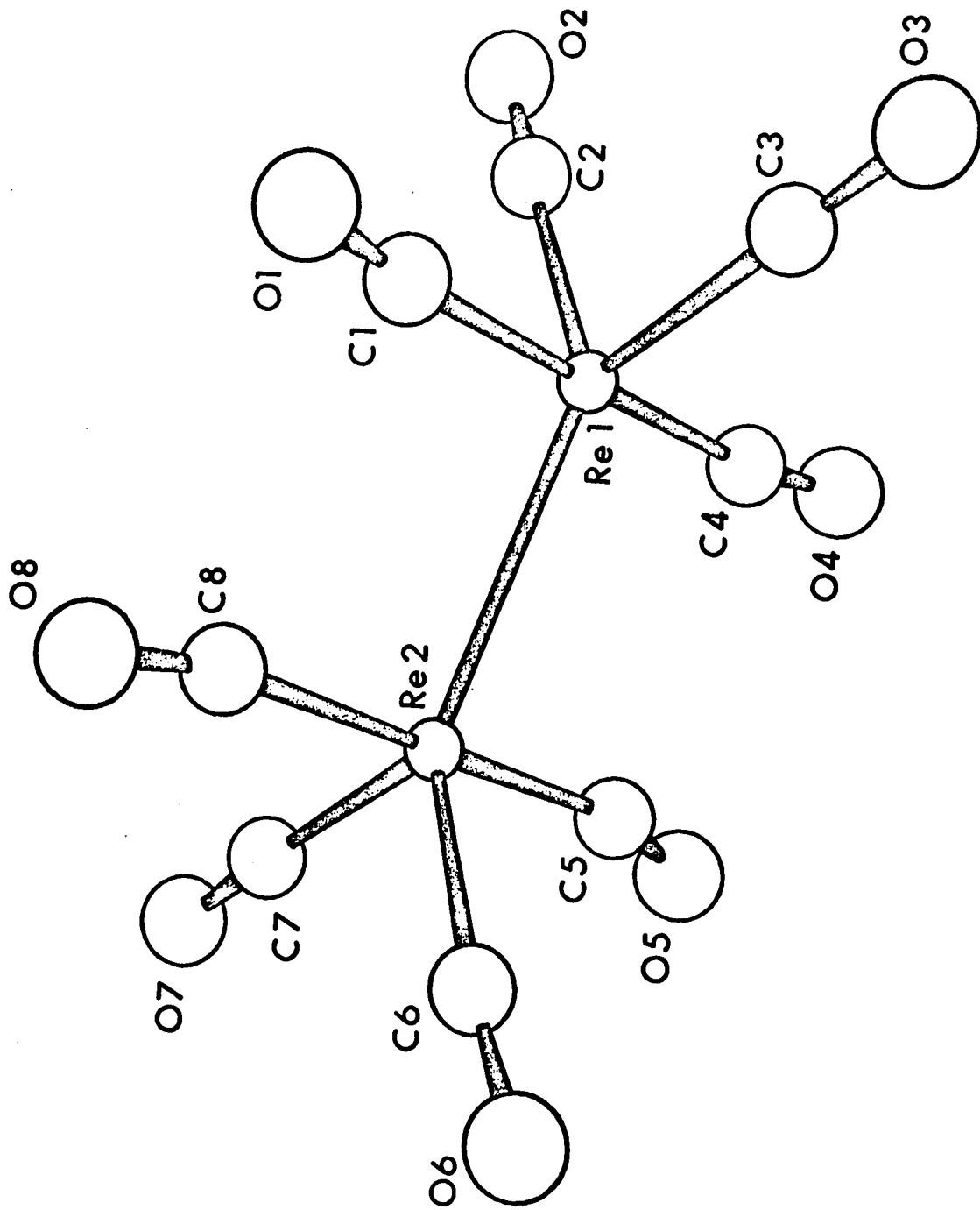


Table XXV

(a) Bond lengths (\AA) in $\text{H}_2\text{Re}_2(\text{CO})_8$

Re1-Re2	2.896(3)	C1-O1	1.17(7)
Re1-C1	1.97(6)	C2-O2	1.05(7)
Re1-C2	2.05(6)	C3-O3	1.17(7)
Re1-C3	1.92(5)	C4-O4	1.13(8)
Re1-C4	2.00(6)	C5-O5	1.03(7)
Re2-C5	2.06(7)	C6-O6	1.13(8)
Re2-C6	1.92(7)	C7-O7	1.17(9)
Re2-C7	1.91(7)	C8-O8	1.12(7)
Re2-C8	2.06(6)		

(b) Bond angles in $\text{H}_2\text{Re}_2(\text{CO})_8$

C1-Re1-C2	87.(2)	C5-Re2-C6	87.(3)
C1-Re1-C4	176.(2)	C5-Re2-C8	178.(2)
C2-Re1-C3	90.(2)	C6-Re2-C7	90.(3)
C3-Re1-C4	90.(2)	C7-Re2-C8	89.(3)
C1-Re1-Re2	89.(2)	C5-Re2-Re1	90.(2)

(c) Intramolecular non-bond contacts

C1-C8	2.89(9)	C4-C5	2.97(10)
O1-O8	3.31(8)	O4-O5	3.27(8)
C1-C2	2.78(8)	C5-C6	2.74(9)
C2-C3	2.82(8)	C6-C7	2.70(10)
C3-C4	2.77(7)	C7-C8	2.78(9)

Table XXVI

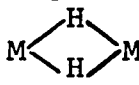
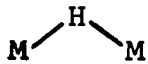
Intermolecular contacts (\AA)

C1-O7	3.40(8)	C2-O7	3.33(8)
C1-O2	3.40(8)	C2-O6	3.37(7)
C1-C7	3.93(9)	C2-C6	3.59(9)
O1-O4	3.13(8)	C2-O4	3.60(8)
O1-O7	3.14(8)	O2-O3	3.12(7)
O1-O5	3.15(7)	O2-O5	3.16(8)
O1-O2	3.15(7)	O2-C3	3.27(7)
O1-O8	3.31(8)	O2-C5	3.30(9)
O1-C8	3.21(8)	O2-C6	3.36(8)
O1-C3	3.32(8)	O2-O7	3.36(8)
O1-O6	3.32(7)	O2-C7	3.41(9)
C3-O4	3.30(7)	O3-O7	3.19(8)
C3-O6	3.38(7)	O3-O4	3.24(8)
C3-O7	3.44(8)	O3-O8	3.33(8)
C4-O5	3.31(8)	O3-O6	3.43(7)
C4-O4	3.34(8)	O4-O4	3.26(12)
C4-O6	3.37(7)	O4-O6	3.38(7)
C5-O8	3.31(9)	O5-C8	3.15(7)
C6-O8	3.23(9)	O6-O8	3.15(7)

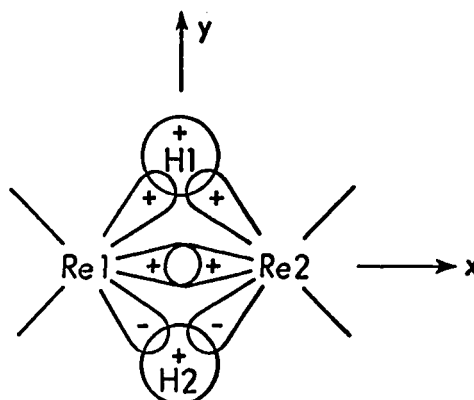
DISCUSSION

The compound $\text{Re}_2\text{H}_2(\text{CO})_8$ shows octahedral geometry about the rhenium atoms if one assumes that the hydrogen atoms occupy the empty region between the Re atoms and complete the octahedron. The molecule as a whole has D_{2h} symmetry, although none is required crystallographically.

There is little deviation from 90° of the C-Re-C angles, the largest being -3.2 degrees. The Re-C bonds range in length from 1.91\AA to 2.06\AA . Those being cis to the hydrogens are longer than those trans (average $2.02(3)\text{\AA}$ as compared to $1.95(4)$). Since the hydrogen-rhenium bond is weaker than rhenium-carbon, the bonds trans to the hydrogen would be stronger than those trans to carbonyl and thus have shorter bond lengths. The hydrogen atoms are assumed to occupy the two remaining octahedral sites. If there is undistorted octahedral symmetry (i.e., H-Re-H of 90°), then a Re-Re distance of $2.896(3)\text{\AA}$ would require a Re-H distance of 2.05\AA . This is rather longer than the average Re-H distance (terminal) in $\text{ReH}_9^{=72}$ of $1.68(1)\text{\AA}$ from neutron diffraction work, and would suggest that there is a slight distortion from octahedral symmetry by the reduction of the H-Re-H angle

in order to shorten the Re-H distance. The Re-H bond length lies between two extremes - 2.05\AA for undistorted octahedral symmetry, and 1.45\AA if the M-H-M unit is linear. Most likely it is close to those found in other Re-H structures of $\sim 1.70\text{\AA}$. This would require a H-Re-H angle of 63° . The Re-Re distance of $2.896(3)\text{\AA}$ is shorter than would be expected for a Re-Re unbridged bond. A Re-Re bond of 3.035\AA was found in $[\text{H}_2\text{Re}_3(\text{CO})_{12}]^{73}$, 2.96 , 2.96 and 3.02\AA in $\text{Re}_4(\text{CO})_{16}^{70}$ and 3.000\AA in $(\text{Si}(\text{C}_6\text{H}_5)_2)_2\text{Re}_2(\text{CO})_8^{77}$. A similar shortening of the metal-metal bond was observed in $\text{H}_2\text{Os}_3(\text{CO})_9^{75}$, also containing a doubly hydrogen bridged Os-Os bond. This shortening of M-M bonds is the opposite to the effect of bond lengthening found in singly bridged bonds, and suggests that the bonding of the  unit is very different from that of the  group.

In order to explain the bonding of the rhenium and hydrogen atoms, a molecular orbital calculation was done. If one considers only the rhenium-hydrogen unit, then the following orbitals can be drawn⁷⁷, assuming no interaction with the carbonyl groups:



It should be borne in mind that such an assumption, as well as the choice of orbitals, can prejudice the results and may invalidate them. Using D_{2h} symmetry, the following orbitals are permitted⁴²:

$$\Gamma_{x^2 - y^2} = A_g + B_{3u}$$

$$\Gamma_H = A_g + B_{2u}$$

$$\Gamma_{xy} = B_{1g} + B_{2u}$$

The orbitals ϕ_1 to ϕ_6 are defined as follows:

ϕ_1	$5d_{x^2 - y^2}$	orbital on Re1
ϕ_2	$5d_{x^2 - y^2}$	orbital on Re2
ϕ_3	1s	orbital on H1
ϕ_4	1s	orbital on H2
ϕ_5	$5d_{xy}$	orbital on Re1
ϕ_6	$5d_{xy}$	orbital on Re2

Then the A_g orbitals can be expressed as

$$\psi'_{A} = \frac{1}{\sqrt{2}} \left(\phi_1 + \phi_2 \right)$$

and
$$\psi''_{A} = \frac{1}{\sqrt{2}} \left(\phi_3 + \phi_4 \right)$$

Symmetry considerations permit that these may combine. Using Hückel molecular orbital theory⁷⁸, the Slater equations may be set up and the determinant obtained:

$$\begin{vmatrix} H_{A'A'} - E & H_{A'A''} \\ H_{A'A''} & H_{A''A''} - E \end{vmatrix} = 0$$

Defining	$\alpha_R = \int \phi_1^{H^0} \phi_1 \partial \tau = \int \phi_2^{H^0} \phi_2 \partial \tau$
$\alpha_{R'} = \int \phi_5^{H^0} \phi_5$	$\alpha_H = \int \phi_3^{H^0} \phi_3 \partial \tau = \int \phi_4^{H^0} \phi_4 \partial \tau$
$= \int \phi_6^{H^0} \phi_6$	$\beta_R = \int \phi_1^{H^0} \phi_2 \partial \tau = \int \phi_2^{H^0} \phi_1 \partial \tau$
$\beta_{R'} = \int \phi_5^{H^0} \phi_6$	$\beta_{R-H} = \int \phi_1^{H^0} \phi_3 \partial \tau = \int \phi_1^{H^0} \phi_4 \partial \tau$
$\beta_{R'H} = \int \phi_6^{H^0} \phi_3$	$= \int \phi_2^{H^0} \phi_3 \partial \tau = \int \phi_2^{H^0} \phi_4 \partial \tau$
$\int \phi_5^{H^0} \phi_3$	$\beta_{H-H} = \int \phi_3^{H^0} \phi_4 \partial \tau = \int \phi_4^{H^0} \phi_3 \partial \tau$

the determinant can then be rewritten as

$$\begin{vmatrix} \alpha_R + \beta_{RR}^{-E} & 2\beta_{R-H} \\ 2\beta_{R-H} & \alpha_H + \beta_{HH}^{-E} \end{vmatrix} = 0$$

If the assumption is made that the overlap between the rhenium and hydrogen atoms is very small, then $\beta_{R-H} \approx 0$ and the expression simplifies to

$$\begin{vmatrix} \alpha_R + \beta_{RR}^{-E} & 0 \\ 0 & \alpha_H + \beta_{HH}^{-E} \end{vmatrix} = 0$$

which can be very easily solved to give

$$E_1 = \alpha_R + \beta_{RR}$$

and $E_2 = \alpha_H + \beta_{HH}$

Similar calculations can be carried out for the other set of orbitals, B_{2u} :

$$\psi'_{B_{2u}} = \frac{1}{\sqrt{2}} \left(\phi_5 + \phi_6 \right) \quad \text{and} \quad \psi''_{B_{2u}} = \frac{1}{\sqrt{2}} \left(\phi_3 - \phi_4 \right)$$

The energies were calculated to be

$$E_3 = \frac{-b + \sqrt{b^2 - 4c}}{2c}$$

and $E_4 = \frac{-b - \sqrt{b^2 - 4c}}{2c}$

where $b = \alpha_{R'} + \beta_{R'} + \alpha_H - \beta_H$

and $c = 4\beta_{R'H}^2 + \alpha_{R'}\alpha_H - \alpha_{R'}\beta_H + \alpha_H\beta_{R'} - \beta_H\beta_{R'}$

If the assumption is made that the β^2 and cross β terms are much smaller than other terms, then E_3 and E_4 can be approximated to

$$E_3 = \alpha_H - \beta_H + \beta_{R'H}$$

and $E_4 = \alpha_{R'} + \beta_{R'} - \beta_{R'H}$

There is only one orbital combination with B_{3u} symmetry:

$$\psi_{B_{3u}} = \frac{1}{\sqrt{2}} \left(\phi_1 - \phi_2 \right)$$

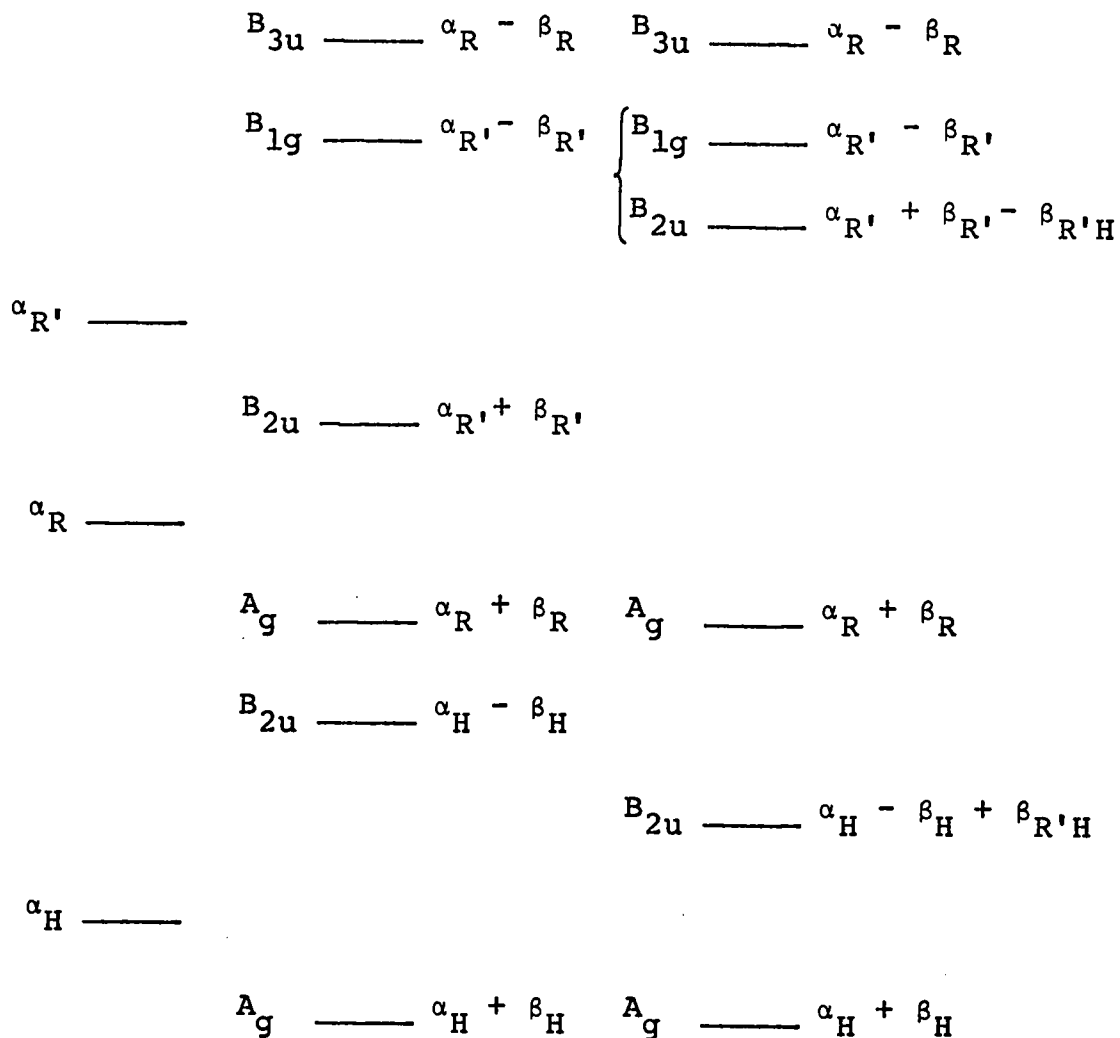
$$E_5 = \alpha_R - \beta_{RR}$$

and one with B_{1g} symmetry:

$$\psi_{B_{1g}} = \frac{1}{\sqrt{2}} \left(\phi_5 - \phi_6 \right)$$

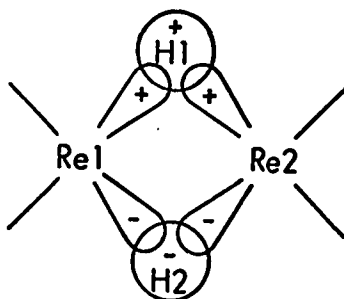
$$E_6 = \alpha_R - \beta_{R'R'}$$

The following energy level diagram will be obtained:

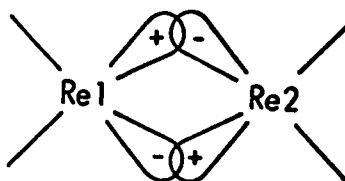


where the order of the levels B_{1g} and the higher B_{2u} is unknown and depends on the relative sizes of $\beta_{R'}$ and $\beta_{R'H}$. If $\beta_{R'H}$ is greater than $2\beta_{R'}$, then B_{1g} will lie below B_{2u} . There are eight electrons which occupy these orbitals so that the bottom four will be filled. The bonding of the Re-H unit will be (1) both A_g orbitals filled (that is, (a) the electrons localized on the

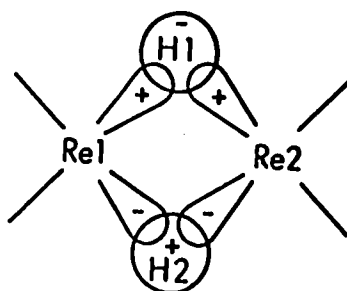
hydrogen atoms, and (b) a Re-Re σ bond), (2) the bonding B_{2u} orbital filled in which the electrons are localized over both rheniums and both hydrogens, forming Re-H bonds:



and (3) one of the antibonding orbitals depending on the relative size of $\beta_{R'}$ and $\beta_{R'H}$. If B_{1g} lies below B_{2u} , then the electrons occupy a Re-Re antibonding orbital:



Otherwise, the two remaining electrons will occupy a Re-H antibonding orbital in which the electrons are delocalized over all four atoms:



The bonding can thus be considered as a Re-Re single bond with delocalization of the remaining electrons over both the rheniums and hydrogens, rather than a protonation of a Re=Re double bond. Examination of the energy level diagram shows that the hydrogens act as a stabilizing unit even if there were no Re-H bond. Removal of the hydrogens to give Re-Re^{++} would result in no bond at all, since all four of the remaining levels would be filled.

REFERENCES

1. International Tables for X-Ray Crystallography,
Vol. I, II and III, Kynoch Press, Birmingham,
England (1962).
 2. G.H. Stout and L.H. Jensen, X-Ray Structure
Determination, MacMillan, New York (1968).
 3. M.J. Buerger, Crystal Structure Analysis,
John Wiley, New York (1960), p. 231.
- Original papers:
- P. Debye, Ann. Physik 43, 49 (1914).
 - I. Waller, Ann. Physik 83, 153 (1927).
 4. D.W.J. Cruickshank, Acta Cryst. 9, 747 (1956).
 5. S.J. La Placa and J.A. Ibers, Acta Cryst. 18,
511 (1965).
 6. L.I. Hodgson and J.S. Rollett, Acta Cryst. 16,
329 (1963).
 7. C. Scheringer, Acta Cryst. 16, 546 (1963).
 8. R. Eisenberg and J.A. Ibers, Inorg. Chem. 4, 773
(1965).
 9. L. Pauling, Physical Review 36, 430 (1930).
 10. J.M. Bijvoet and J.A.A. Ketelaar, J. Am. Chem.
Soc. 54, 625 (1932).
 11. W.H. Zachariasen, Theory of X-Ray Diffraction
in Crystals, Wiley, New York (1945).

12. E.G. Cox, D.W.J. Cruickshank and J.A.S. Smith, Proc. Roy. Soc. A247, 1 (1958).
13. D.W.J. Cruickshank, Acta Cryst. 9, 754 (1956).
14. D.W.J. Cruickshank, Acta Cryst. 9, 757 (1956).
15. V. Schomaker and K.N. Trueblood, Acta Cryst. B24, 63 (1968).
16. G.S. Pawley, Acta Cryst. 20, 631 (1966).
17. M.V. King and W.N. Lipscomb, Acta Cryst. 3, 155 (1950).
18. R.A. Schunn, C.J. Fritchie and C.T. Prewitt, Inorg. Chem. 5, 892 (1966).
19. F.B. Hildebrand, Introduction to Numerical Analysis, McGraw-Hill, New York (1956).
20. G.N. Watson, Bessel Functions, MacMillan, London (1944).
21. I.S. Sokolnikoff and R.M. Redheffer, Mathematics of Physics and Modern Engineering, McGraw-Hill, New York (1958).
22. G.L. Hardgrove and D.H. Templeton, Acta Cryst. 12, 28 (1959).
23. M.R. Churchill and T.A. O'Brien, J. Chem. Soc. (A), 1110 (1969).
24. A.F. Berndt and R.E. Marsh, Acta Cryst. 16, 118 (1963).
25. M.F. Bailey and L.F. Dahl, Inorg. Chem. 4, 1314 (1965).

26. M.J. Bennett, F.A. Cotton, P. Legzdins and S.J. Lippard, *Inorg. Chem.* 7, 1770 (1968).
27. E.R. Andrews and R.G. Eades, *Proc. Roy. Soc. A218*, 537 (1953).
28. C.H. Holms and J.A. Ibers, *J. Chem. Phys.* 30, 885 (1958).
29. B.P. Stoicheff, *Can. J. Phys.* 32, 339 (1954).
30. D.W.J. Cruickshank, D.W. Jones and G. Walker, *J. Chem. Soc.* 1303 (1964).
31. Brockway and Schevendeman, reported in (30).
32. H.J.M. Bowen, *Trans. Faraday Soc.* 50, 452 (1954).
33. W.C. Hamilton, *Acta Cryst.* 18, 502 (1965).
34. M.J. Bennett, W.L. Brooks, M. Elder, W.A.G. Graham, D. Hall and R. Kumer, *J.A.C.S.* 92, 208 (1970).
35. J.D. Dunitz, L.E. Orgel and A. Rich, *Acta Cryst.* 9, 373 (1956).
36. Kathleen A. Simpson, private communication.
37. Ester Lorah, University of Wisconsin thesis, Ph.D. (1969).
38. D.W.J. Cruickshank and W.S. MacDonald, *Acta Cryst.* 23, 9 (1967).
39. K. Maartmann-Moe, *Acta Cryst.* B25, 1452 (1969).
40. A.T. Armstrong, F. Smith, E. Elder and S.P. McGlynn, *J. Chem. Phys.* 46, 4321 (1967).
41. R.C. Pettersen, University of California, Berkeley, thesis, Ph.D. (1966).

42. F.A. Cotton, Chemical Application of Group Theory, Wiley, New York (1963).
43. W. Moffit, J. Am. Chem. Soc. 76, 3386 (1954).
44. R. Prins and J.D.W. van Voorst, J. Chem. Phys. 49, 4665 (1968).
45. Y.S. Sohn, D.N. Hendrickson and H.B. Gray, J. Am. Chem. Soc. 92, 3233 (1970).
46. D.R. Scott and R.S. Becker, J. Phys. Chem. 69, 3207 (1965).
47. D.A. Levy and L.E. Orgel, Mol. Phys. 4, 93 (1961).
48. R. Prins, F.J. Reinders, J. Am. Chem. Soc. 91, 4929 (1969).
49. J.K. Hoyano, private communication.
50. D.T. Cromer, Acta Cryst. A24, 321 (1968).
51. R. Mason and G.B. Robertson, in Advances in Structure Research by Diffraction Methods, Vol. 2, R. Brill and R. Mason (Eds.), Interscience Division, Wiley, New York (1966).
52. B.R. Davis, N.C. Payne and J.A. Ibers, Inorg. Chem. 8, 2719 (1969).
53. A.L. Beauchamp, M.J. Bennett and F.A. Cotton, J. Am. Chem. Soc. 90, 6675 (1968).
54. M.R. Churchill and F.R. Scholer, Inorg. Chem. 8, 1950 (1969).

55. M.R. Churchill and P.H. Bird, *Inorg. Chem.* 7, 1793 (1968).
56. M.J. Bennett and R. Mason, *Proc. Chem. Soc.* (1964), 395.
57. S.J. La Placa, W.C. Hamilton, J.A. Ibers and A. Davidson, *Inorg. Chem.* 8, 1928 (1969).
58. R.J. Doedens, W.T. Robinson and J.A. Ibers, *J. Am. Chem. Soc.* 89, 4323 (1967).
59. L.F. Dahl and R.E. Rundle, *Acta Cryst.* 16, 419 (1963).
60. M.R. Churchill and R. Bau, *Inorg. Chem.* 6, 2086 (1967).
61. G. Simon and L.F. Dahl, private communication to W.A.G. Graham.
62. R.S. Hamilton and E.R. Corey, Abstracts, 156th National Meeting of the American Chemical Society, September 1968, #INORO25.
63. L. Pauling, Nature of the Chemical Bond, Cornell University Press, Ithaca, New York (1960).
64. F.A. Cotton and D.C. Richardson, *Inorg. Chem.* 5, 1851 (1966).
65. R.F. Stewart, E.R. Davidson and W.T. Simpson, *J. Chem. Phys.* 42, 3175 (1964).
66. M. Elder, *Inorg. Chem.* 9, 762 (1970).
67. A.F. Wells, Structural Inorganic Chemistry, 3rd edition, Oxford University Press, London (1962), p. 696.

68. L. Manojlović-Muir, K.W. Muir and J.A. Ibers,
Inorg. Chem. 9, 447 (1970).
69. A. Hart-Davis, private communication.
70. R. Bau, B. Fontal, H.D. Kaesz and M.R. Churchill,
J. Am. Chem. Soc. 89, 6374 (1967).
71. L.B. Handy, P.M. Treichel, L.F. Dahl and
R.G. Hayter, J. Am. Chem. Soc. 88, 366 (1966).
72. S.C. Abrahams, A.P. Ginsberg and K. Knox,
Inorg. Chem. 3, 558 (1964).
73. M.R. Churchill, P.H. Bird, H.D. Kaesz, R. Bau
and B. Fontal, J. Am. Chem. Soc. 90, 7135
(1968).
74. H.D. Kaesz, B. Fontal, R. Bau, S.W. Kirtley and
M.R. Churchill, J. Am. Chem. Soc. 91, 1021
(1969).
75. R. Mason, private communication.
76. A.L. Patterson and W.E. Love, Am. Minn. 45,
325 (1960).
77. T.E. Haas, private communication.
78. W. Kauzmann, Quantum Chemistry, Academic Press,
New York (1964).

Appendix A

SUBROUTINES ROTOR AND BESSEL
OF SFLS5HR


```
SUBROUTINE ROTOR
COMMON TITLE(18),MODE,INV,NAD,ISAN,NPU,NEW(5),NFSQ,NFOUR,
INCR,KARD,LD,LV,NLV,NS,NU,MU,MLSC,KRIT,RPAR,NATE,ICENT
2,NRIG,NONR,NHIN
COMMON A,B,C,AL,BE,GA,AQ,BQ,CQ,ALQ,BEQ,GAQ,NSL,SUMDL
COMMON NPAR,NVAR,NCNT,KSEL(921)
COMMON S(50),PO,GP(70),GQ(60),GR(60),MF(60),MG(60),MI(60),
2X(140),Y(140),Z(140),B11(140),B22(60),B33(60),B12(60),
2B13(60),B23(60),NA(70),NAME(140),XC(10),YC(10),ZC(10),
3P(10),R(10),U(10),RPE(10,8),NSTEP(10),NORD(10),RID(10)
COMMON MLSW,AW,BW,CW,DW,EW,FW,GW,HW,SIZE1,SIZE2
COMMON SAER(10,10),NSAFR(10,10),SAES(10),NSAES(10),SAEF(10),
INSAEF(10)
COMMON NTRAN(4,12,12),NVTN(4,36)
COMMON NF,FM(32,20),F(20),FP(20),FPP(20),RHO,RHOSQ
COMMON FOBS,FCAL,SFC,ADBS,ACA,BOBS,BCAL,DFL,SIGMA,EXT1,EXT2
1,MS1,MREJ,Q,MH,MK,ML,TH,TK,TL,DA(180),DB(180),DF(180)
COMMON CHG(921),STD(921),EPS(180),DIAG(180),V(180)
COMMON A11,A12,A13,A22,A23,A33,BA1,BA2,BA3,BA4,BA5,BA6
COMMON SN(50),BON,GPN(70),GQN(60),GRN(60),XN(140),YN(140),
1ZN(140),B11N(140),B22N(60),B33N(60),B12N(60),B13N(60),
2B23N(60),XCN(10),YCN(10),ZCN(10),PN(10),RN(10),UN(10),
3BRB(10,8),RIDN(10)
COMMON/SPSY/I,J,N,RH,RK,RL,T,RHH,RKK,RLL,RHK,RHL,RKL,NR
COMMON /PDC/SPK,SPL,SPP,SPR,SPU,CPH,CPK,CPL,CPP,CPR,CPU,WL,
1SACAL,WB,SBCAL,K,L,TPI,JF,LC,SPH,INVI
COMMON/BESS/DBJB(10,20),LM(6),BR,BEA,TE,TD,BDD,BD,BIA(10,20)
1,DBIB(10),BID(10),JPA
DIMENSION WL(20),WB(20)
EQUIVALENCE(BI,B11),(BIN,B11N),(AR,SN)
DIMENSION AR(20100)
DIMENSION BI(140),BIN(140)
DIMENSION SUH(6),DELMS(2,6),DELMC(2,6),DELC(2,3),DELS(2,3)
REAL MTERM
REAL*8 CC,DD,AP,AP2
COMMON/RIGID/CLIMIT
TE=0.
TD=0.
QW=0.
BPOS=1.0
BNEG=-1.0
BD=BRB(I,2)
NK=MOD(NORD(I),2)+1
CD=COS(P(I))
CF=COS(R(I))
SD=SIN(P(I))
SE=SIN(R(I))
TPI=6.283185
XK=TPI*RID(I)
TF=EXP(-BRB(I,1)*RHOSQ)*GP(I+NU)*ICENT*NSTEP(I)
IF(NAD.EQ.2) TF=TF*2.
TF=TF*F(JF)
DO 14 IWA=1,2
DO 10 IW=1,6
```

```
      DELMC(IWA,IW)=0.
      DELMS(IWA,IW)=0.0
      IF(IW.GT.3) GO TO 10
      DELC(IWA,IW)=0.
      DELS(IWA,IW)=0.
10  CONTINUE
14  CONTINUE
      CODE=0.
      DO 23 J=1,MU
          ICCODE=0
          CALL SYM
          PHI=TPI*(RH*XC(I)+RK*YC(I)+RL*ZC(I)+T)
          CP=COS(PHI)*TF
          SP=SIN(PHI)*TF
          XK1=RH*BA1+RK*BA2+RL*BA3
          XK2=RL*BA6
          XK3=RK*BA4+RL*BA5
          CC=XK*(XK1*CE-XK2*SE)
          DD=XK*(XK1*SD*SE+XK3*CD+XK2*CE*SD)
          AP=DSQRT(CC*CC+DD*DD)
          XNU=DARCOS(CC/AP)
          IF(DD.LT.0.0)XNU=-XNU
          ANGLE=NORD(I)*(U(I)-XNU)
          IF(MODE.EQ.1) GO TO 2
          IF(KSEL(L+7).EQ.0.AND.KSEL(L+8).EQ.0) GO TO 2
          DELCE=-XK*(XK1*SE+XK2*CE)
          DELDE=XK*(XK1*SD*CE-XK2*SD*SE)
          DELDD=XK*(CD*SE*XK1-SD*XK3+CE*CD*XK2)
          AP2=AP*AP
          DELAPD=DD*DELD/AP
          DELAPE=(CC*DELCE+DD*DELDE)/AP
          TE=DELAPE/AP
          TD=DELAPD/AP
```

```
C
C      ***** THIS NEXT SECTION WILL CAUSE DIVIDE BY ZERO ERRORS
C      FOR CERTAIN REFLECTIONS IF D JR E ARE 0,90,180,OR 270DEGS
C      BY PASS IS TO OMIT THESE REFLECTIONS FROM LEAST SQUARES
C
```

```
      CW=AP2*DSQRT(1.-CC*CC/AP2)
      IF (ABS(CW).LT.0.00001) GO TO 1
      DXNU=1./CW
      DXNUE=-DXNU*(AP*DELCE-CC*DELAPE)
      DXNUE=DXNU*CC*DELAPD
      GO TO 2
```

```
1  ICODE=1
2  IF(NK.EQ.2) GO TO 3
```

```
C
C      ***** CALC'N OF REAL TERMS *****
```

```
15  NPRIME=NK*NORD(I)/2
      NAA=1
      GO TO 21
22  F=SNGL(AP)
      CALL BFSSEL (BJ,OW,E ,BNEG)
```

```
SUM(1)=DBIB(I)*BJ
SUM(2)=BR
SUM(3)=BOD
SUM(4)=BEA
SUM(5)=0.
SUM(6)=BJ
GO TO 5
```

C
C
C

```
***** CALC'N OF IMAG TERMS *****
```

```
3 NPRIME=(NORD(I)-1)/2
  DO 4 IA=1,6
    SUM(IA)=0.
4 CONTINUE
  NAA=2
21 DO 24 IA=1,5
    LM(IA)=KSEL(IA+L+4)
24 CONTINUE
  LM(6)=1
  IF(NAA.EQ.1) GO TO 22
5 PSIGN=1.
  IF(ICODE.FO.0) GO TO 16
  SUM(3)=0.
  SUM(4)=0.
  LM(3)=0
  LM(4)=0
16 DO 6 IA=1,NPRIME
    PSIGN=PSIGN*(-1)
6 CONTINUE
  SIGN=PSIGN
  IF(NK.EQ.2) PSIGN=-1.
  NL=1
  IF(NAA.NE.NK) NL=2
```

C
C
C

```
***** CALC'N OF M AND DERIVATIVES *****
```

```
DO 11 JP=NL,20,NK
  JPA=JP
  PA=FLOAT(JP)
  PNA=PA*NORD(I)
  CU=COS(PA*ANGLE)
  SU=SIN(PA*ANGLE)
  TCOM=2.*SIGN*BIA(I,JP)/BIO(I)
  E=SNGL(AP)
  CALL BESSEL (BJ,PNA,E ,BNEG)
  IF(MODE.EQ.1) GO TO 34
  IF(LM(1).EQ.0) GO TO 30
```

C
C
C

```
***** CALC'N OF DM/D(BD) *****
```

```
BDTERM=2.*SIGN*CU*DBJB(I,JP)*BJ
SUM(1)=SUM(1)+BDTERM
IF(ABS(BDTERM/SUM(1)).LE.CLIMIT) LM(1)=0
30 IF(LM(2).EQ.0) GO TO 31
```

C
C
C

***** CALC'N OF DM/DR *****

RTERM=TCOM*BR*CU
SUM(2)=SUM(2)+RTERM
IF (ABS(RTERM/SUM(2)).LE.CLIMIT) LM(2)=0
31 IF(LM(3).EQ.0) GO TO 32

C
C
C

***** CALC'N OF DELMD *****

DMD=SU*PNA*DXNUD
DTERM=TCOM*(BDD*CU+BJ*DMD)
SUM(3)=SUM(3)+DTERM
IF (ABS(DTERM/SUM(3)).LE.CLIMIT) LM(3)=0
32 IF(LM(4).EQ.0) GO TO 33

C
C
C

***** CALC'N OF DM/DE *****

DME=SU*PNA*DXNUE
ETERM=TCOM*(BEA*CU+BJ*DME)
SUM(4)=SUM(4)+ETERM
IF (ABS(ETERM/SUM(4)).LE.CLIMIT) LM(4)=0
33 IF(LM(5).EQ.0) GO TO 34

C
C
C

***** CALC'N OF DM/DG *****

GTERM=-PNA*TCOM*SU*BJ
SUM(5)=SUM(5)+GTERM
IF (ABS(GTERM/SUM(5)).LE.CLIMIT) LM(5)=0
34 IF(LM(6).EQ.0) GO TO 35

C
C
C

***** CALC'N OF M *****

MTERM=TCOM*CU*BJ
SUM(6)=SUM(6)+MTERM
IF (ABS(MTERM/SUM(6)).LE.CLIMIT) LM(6)=0
35 LSUM=LM(1)+LM(2)+LM(3)+LM(4)+LM(5)+LM(6)
IF(MODE.EQ.1) LSUM=LM(6)
IF(LSUM.EQ.0) GO TO 12
SIGN=SIGN*PSIGN

11 CONTINUE

WRITE(6,201)RH,RK,RL

12 IF (MODE.EQ.1) GO TO 7

SUM(1)=(SUM(1)-SUM(6)*DBIB(I))/BIO(I)

DO 36 IA=1,5

DELMC(NAA,IA)=SUM(IA)*CP+DELMC(NAA,IA)

DELS(NAA,IA)=SUM(IA)*SP+DELS(NAA,IA)

36 CONTINUE

IF((KSEL(L+1)+KSEL(L+2)+KSEL(L+3)).EQ.0) GO TO 7

DELC(NAA,1)=DELC(NAA,1)+CP*SUM(6)*RH

DELC(NAA,2)=DELC(NAA,2)+CP*SUM(6)*RK

DELC(NAA,3)=DELC(NAA,3)+CP*SUM(6)*RL

DELS(NAA,1)=DELS(NAA,1)+SP*SUM(6)*RH

DELS(NAA,2)=DELS(NAA,2)+SP*SUM(6)*RK

```
DELS(NAA,3)=DELS(NAA,3)+SP*SUM(6)*RL
7 DELMC(NAA,6)=SUM(6)*CP+DELMC(NAA,6)
  DELMS(NAA,6)=SUM(6)*SP+DELMS(NAA,6)
  IF(NAA.EQ.2) GO TO 15
23  CONTINUE
  8 AT=DELMC(1,6)-DELMS(2,6)
    ACAL=ACAL+AT
    IF(NAD.EQ.2) GO TO 40
    BT=DELMC(2,6)+DELMS(1,6)
    BCAL=BCAL+BT
40  IF(MODE.EQ.1) GO TO 9

C
C
C    ***** CALC'N OF DELF(POPULATION FACTOR) *****

    IF(KSEL(L).EQ.0) GO TO 58
    DA(K)=AT/GP(I+NU)
    IF(INV1.FQ.1) GO TO 59
    DB(K)=BT/GP(I+NU)
59  K=K+1
58  L=L+1

C
C
C    ***** DERIVATIVES W.R.T. CENTRE OF RING *****

DO 56 IA=1,3
  IF(KSEL(L).EQ.0) GO TO 55
  DA(K)=-TPI*(DELS(1,IA)+DELC(2,IA))
  IF(INV1.EQ.1) GO TO 57
  DB(K)=TPI*(-DELS(2,IA)+DELC(1,IA))
57  K=K+1
55  L=L+1
56  CONTINUE
  IF(KSEL(L).EQ.0) GO TO 53

C
C
C    ***** CALC'N OF DELF(TEMP) *****

  DA(K)=-RHOSQ*(DELMC(1,6)-DELMS(2,6))
  IF(INV1.EQ.1) GO TO 54
  DB(K)=-RHOSQ*(DELMC(2,6)+DELMS(2,6))
54  K=K+1
53  L=L+1

C
C
C    ***** CALC'N OF DELFD TO DFLF3 *****

DO 50 IA=1,5
  IF(KSEL(L).EQ.0) GO TO 51
  DA(K)=DELMC(1,IA)-DELMS(2,IA)
  IF(INV1.EQ.1) GO TO 52
  DB(K)=DELMC(2,IA)+DELMS(1,IA)
52  K=K+1
51  L=L+1
50  CONTINUE
  9  RETURN
201 FORMAT(' REFLECTION ',3F3.0,' HAS NOT CONVERGED')
  END
```

```
SUBROUTINE BESSEL (BSUM, PP, XZ, BSIGN )
COMMON TITLE(18),MODE,INV,NAD,ISAN,NPJ,NEW(5),NFSQ,NFOUR,
INCOR,KARD,IO,LV,NLV,NS,NU,MU,MLSC,KRIT,RPAR,NATE,ICENT
2,NRIG,NONR,NIIN
COMMON A,B,C,AL,BE,GA,AQ,BQ,CQ,ALQ,BEQ,GAQ,NSL,SUMDL
COMMON NPAR,NVAR,NCNT,KSEL(921)
COMMON S(50),BC,GP(70),GQ(60),GR(60),MF(60),MG(60),MI(60),
2X(140),Y(140),Z(140),B11(140),B22(60),B33(60),B12(60),
2B13(60),B23(60),NA(70),NAME(140),XC(10),YC(10),ZC(10),
3P(10),R(10),U(10),BRB(10,8),NSTEP(10),NORD(10),RID(10)
COMMON MLSW,AW,BW,CW,DW,EW,FW,GW,HW,SIZE1,SIZE2
COMMON SAER(10,10),NSAER(10,10),SAES(10),NSAES(10),SAEF(10),
INSAEF(10)
COMMON NTRAN(4,12,12),NVTN(4,36)
COMMON NF,FM(32,20),F(20),FP(20),FPP(20),RHO,RHOSQ
COMMON FOBS,FCAL,SFC,AOBS,ACAL,BOBS,BCAL,DEL,SIGMA,EXT1,EXT2
1,MS1,PREJ,Q,MH,NK,ML,TH,TK,TL,DA(180),DB(180),DF(180)
COMMON CHG(921),STD(921),EPS(180),DIAG(180),V(180)
COMMON A11,A12,A13,A22,A23,A33,BA1,BA2,BA3,BA4,BA5,BA6
COMMON SN(50),BON,CPN(70),CQN(60),GRN(60),XN(140),YN(140),
1ZN(140),B11N(140),B22N(60),B33N(60),B12N(60),B13N(60),
2B23N(60),XCN(10),YCN(10),ZCN(10),PN(10),RN(10),UN(10),
3BRB(10,8),RIDN(10)
COMMON/SPSY/I,J,N,RH,RK,RL,T,RHH,RKK,RLL,RHK,RHL,RKL,NR
COMMON /PDC/SPK,SPL,SPP,SPP,SPJ,CPH,CPK,CPL,CPP,CPR,CPU,WL,
1 SACAL,WB,SBCAL,K,L,TPI,JF,LC ,SPH,INV1
COMMON/BFSS/DBJB(10,20),LM(6),BR,BEA,TE,TD,BDD,8D,BIA(10,20)
1,DBIB(10),BIO(10),JPA
COMMON/RIGID/CLIMIT
DIMENSION WL(20),WB(20)
EQUIVALENCE(BI,B11),(BIN,B11N),(AR,SN)
DIMENSION BI(140),BIN(140)
DIMENSION AR(20100)
DIMENSION LB(5)
```

C

```
BTERM=1.
BRTERM=0.
FRTERM=0.
DRTERM=0.
BJTERM=0.
LB(5)=1
IF(PP.EQ.0.) GO TO 17
FACP=1.
JP=IFIX(PP)
DO 1 M=1,JP
    XM=FLOAT(M)
    BTERM=BTERM*XZ/(2.*XM)
1 CONTINUE
17 IF(BSIGN.LE.0.) GO TO 22
C ***** CALC'N OF I TERMS *****
LB(1)=1
DO 13 M=2,4
    LB(M)=0
13 CONTINUE
```

```
IF (PP.NE.0.)BJTERM=PP*BTERM/BD
DBJB(I,JPA)=BJTERM
GO TO 5
C ***** CALC'N OF M TERMS *****
22 LB(1)=0
DO 14 M=2,4
    LB(M)=LM(M)
14 CONTINUE
IF (PP.EQ.0.) GO TO 5
BRTERM=BTERM*PP/RID(I)
ERTERM=PP*BTERM*TF
DRTERM=PP*BTERM*TD
5 BSUM=BTERM
BR=BRTERM
BEA=ERTERM
BDD=DRTERM
IF (BSIGN.GT.0) DBJB(I,JPA)=BJTERM
DO 2 M=1,30
    BTERM=(BSIGN*BTERM*XZ*XZ)/(4.*M*(M+PP))
IF (MODE.EQ.1) GO TO 11
IF (LB(1).EQ.0) GO TO 6
C
C ***** CALC'N OF DM/DBD TERM *****
C
BJTERM=(2.*M+PP)*BTERM/BD
DBJB(I,JPA)=DBJB(I,JPA)+BJTERM
IF (ABS(BJTERM/DBJB(I,JPA)).LE.CLIMIT)LB(1)=0
6 IF (LB(2).EQ.0) GO TO 7
C
C ***** CALC'N OF DM/DR TERM *****
C
BRTERM=BTERM*(2.*M+PP)/RID(I)
BR=BR+BRTERM
IF (ABS(BRTERM/BR).LE.CLIMIT) LB(2)=0
7 IF (LB(3).EQ.0) GO TO 8
C
C ***** CALC'N OF DM/DD *****
C
DRTERM=BTERM*(2.*M+PP)*TD
BDD=BDD+DRTERM
IF (ABS(DRTERM/BDD).LE.CLIMIT) LB(3)=0
8 IF (LB(4).EQ.0) GO TO 11
C
C ***** CALC'N OF DM/DE TERM *****
C
ERTERM=BTERM*(2.*M+PP)*TE
BEA=BEA+ERTERM
IF (ABS(ERTERM/BEA).LE.CLIMIT) LB(4)=0
```

11 IF (LB(5).EQ.0) GO TO 12

C
C
C

***** CALC'N OF BESSEL SUMMATION *****

BSUM=BSUM+BTERM

IF(ABS(BTERM/BSUM).LE.CLIMIT) LB(5)=0

12 LSUM=LB(1)+LB(2)+LB(3)+LB(4)+LB(5)

IF(MODE.EQ.1) LSUM=LB(5)

IF(LSUM.EQ.0) GO TO 3

2 CONTINUE

3 RETURN

END

Appendix B

PROGRAMMES USED

<u>Author</u>	<u>Title</u>	<u>Description</u>
D.P. Shoemaker	MIXG2	calculates Picker diffractometer settings modified by M. Elder to sort data
M.J. Bennett	PMMO	calculates intensities, makes I_p corrections for Picker data
M. Elder	Datap	as for PMMO, except for PAILRED data
M. Elder and K. Simpson	D-refine	refines axial lengths
A. Zalkin	FORDAP	Fourier summation for Patterson or Fourier maps
M.J. Bennett	MMMR	calculates starting parameters for rigid bodies and hindered rotors
W.C. Hamilton	GONO9	absorption corrections - Picker data
D.P. Shoemaker	GNABS	absorption corrections - PAILRED data
C.T. Prewitt	SFLS5HR	structure factor calculation and least squares refinement of parameters modified by B.M. Foxman, M.J. Bennett and W.L. Brooks for rigid body and hindered rotor routines
G.J. Williams	CROMERS	calculates form factor curves using Cromer coefficients
J.S. Wood	MGEOM	calculates bond lengths, angles and best planes

Programmes Used (Contd.)

<u>Author</u>	<u>Title</u>	<u>Description</u>
W. Busing and H.A. Levy	ORFFE2	calculates bond lengths, angles and associated errors modified by B. Penfold for IBM 360, and W.L. Brooks and M. Elder for hindered rotors and rigid bodies
C. Johnson	ORTEP	writes plot command tape for Calcomp plotter
M. Elder and W.L. Brooks	SFLIST	lists structure factors for publication

Appendix C

CONVENTIONAL CRYSTALLOGRAPHIC SYMBOLS
AS DEFINED IN VOL. I, PAGE xi, OF THE
INTERNATIONAL TABLES FOR X-RAY CRYSTALLO-
GRAPHY

h, k, l	indices of the reflection from a set of parallel planes; co-ordinates of a reciprocal lattice point
F_{hkl}	structure factor for the unit cell, corresponding to the Bragg reflection hkl
$a, b, c,$	lengths of unit cell edges
α, β, γ	interaxial angles
a^*, b^*, c^*	lengths of reciprocal lattice unit cell edges
$\alpha^*, \beta^*, \gamma^*$	interaxial angles in reciprocal space
x_i, y_i, z_i	fractional co-ordinates of an atom i (co-ordinates of atom i in units of a, b, c)
$\rho_{x, y, z}$	electron density at the point x, y, z
μ	linear absorption coefficient
\bar{u}^2	mean square amplitude of atomic vibration
B	Debye isotropic temperature parameter $B = 8\pi^2 \bar{u}^2$
$\beta_{11}, \beta_{22}, \beta_{33},$	anisotropic temperature parameters used to describe ellipsoidal electron distribution of the anisotropically vibrating atom; the temperature factor expression is then: $\exp[-(\beta_{11}h^2 + \beta_{22}k^2 + \beta_{33}l^2 + 2\beta_{12}hk + 2\beta_{13}h\ell + 2\beta_{23}k\ell)]$
$\beta_{12}, \beta_{13}, \beta_{23}$	

F_o observed structure factor
 F_c calculated structure factor